Sitting Up System

M.H.J. Groen

A novel concept for large integrated offshore wind turbine installation

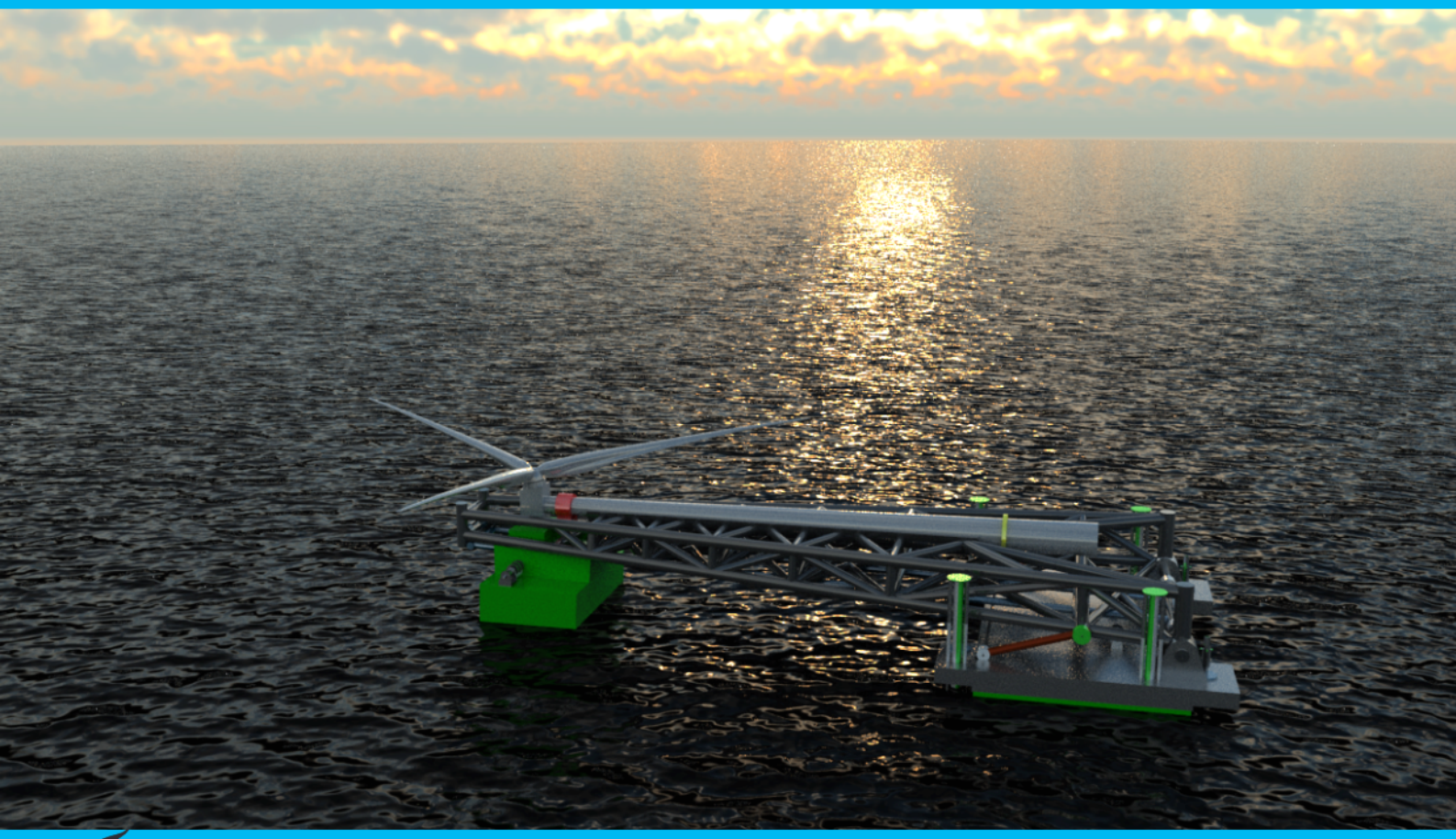

TU Delft

Sitting Up System

by

M.H.J. Groen

to obtain the degree of Master of Science
at the Delft University of Technology,
to be defended publicly on Friday August 30, 2019 at 9:30 AM.

Student number:	4079507	
Project duration:	September 1, 2018 – August 30, 2019	
Thesis committee:	Prof. dr. ir. M. Metrikine,	TU Delft, supervisor
	Dr. J. S. Hoving,	TU Delft
	Ir. J. Lanser,	Marine Innovators B.V.

This thesis is confidential and cannot be made public until 30 august, 2019.

TU Delft

Preface

This master thesis is written to obtain a Master of Science degree for Offshore and Dredging Engineering at Delft University of Technical, involving Bottom Founded and Floating Offshore Structures. Above that, it is a feasibility study on the upending of the SUS concept which is newly developed installation method for fully assembled wind turbines at moderate water depths.

This project is done in name of Marine Innovators B.V. and executed through out KCI the Engineering B.V. at which I was contracted during this thesis from 1 September 2018 up and till 31 July 2019. At first I want to grant my sincere thanks to Jan Lanser whom I was working with at a daily basis, he helped me throughout this thesis as a soundboard on both the conceptual optimisation and theoretical approach. Secondly, I want to thank KCI Engineering B.V. for supporting me throughout this thesis.

During this journey I learned about doing research, modeling complex submerged structures and the path of a start-up finding a way up into the offshore business. This involved visiting conferences, fairs and meetings with multiple well-established engineering companies.

Another thanks go to my supervisors Jeroen Hoving and Andrei Metrikine from Delft University of Technology, for giving constructive criticism helping this research into the right direction. Especially Jeroen, who was always ready to help with all the challenges within this thesis.

Finally, I would like to thank my girlfriend, family and friends who have always been a listening ear throughout my thesis. They helped me see things in another perspective and criticized or complimented my work to get the thesis as far as it finally is.

M.H.J. Groen
Delft, August 2019

Summary

The offshore wind industry has great prospects in the near future. It is expected by the EWEA that in the North Sea only the wind turbine capacity will increase to 45 GW. In 2015 the capacity was only 5.2 GW, implying big business for coming years. Offshore contractors should be capable of installing lots of turbines and just that is a problem. As offshore wind turbines increase in size installation vessels need significant upgrades, which leads to excessive cost. Therefore, most contractors look for cheaper and better solution for installing these large offshore wind turbines. The Sitting Up System or SUS is a new concept designed by Marine Innovators B.V. and will install fully assembled wind turbines with their foundation. It decreases offshore installation time and therefore decreases operational cost significantly. The SUS is designed to transport fully assembled wind turbines horizontally and upend them to a vertical position while anchored to the seabed. For now, the SUS is a concept and has multiple design possibilities using either a hydraulic or a buoyant lifting system. Analysis on these lifting methods and their operational functionality resulted in a buoyant type lifting system. The SUS 3: 'Buoyant upend 2' concept consists of latticed structure and two buoyant modules. The large module is sunk to anchor the SUS and the small buoyancy module is pulled along the lattice to create an upending moment.

Using the software Matlab the upending motion of SUS 3 is modelled as a rigid body to find limiting wave conditions. The model uses second order stokes theorem and Jonswap to simulate waves on the structure. Loads on the structure are calculated using the Morison equation. Two DOFs are considered as the SUS can only rotate around a hinge at the seabed and move the buoyancy module.

In the simulation a wind turbine of 200 meters height is upended in 30 minutes, while operating at 40 meters water depth. The first phase of the upending wave loads is most critical. The criteria for the SUS to operate depends on the acceleration of the top tower assemble of the wind turbine, these cannot exceed 0.1 g. In this case the limiting sea state is a H_s of 1 m with a T_p of 4.5 s. This leads to a workability of about 16 percent. During the beginning stages of the upending the natural frequency of the system operates around 10 seconds. This is critical as waves oscillate near this frequency. Though the simulation does not account for radiation or diffraction, the performance in later stages of upending gives a better result. Here, it can operate with a H_s of 2.5 meters resulting in a workability of 75 percent.

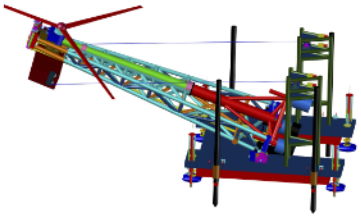

Figure 1: Sitting Up System concept

The SUS 3 is anchored with spudcans during upending and shear loads are most significant. These spudcans can experience a shear load of 24 MN when considering a H_s of 3.5 with a T_p of 8.5. Therefore, anchoring method should be designed such that it can comprehend these shear loads more efficiently.

The work done by the winches pulling the buoyancy module is 13 percent more than the potential energy gained after upending with no waves. When waves are applied, energy is gained due to the uplifting force of waves. As the structure is lifted, resistance of pulling the buoyancy module decreases and can move more efficiently. Considering a H_s of 1.5 m and a T_p of 5.5 s will results in an energy gain of 5 percent. Therefore, this method is quite efficient in upending wind turbines offshore.

Contents

1

Introduction to offshore wind turbine installation

The world energy production in 2017 was about 163.400 TWh [8] and is growing with roughly 2 percent yearly. In 2018 the growth was mainly caused by emerging industries in China and India, namely about an addition 40 percent of their previous consumption. Although it is commonly known that global warming is present, which is thought to be mainly caused by greenhouse gas produced by energy producing companies, the means to decrease pollution with new and cleaner technologies are not being sufficiently deployed. As most industries are conditioned to coal, oil and gas infrastructures and its cost effectiveness, their effort to change to renewable energy will be fairly low. It is safe to say all large industries follow the most basic rules of economics; supply, demand and cost. These industries do not get acquainted with new technologies because renewable energy is yet too expensive. The two most realistic options to change this phenomenon would be either taxing pollution excessively or reducing cost of renewable energy. This thesis is investigating on the last one, reducing the costs. More specifically the cost of installing wind turbines offshore.

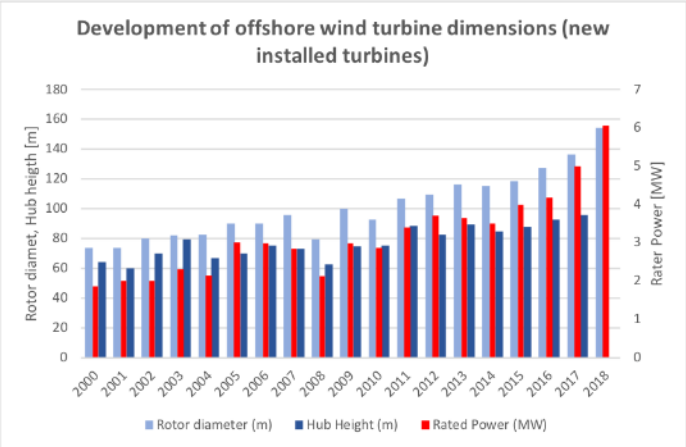

Figure 1.1: Development of offshore wind turbines

1.1. State of the art

The first installation of an offshore wind farm was done in 1991, 'Vindeby' in Denmark [1]. The eleven 450 kW turbines were installed on gravity-based foundations at a water depth of 4 meters. The installation of the turbine was done using a barge with a crane on it. This

crane then installed the turbine with nacelle and blades as a whole. Since then a total of about 23 GW offshore wind power is installed. A forecast from Norwegian Energy Partners expects a growth to 46.5 GW [5] installed power by 2022. The market is thought to have an annual growth of 16-22% for the coming years as turbines get bigger and more efficient. But these new wind turbines need innovative installation methods, as offshore contractors are not yet able to install these enormous structures. For these companies most obvious step would be increasing the size of installation vessels, but costs and thus time are an issue.
The installation time, for a fully installed wind turbine including monopile, decreased from 7.6 days in 2000-2003 to 5.9 days in 2016-2017 [18]. The installation duration of monopile decrease significantly from 4 days to almost 1.06 days per MW and many contributes to the decreased installation duration. As turbine sizes increase obviously the duration per MW can be decreased significantly, however installation time of only a wind turbine decreased from 5 days to 4 days on average. Therefore, for turbine installation significant improvement would be desirable in the near future. During the short history of offshore wind, there have been installed various turbine design types. The outer design of tower, nacelle and blades have been basically the same for all wind turbines, and were mainly optimized for power by increasing size, decreasing material weight and optimizing generators [16]. Figure 1.1 illustrates how these optimizations result in increased performance since 2000. This trend is thought to proceed for future wind turbines. New turbines with a capacity beyond thought possible are ready for offshore testing, the Haliade-X [3] 12 MW wind turbine of General Electric with a hub height of 150 meters and a rotor span of 220 meters is being installed at the port of Rotterdam in the summer of 2019. It will be installed onshore for testing, however for offshore installation, methods are still unknown as these structures are too large for most conventional turbine installation vessels. The first challenge for these enormous turbines is the foundation and the depth these are to be placed. However, foundations have more freedom of in design which creates opportunities.

Figure 1.2: Offshore foundation types

1.1.1. Foundations

The first offshore foundations for wind turbines were gravity based structures or GBS. After that multiple other structures types where used, namely monopiles, suction buckets, piled lattice, tripods, and floating structures with tension legged tripods or ballast as shown in figure 1.2 accordingly. Table 1.1 shows the quantity of each foundation in Europe and clearly monopiles are used significantly more than others. But with increasing length and diameter these monopile XL variants come with lots of design issues. The research [14] found that for a 10 MW turbine the global buckling load will exceed to some extent, however it is thought that this issue can be overcome. Alternatives like hybrid monopiles are investigated and could probably solve these structural problems. However, its questionable how many optimizations for these XL monopiles are realistic before other foundations tend to becoming more fitting.

Sticking with known methods may eventually lead to less efficient and possibly more costly solutions.

Table 1.1: Installed foundations in 2018 [11]

Type	#	%
Monopile	3720	81.7
Lattice	315	6.9
GBS	283	6.2
Tripod	132	2.9
Tripile	80	1.8
Floating	7	0.2
Other	18	0.4
Total	4555	100

1.1.2. Existing installation methods

As for installation methods, there has been little changes during the short history of offshore wind. The first turbines were installed using a barge with an onshore crane placed on deck. Later on, as turbines increased in size and the offshore wind business grew vessels were made specifically for this operations. Since then heavy lift vessels and jack-up barges with large cranes are installing turbines these wind turbine. Figures 1.3 to 1.6 illustrate some installation vessels of some leading offshore wind contractors. These vessels are an evolution of the barge with an onshore crane and at the moment their functionality extends beyond the offshore wind industry. However still these vessels need some sort of upgrade for wind turbines of the future and the questions is whether this is feasible.

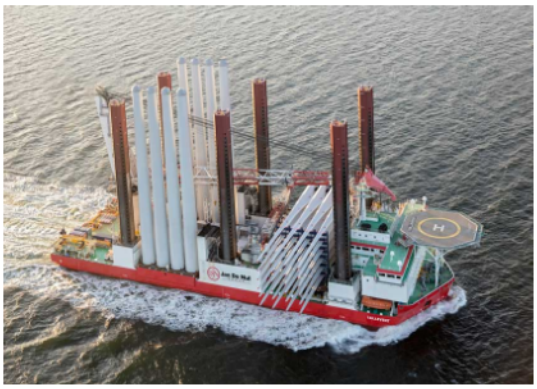

Figure 1.3: Taillevent, Jan de Nul

Figure 1.4: Orion, DEME

Figure 1.5: Seajacks Scylla, Boskalis contracted

Figure 1.6: Svanen, Van Oord

At the moment the newest vessel to install these larger wind turbines is ordered by Jan de Nul, the Voltaire [7] shown in figure 1.7. This vessel will be equipped with a crane capable

of lifting 3,000 tonnes. The company is the first taking the risk in installing these larger turbines. However, as new installation concepts are being designed to operate more efficient it could well be a resulting in a costly investment.

Figure 1.7: Voltaire, Jan de Nul Group

1.1.3. Concept installation methods

The need for more efficient and capable installation methods is a problem that has been spooking around for a few years already. Innovative ideas pop up quite often. For it to be successful a concept it needs significantly more potential than existing technology. Unfortunately, the offshore industry is very conservative which makes creativity hard. As these structures are really gigantic there is no margin for failed concepts, costing millions of euros when failing.

Though it is a tough market there are a few concepts who got attention. One of these is the WindFlip system. It should transport and install floating wind turbine and was made knowledgeable to the world in 2009. As figure 1.8 shows the wind turbine is placed on a ship like structure as a whole. At location the vessel is filled up with water starting at the bottom. Eventually the wind turbine is position vertically and can be anchored with some sort of mooring system. Unfortunately, for the developers it has stayed a concept for now.

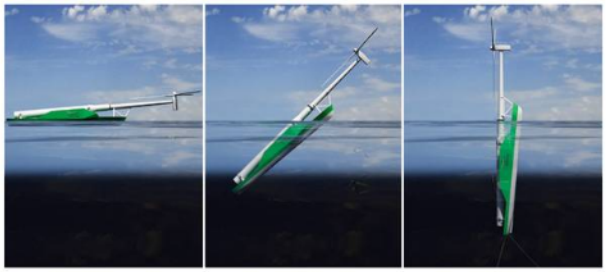

Figure 1.8: Windflip concept

Another concept is the MonobaseWind figure 1.9, this idea is still in the running for production. It uses two ballast structures of steel and concrete to float the turbine to its position, where after the lower foot is lowered to the seabed. In the last phase the upper ballast is lowered to finally be stable. The system should be able to install 10+ MW wind turbines at depths over 40 meters. This company has already done model tests at Marin and is waiting for a golden opportunity to realize their idea.

Furthermore, there are several concepts for floating wind turbine installations, from which

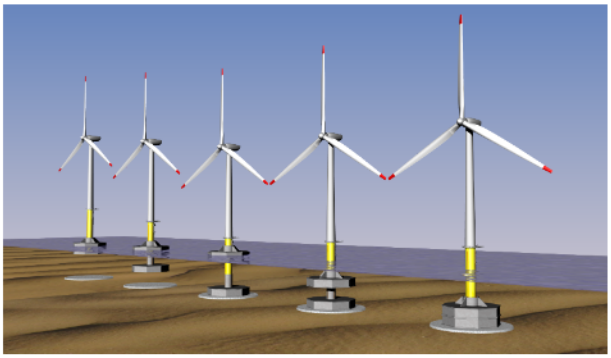

Figure 1.9: MonobaseWind concept

most rely on its floating system for transportation and operation. These floating systems are then anchored at the seabed with mooring systems.

2

Methodology

In this chapter the methodology is discussed. First, a short introduction will elaborate on the Sitting Up System. Secondly, a short note on the total extend of the research on the new wind turbine installation method is explained. Hereafter, the problem statement and outline of this thesis are elaborated. Lastly the assumptions made during this thesis are stated.

2.1. Design study on Sitting Up System

The existing installation methods of wind turbine are becoming excessively more expensive as future offshore wind turbines increase in size. Offshore contractors are desperately looking for faster and cheaper installation methods. Therefore, Marine Innovators B.V. developed the Sitting Up System (SUS). A completely new method of installing bottom founded offshore wind turbines. By transporting a fully assembled turbine horizontally, possibly including foundation. Hereafter the aft or bottom of the SUS is submerged and is temporary fixed to the seabed. The system then upends the turbine to a vertical position by using a system which is best capable of doing so. The overall objective of this design study is to optimize the design of the SUS. This design study covers the following five installation phases;

I Positioning the wind turbine onto the SUS

II Transportation of the wind turbine

III Submersing and anchor the SUS onto the seabed

IV Upending the SUS with wind turbine to a vertical position

V Installation of the wind turbine

2.2. Objective thesis and problem statement

The objective of this thesis is the design optimization of the fourth phase; Upending the SUS with wind turbine to a vertical position. An operation of this kind has never been attempted before. Therefore, the extend of literature is limited and will this operation require extensive research before the SUS can operate. To obtain a significant knowledge, validating the principle of the upending mechanism of SUS, two problem statements are formulated. Within each problem statement sub-questions are stated to solve the problem.

1. Improve the SUS design for upending and select the optimal concept
   (a) Which mechanisms are feasible to upend a wind turbine with the SUS?
   (b) What are the static loads during a upend of each concept?
   (c) How would each concept perform operationally during the whole installation cycle?
   (d) Which concept is most efficient in upending a wind turbine?

2. Determine the dynamic behavior during upending of the selected SUS concept
   (a) What are the natural frequencies of the system throughout the upend?
   (b) What is the optimal method of upending for the SUS?
   (c) What is the maximal wave condition the concept can operate?
   (d) What dynamic loads should the seabed be able to comprehend during the upend?

2.3. Study approach

In the first phase all upending mechanisms will be assessed on their performance taken into account only mass, buoyancy and external lifting loads. Hereafter the optimal SUS concept is analyzed more in depth. This is done by generating a geometrical model of the SUS its structure with a wind turbine positioned on the SUS structure. The model is assumed rigid for simplification and is then tested on its performance in still waters. Hereafter, the structure is modeled such that it is loaded with environmental loads. From the output, responses will be generated to validate which sea states the SUS is able to operate the upending of a wind turbine. The loads from the model are then used to validate the stability of the SUS at the seabed.

2.4. Assumption and conditions

In this section the basic assumptions and conditions are presented. First the to be installed wind turbine is evaluated, where after the design parameters of SUS are presented. Finally, the environmental loads and conditions discussed.

2.4.1. Future wind turbines specifications

In this section the sizes and weights of future wind turbines and their foundation are discussed. During the history of the offshore wind turbine a lot optimization and innovation has taken place. Estimating the parameters of future turbines has proven to be quite hard as constructions rely very much on newly developed material which are lighter and stronger. Also efficiency increases with innovative optimization, therefore prospects are fairly uncertain. In the book "Innovation in wind turbine design" of P. Jamieson [12],[13] does try to develop a prospects and does estimations of weight, size and efficiency for these future turbines.

Blades

The power a turbine can deliver is correlated with its rotor radius, $P \sim R^2$. So in order to increase the rated power, bigger rotor diameter should be used which then increases its weight. To accommodate these parameters, the technology of blades and generators is research excessively, making wind harvest more efficient. This rapidly changing technology makes predictions on sizing rather difficult. At the moment blades are expected to increase weight as in figure 2.1. The torque these blades can harvest are as in figure 2.2. For wind turbines of 15 to 20 MW the rated speed will be between 6 and 12 RPM. For a RPM of 8 that would mean a such turbines should generate about 18 to 24 MNm. Reading from the graph the span diameter would reach about 230 meters, which means blades would have a mass of 60 tonne.

Nacelle and top tower

When the rated power output is increased, the capability of the generator and drive within the nacelle increase in size and weight. Similarly, the top tower will increase which is the weight of the blades, nacelle and rotor combined. Following the predictions of Jamieson [13] in figure 2.3, the nacelle weight alone would be higher than the top tower assembly, which is obviously incorrect. The predictions made by Jamieson are based on a maximum wing span of about 120 meters and are extrapolated towards higher spans. Even though these values are incorrect one can get a feeling for realistic values. In order to verify this data wind turbine fabricator Lagerwey is consulted. Their estimate would be that the top tower weight of wind turbine of 20 MW would be in the order of 1200 tonne, which is quite in line with the average of the nacelle weight and the top tower weight.

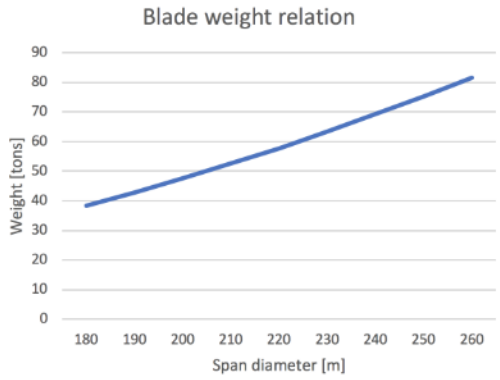

Figure 2.1: Blade weight vs span

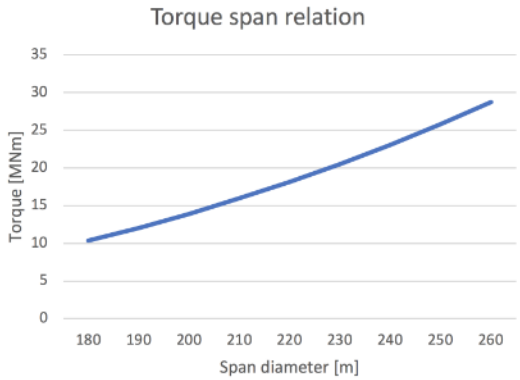

Figure 2.2: Torque vs span

Tower

Towers are basically the foot of a wind turbine. Therefore, it needs to by as light weight as possible though as stiff as dynamically optimal. As hub heights increase with bigger turbines the size of towers increase. Obviously these structures will have larger weights as more material is needed. Considering the current design of steel tubular towers the weight verses rotor diameter will be as in figure 2.3, which would mean it has a weight of about 2400 tonne. When calculating a tower of a bottom diameter of 12 meters, a top diameter of 8 meters and average thickness of 40 millimeters it would have a mass of about 2000 tonne, which is plausible.

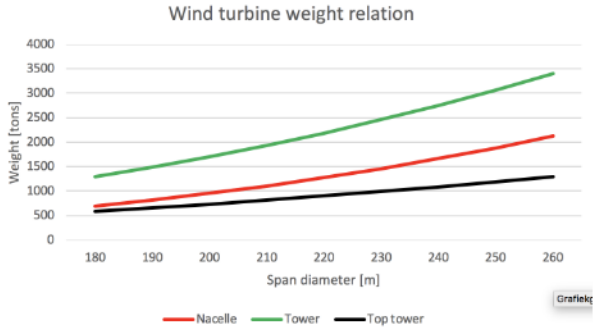

Figure 2.3: Mass tower vs rotor diameter

Foundations

The weight of foundations is depending very much on the water depth and the type installed. As for the SUS concept these would most likely be either latticed jacket structures or tripod structures. When calculating the weight of structures this size this concurs with weights between 1200 to 1800 tonne.

2.4.2. Presumed installation location

The SUS concept is designed to install wind turbines in the North Sea. Therefore, it will operate at medium water depths ranging from 30 to 60 meters. Many wind turbines are to be placed in the North Sea to reach CO2 emission reduction dedicated by the European Union. The bathymetry of the North Sea is illustrated in figure 2.4. Most of the North Sea is not deeper than 60 meters and vast areas are within the range 30 to 50 meters. These locations are all feasible for wind turbine installation using the SUS. At the moment wind farms are mostly installed near shore at depths ranging from 5 to 30 meters. The expansion of wind energy farms offshore will automatically result in deeper water installations. Figure 2.5 illustrates future wind farm development areas within the North Sea. The next 20 years more

development areas are to be opened for tendering. Making clear that there are a lot of opportunities of using the SUS to install wind turbines. The location used during this research is based on the Gemini parks. This wind farm is positioned 85 kilometers north from the dutch north coast, denoted as a black dot in figure 2.4. As the company Marine Innovators is dutch the first installations are most likely done in dutch sea waters at depths of about 40 to 50 meters. The Gemini parks are located in these kinds of conditions and therefore a good measure for this research.

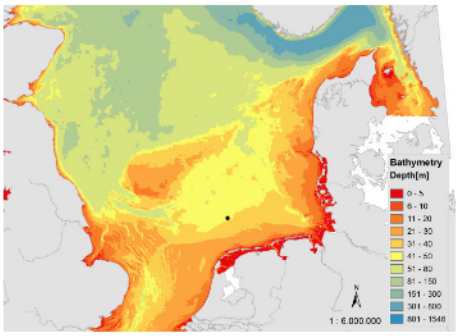

Figure 2.4: Bathymetry North Sea [2]

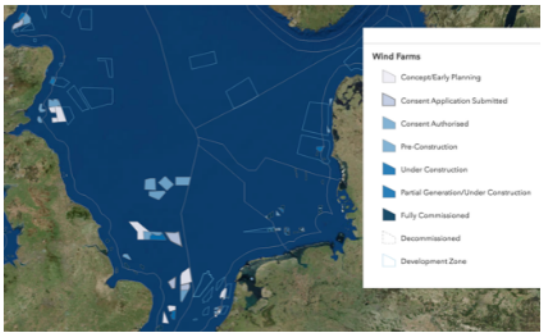

Figure 2.5: Wind farm development [1]

2.4.3. Local wave conditions

The wave condition in the North Sea can be fairly rough as it is a relatively wind area. As for the Gemini park, the wave conditions are on the mild side of the North Sea. In the Annual wave scatter diagram[4] in table 2.1 the percentage of wave appearance can be found. The peak periods are counted together with their wave height. From this it can be concluded that for waves lower than an 8 second period and 3 meter wave height the probability is 72 percent. Within these wave conditions future installation vessels be able to operate to have sufficient operational workability.

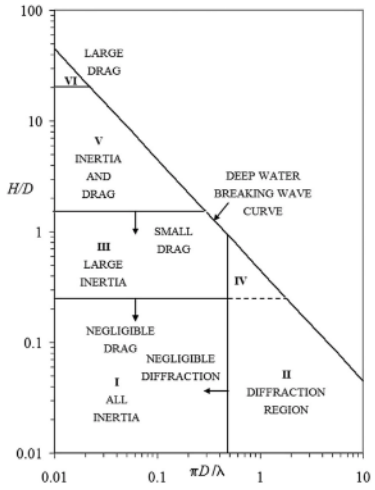

Figure 2.6: Wave load domains

2.4.4. Wave load assumptions

When calculating wave loads on a structure there are four components to take into account. These are radiation due to reflecting waves, approaching waves on the body which are not reflected, diffracting waves of the body and hydrostatic buoyancy of the body. Summed up it will result in the total load on the body as in equation 2.1.

$$\vec{F} = F_r + F_w + F_d + F_s \tag{2.1}$$

where; $\vec{F}$ = Total wave load on body
F_r = Waves radiated from the oscillating body in still water
F_w = Approaching waves on the fixed body
F_d = Diffracted waves of the fixed body
F_s = Hydrostatic buoyancy in still water

During this research the radiation of the body is neglected as well as the diffraction. For slender cylindrical bodies this approximation can be considered valid. Though for bodies with a waterline D and a wave length, , that is smaller than $2\pi D \leq \lambda$ diffraction should be accounted for. Figure 2.6 shows a graph that divides the loading domains into sections based on the wave length, wave height and structures diameter. Consulting this graph, it can be concluded that neglecting these loads could influence the validity of the model and therefore its significance should be assessed. As for radiation it would dampen larger bodies quite significant, therefore it is safe to say that neglecting radiation is conservative. The load considered during this research will be such as in equation 2.2.

$$\vec{F} = F_w + F_s \tag{2.2}$$

2.4.5. Seabed conditions

During this research the geotechnical analysis is not done extensively. The structure is considered to be fixed on the seabed and will not influence any motion. For a preliminary study the loads conducted from the structure onto the seabed are used to calculate the operation stays within the soil's capacity. The soil condition is taken to be homogeneous sandy. The unit weight is taken to be 19 $^{kN}/_{m^3}$ with a friction angle of 32°. As the design of the SUS footing is not yet developed a preliminary loading can assist the design process.

Table 2.1: Annual wave percentage diagram North Sea 0.033° 54.35N 5.3E

H, T_p	0-1	1-2	2-3	3-4	4-5	5-6	6-7	7-8	8-9	9-10	10-11	11-12	12-13	13-14	14-15	15-16	16-17	17-18	18-19	19-20
0-0.5	0	0,001	0,313	1,882	1,182	0,349	0,110	0.083	0.096	0.114	0.119	0.147	0.162	0.157	0.067	0.025	0.005	0.002	0.002	0
0.5-1	0	0	0.011	3.174	8.425	6.080	2.792	1.583	0.929	0.581	0.417	0.264	0.340	0.614	0.476	0.370	0.162	0.067	0.027	0.006
1-1.5	0	0	0	0.009	3.219	8.718	4.963	3.048	2.026	1.686	0.820	0.384	0.144	0.194	0.128	0.108	0.086	0.062	0.007	0
1.5-2	0	0	0	0	0.044	4.227	5.809	3.319	1.398	1.028	1.180	0.571	0.148	0.062	0.039	0.027	0.015	0.014	0.003	0
2-2.5	0	0	0	0	0	0.268	4.064	3.881	1.121	0.500	0.545	0.461	0.225	0.080	0.010	0.008	0	0	0.001	0
2.5-3	0	0	0	0	0	0.001	0.781	3.857	1.548	0.330	0.225	0.209	0.098	0.097	0.014	0	0	0	0	0
3-3.5	0	0	0	0	0	0	0.034	1.921	2.135	0.397	0.093	0.067	0.022	0.020	0.007	0	0	0	0	0
3.5-4	0	0	0	0	0	0	0	0,284	2.149	0.485	0.048	0.027	0.010	0.004	0	0	0	0	0	0
4-4.5	0	0	0	0	0	0	0	0.015	0.996	0.863	0.065	0.006	0.001	0.001	0	0	0	0	0	0
4.5-5	0	0	0	0	0	0	0	0	0.173	0.929	0.122	0.004	0	0	0	0	0	0	0	0
5-5.5	0	0	0	0	0	0	0	0	0.011	0.482	0.180	0.003	0	0	0	0	0	0	0	0
5.5-6	0	0	0	0	0	0	0	0	0	0.145	0.222	0.013	0	0	0	0	0	0	0	0
6-6.5	0	0	0	0	0	0	0	0	0	0.008	0.165	0.018	0	0	0	0	0	0	0	0
6.5-7	0	0	0	0	0	0	0	0	0	0	0.085	0.014	0	0	0	0	0	0	0	0
7-7.5	0	0	0	0	0	0	0	0	0	0	0.018	0.027	0.001	0	0	0	0	0	0	0
7.5-8	0	0	0	0	0	0	0	0	0	0	0.001	0.007	0	0	0	0	0	0	0	0
8-8.5	0	0	0	0	0	0	0	0	0	0	0	0.003	0.001	0	0	0	0	0	0	0
8.5-9	0	0	0	0	0	0	0	0	0	0	0	0.001	0	0	0	0	0	0	0	0
9-9.5	0	0	0	0	0	0	0	0	0	0	0	0	0	0	0	0	0	0	0	0

3

Sitting Up System concept evaluation

In this chapter the Sitting Up System is introduced, analysed and evaluated. At the moment the SUS is still in concept design phase, therefore calculations of the initial concepts are done to evaluate the different concepts. In this stage there are 3 concepts which are considered, the first two are quite different concepts and the last is a minor adjustment to the one before.

3.1. Concepts for SUS

The ideology of the Sitting Up System, or SUS, is to install wind turbines including their foundation in a single operation. The wind turbine with foundation is loaded on a frame horizontally at an onshore site. Then the SUS is towed to the installation location. Hereafter, the turbine is installed and towed back to the onshore site where the whole cycle starts over. The installation principle of a SUS relies on a simple mechanism. By rotating the horizontal frame with a turbine to a vertical position by exerting an upending moment, as display in figure 3.1. The hinge is connected to a submersible frame or barge which is anchored to the seabed. This enables the frame to turn around a fixed axis. Now a force, of any kind, is exerted to generate an upending moment lifting the frame and thus the wind turbine to a vertical position.

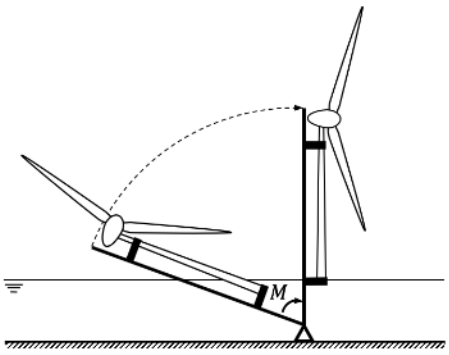

Figure 3.1: SUS concept principle

The mechanisms used to generate the upending force can be done by several methods. For this thesis four concepts are being addressed, shown in the figures 3.2 to 3.5. These concepts are a result of an optimisation process during the basic design phase. The first concept, SUS 1: 'Hydraulic upend', upends the wind turbine with hydraulic cylinders. By pushing the cylinders towards the edge of the frame, it forces the frame to move upward to a vertical position. The second concept, SUS 2: 'Buoyant upend', makes use of a buoyant module, which is pulled along the frame by wire ropes operated by a winch. While the buoyant module is pulled down its submersing and will generate additional buoyancy. By creating

enough buoyancy, a force perpendicular to the frame is generated, realizing a moment capable of upending the structure. The third concept, SUS 3: 'Buoyant upend 2', is quite similar as the second concept, except in this case the buoyancy module is not pulled downwards. Namely, via an addition construction above the hinge the buoyancy module is pulled along the waterline. Therefore, the buoyant module is not pulled down against its buoyancy and is pulled along the path which it would move at the second concept as well. The fourth concept, SUS 4: 'Stiffening system', is an addition to SUS 2 and SUS 3. As the frame is loaded quite heavily at the top by the nacelle and turbine blades, the frame will have to be significantly stiffened. This will result in additional weight and therefore additional stiffness. To mitigate on this problem an additional winch can be installed to prevent the frame from deflecting or even generate additional moment for upending. This concept is not further discussed as structural integrity of the SUS in not yet assessed.

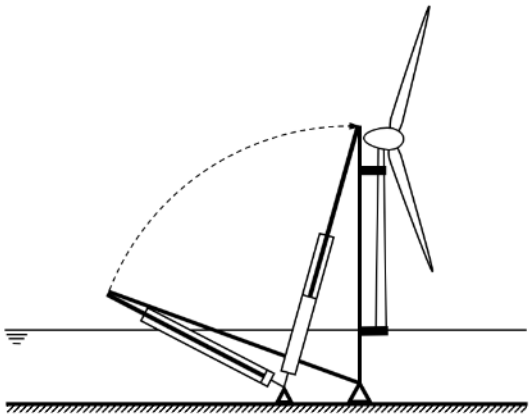

Figure 3.2: SUS 1: 'Hydraulic upend'

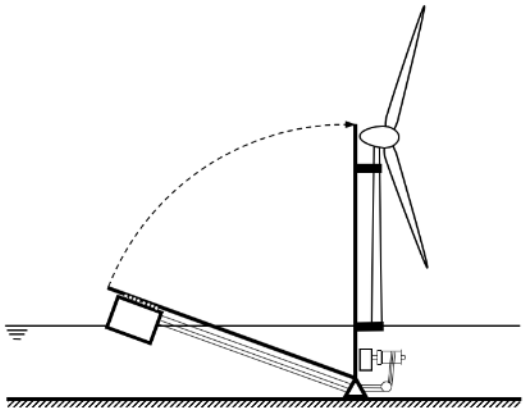

Figure 3.3: SUS 2: 'Buoyant upend 1'

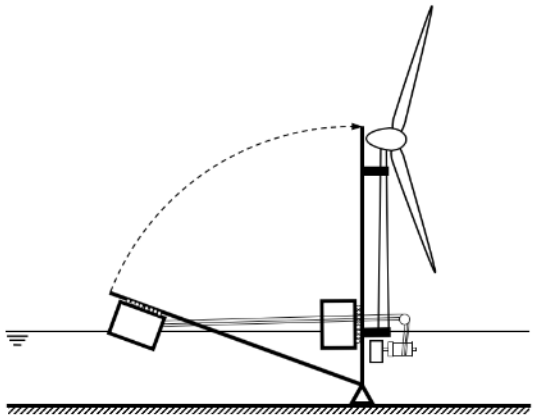

Figure 3.4: SUS 3: 'Buoyant upend 2'

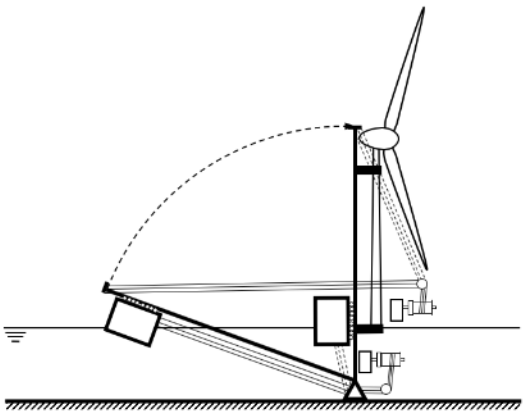

Figure 3.5: SUS 4: 'Stiffening system'

3.2. SUS 1: 'Hydraulic upend'

The original idea of the SUS is based on a hydraulic system as illustrated in figure 3.2. The design of SUS 1 is illustrated in figures 3.6 and 3.7. It consist of a surrounding framework to hold all other sub systems, the turquoise frame. This framework is submersible and is hold in place by a large barge, in red. Figure 3.7 illustrates the submerged turquoise framework, which is lowered via a winch system on the red barges. The submerged framework then functions as stability at the seabed during upending and installation. At the corners it has systems to anchor and level the frame at the seabed while submersed.
Furthermore, there are two frames for the lifting mechanism, namely one holding the wind

turbine into place and another to accommodate the hydraulic system and pushes the first frame to a vertical position. At the bottom of the hydraulic frame there is a buoyancy module installed to generate an additional upending moment. Another important system is the hinge facilitating the rotation of the wind turbine. The wind turbine is hold in place by clamps and a lowering mechanism is incorporated with the clamp at the at the foundation. Finally, the nacelle is protected by a buoyancy module which should clear the asset sufficiently from the waterline.

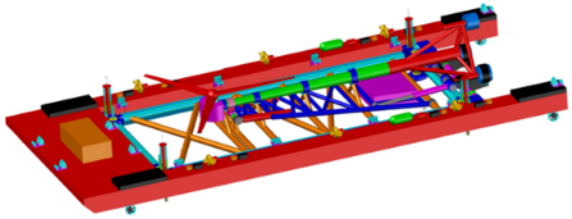

Figure 3.6: Installation barge SUS 1

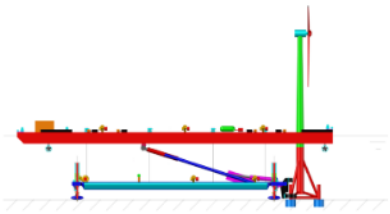

Figure 3.7: SUS 1 during operation

The dimensions of SUS 1 depend on the to be installed wind turbines. In figures 3.8 and 3.9 the main dimension are given. While operating the SUS 1 fully surrounds a wind turbine and is submerged to the seabed. The illustration shows the parameters can vary depending on the desired value. The values used for this thesis are mostly the maximum value of each parameter. Also, as the design is not fully developed yet, the parameters are kept as configurable as possible to be able to adjust and test the system on the parameters.

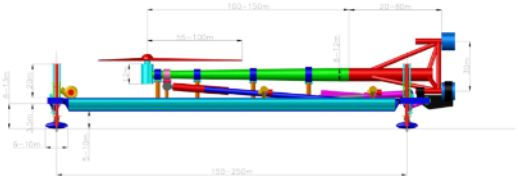

Figure 3.8: SUS 1 side view

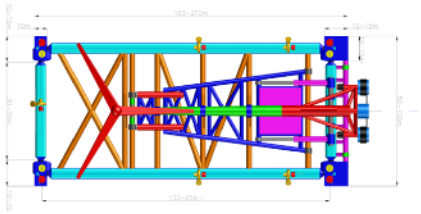

Figure 3.9: SUS 1 top view

To test the feasibility of SUS 1 an operation calculation is done. The loads in the hydraulic cylinders are calculated during the upend and the weights of the whole structure with a wind turbine attached. For the following calculations the structure is presumed to be a rigid body. Table 3.1 shows the design variables used for the calculation.

Table 3.1: Design parameters SUS 1

Design main parameters	[m]
Length surrounding framework	250
Width surrounding framework	70
Length wind turbine with foundation	226
Radius turbine blades	115
Width foundation	60
Nacelle clearance to waterline	15
Length upend frame	203

In figure 3.10 the reactions loads of the frame are displayed. At the left all forces due to gravity, buoyancy and hydraulics are given. Hereafter, the middle figure shows the corresponding hydraulic reaction forces and moments around the two frames. The illustration on the right shows the dimensions of where the forces are applied and the angles of the two bodies. The buoyancy loads and lengths change accordingly depending on their submerged state.

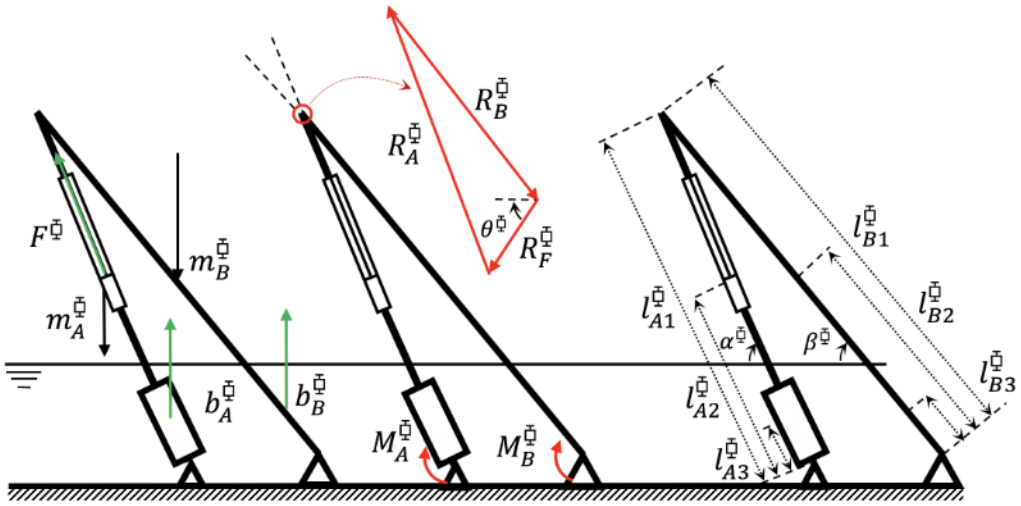

Figure 3.10: SUS 1 General loads

From the mass and buoyancy of the structure the moments around both hinges can be calculated as in equation 3.1. Both the mass and buoyancy of these rigid beams are calculated using combined weights and underwater volumes of the structure, together with the wind turbine. The rigid beam, which needs to push with hydraulics, $A^{\square}$, is referred as the upending arm. Whereas the other, $B^{\square}$, which carries the wind turbine is referred as the carrying arm.

$$\begin{aligned} M_A^{\square} &= \cos\alpha^{\square}(l_{A3}^{\square} b_A^{\square} - l_{A2}^{\square} m_A^{\square})g \\ M_B^{\square} &= \cos\beta^{\square}(l_{B3}^{\square} b_B^{\square} - l_{B2}^{\square} m_B^{\square})g \end{aligned} \tag{3.1}$$

During lifting these moments, $M_A^{\square}$ and $M_B^{\square}$, will have a combined moment which is negative. To compensate for this moment, the hydraulic cylinders can exert a internal axial force which results in an equilibrium of $R_F^{\square}$, $R_A^{\square}$ and $R_B^{\square}$. The reaction force magnitude and angle of $R_F^{\square}$ can be calculated with equations 3.2.

$$\begin{aligned} R_F^{\square} &= \sqrt{\left(\frac{M_A^{\square}}{l_{A1}^{\square}}\sin\alpha^{\square} + \frac{M_B^{\square}}{l_{B1}^{\square}}\sin\beta^{\square}\right)^2 + \left(\frac{M_A^{\square}}{l_{A1}^{\square}}\cos\alpha^{\square} + \frac{M_B^{\square}}{l_{B1}^{\square}}\cos\beta^{\square}\right)^2} \\ \theta^{\square} &= \frac{\frac{M_A^{\square}}{l_{A1}^{\square}}\cos\alpha^{\square} + \frac{M_B^{\square}}{l_{B1}^{\square}}\cos\beta^{\square}}{\frac{M_A^{\square}}{l_{A1}^{\square}}\sin\alpha^{\square} + \frac{M_B^{\square}}{l_{B1}^{\square}}\sin\beta^{\square}} \end{aligned} \tag{3.2}$$

Knowing the angles of the upending arm and carrying arm, the resulting axial reaction forces can be calculated using the law of sines. As figure 3.10 suggests, the upending arm will experience a compression force and the carrying arm a tension force.

$$\frac{R_F^{\square}}{sin(\alpha^{\square} - \beta^{\square})} = \frac{R_A^{\square}}{sin(\theta^{\square} + \beta^{\square})} = \frac{R_B^{\square}}{sin(\pi - \theta^{\square} - \alpha^{\square})} \tag{3.3}$$

As these reaction forces are considered as an static equilibrium the following statement, equation 3.4, can be made. Which concludes that the hydraulic force $F^{\square}$ needs to overcome the internal axial static force plus a load to upend the wind turbine.

$$F^{\square} > R_A^{\square} \tag{3.4}$$

Figure 3.11 displays the axial load of the hydraulic cylinders, $R_A^{\square}$, at static equilibrium for all operational angles. The axial load that these hydraulic cylinders should be able to push

is about 188 MN considering some additional dynamic loads. Cylinders use in these kind of operations can handle about $350MPa$, and taken that such a cylinder has a diameter of about $1.2m$ this will mean that the system will need 6 of these cylinders. Equation 3.5 shows corresponding calculation.

$$n_{cylinders} = \frac{R_A^{\bar{\square}}}{p_{max}^{\bar{\square}} \frac{\pi D_{cylinder}^{\bar{\square}}}{4}} \tag{3.5}$$

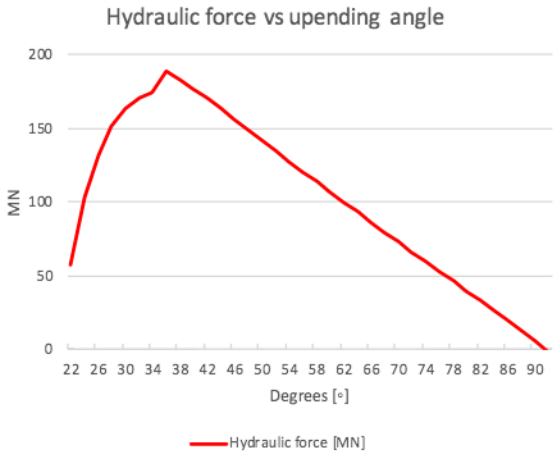

Figure 3.11: SUS 1 Static axial load in upending arm for upending angles

3.3. SUS 2: 'Buoyant upend 1'

Due to the high loads in the hydraulic upend system and bending moments at the cylinders a new concept is developed. As the whole structure is submerged a logical step is to make use of immersed bodies. A buoyant force generating the upending moment was already incorporated into the SUS 1. Although a more efficient way to use this buoyancy is to increase the arm of this buoyant upending force. This resulted in the SUS concept to evolve in SUS 2: 'Buoyant upend'. To prove whether this new concept is more fit than SUS 1, it is tested similarly. In this case there is no addition upending arm, which makes the problem less complex and therefore a more elementary system. Figure 3.12 illustrates the design of the buoyant upending system.

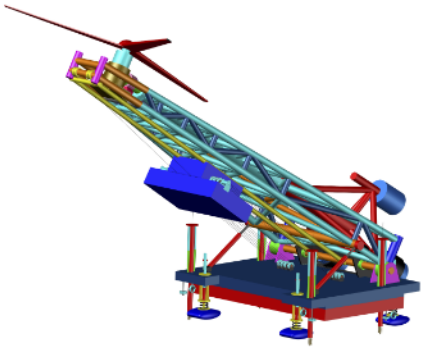

Figure 3.12: SUS 2 Design

The design parameters of SUS 2 are somewhat different from SUS 1. Table 3.2 presents the values of these parameters.

Table 3.2: Design parameters SUS 2

Design main parameters	[m]
Length latticed framework	205
Width latticed framework	65
Main barge length	70
Main barge width	70
Main barge height	10
Buoyancy module length	38
Buoyancy module width	38
Buoyancy module height	12

Different from SUS 1, SUS 2 has no need for a surrounding framework, instead it has just a upending frame carrying the wind turbine, a submersible barge with a hinge system and a buoyancy module at the end of the structure. During the upend operation this buoyancy module is pulled down perpendicular to the length of the frame to create an upending moment. Figure 3.13 illustrates the SUS 2 concept basic drawing.

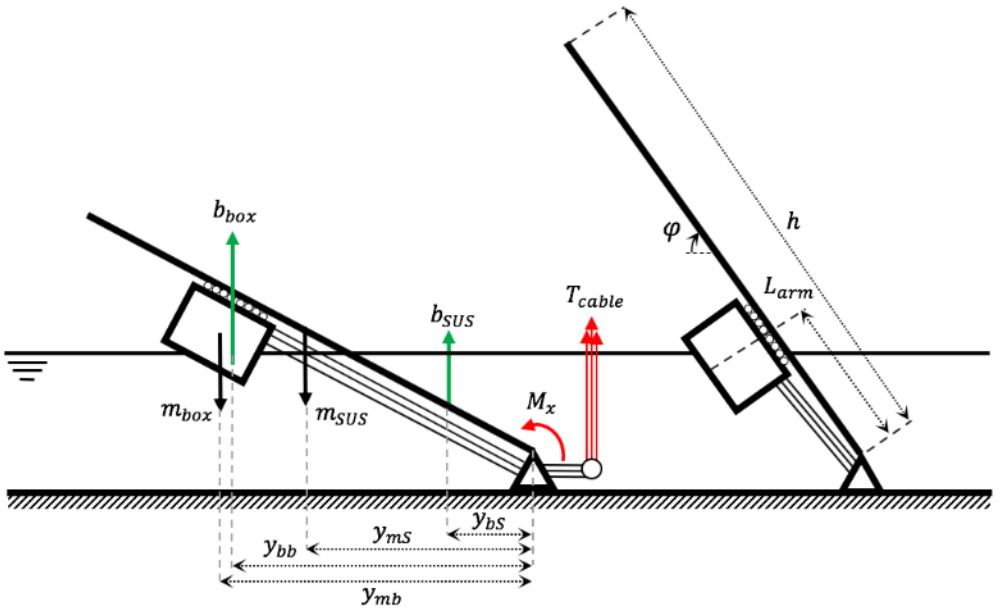

Figure 3.13: SUS 2 General loads

The moment around the hinge, M_x, should be zero to acquire an equilibrium, which results in equation 3.6. Compared to SUS 1, the arm of each mass or buoyancy is expressed in the projected length to the hinge axis, as the mass and buoyancy of the module do not align the axial of rigid frame.

$$\begin{aligned} \sum M_x &= 0 \\ &= m_{SUS} \cdot y_{mS} + m_{box} \cdot y_{mb} - b_{SUS} \cdot y_{bS} - b_{box} \cdot y_{bb} \end{aligned} \tag{3.6}$$

where; m_{SUS} = total mass of the SUS frame, foundation, tower and nacelle
b_{SUS} = buoyancy generate by the SUS frame, foundation and tower
m_{box} = mass of the buoyancy box
b_{box} = distance in y from the CoB of b_{box} till the hinge
y_{mS} = distance in y from the CoG of m_{SUS} till the hinge
y_{mb} = distance in y from the CoG of m_{box} till the hinge
y_{bS} = buoyancy of the SUS frame
y_{bb} = buoyancy of the SUS frame

For the equilibrium at the lattices frame, the buoyancy module is considered to exert a force on the frame at the connection between the two systems, therefore $y_{mb} = y_{bb} = L_{arm} \cos \varphi$. The buoyancy module itself has another equilibrium shown in figure 3.14. The buoyancy module is free to move over the length of the rigid beam and therefore the forces are decomposed into an orthogonal and a parallel force to the latticed frame depending on φ. The parallel force of the buoyancy module is then cancelled by the tension force of the cable to keep the module in position.

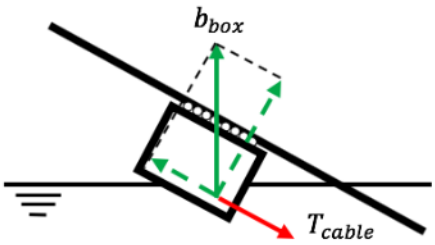

Figure 3.14: SUS 2 Buoyancy module loads

In figure 3.15 the results of the buoyancy loads are presented. The maximal buoyancy the module can exert is shown with the red line and is about 174 MN. The buoyancy that is needed for the upend is displayed with the green line. The black lines show the tension that the cable should have to keep the buoyancy module in position. At first the tension is smaller than the buoyancy as the module is mostly pulled in horizontal direction. After about 70 degrees the tension and buoyancy are almost equal as the cable needs to pull the buoyancy module downward against its buoyancy. The maximal buoyancy needed is roughly 162 MN and the maximal tension about 145 MN.

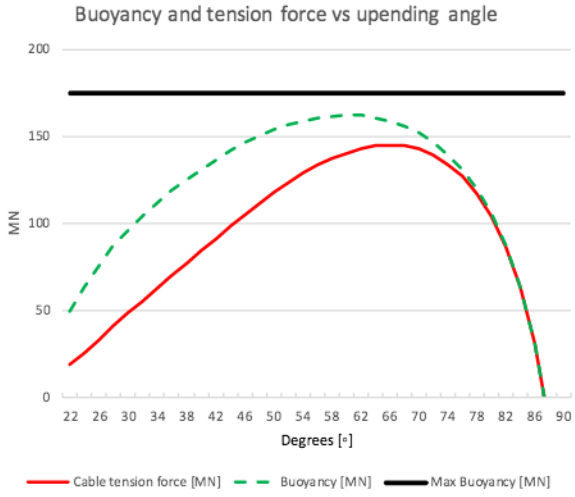

Figure 3.15: SUS 2 Buoyancy and tension force

3.4. SUS 3: 'Buoyant upend 2'

During a concept phase it is usual to access more than one scenario. In figure 3.16 the SUS 3 concept is illustrated. The additional framework holding the winches is not yet optimally designed as the loads are not yet known. The design is similar as SUS 2 the design, therefore the parameters quite similar such as in table 3.2.

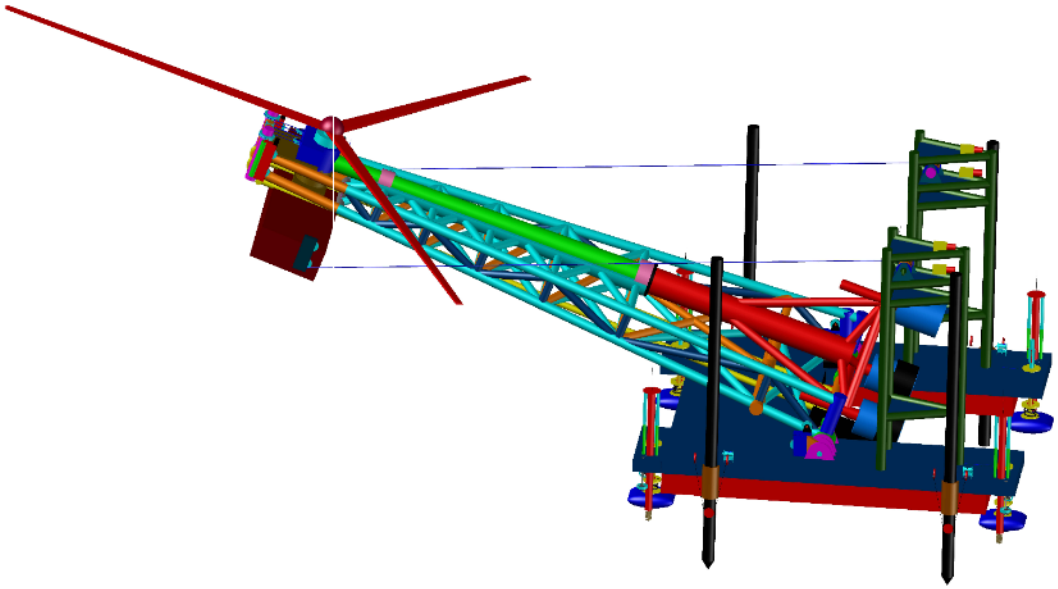

Figure 3.16: SUS 3 Design

SUS 3 is another considered concept to keep the buoyancy module positioned. Here, instead of pulling the buoyancy along the latticed frame, it is pulled along the waterline as illustrated in figure 3.17. Doing so, the buoyancy module does not have any tension force losses due pulling against the buoyancy along the lattice. Also, as the path of the buoyancy module in SUS 2 is moving over the waterline, it is a logical step to investigate the possibilities of SUS 3. As the design is similar as SUS 2 the design parameters are such as in table 3.2.

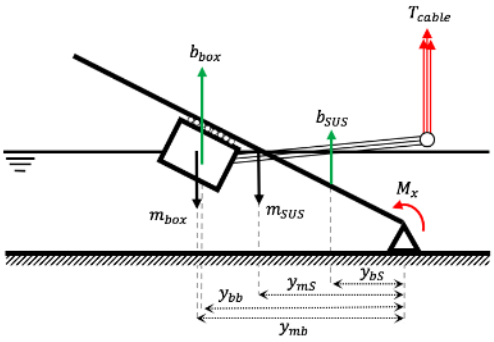

Figure 3.17: SUS 3 General loads

The tension which the cable exerts on the buoyancy module can be decoupled as in figure 3.18. The tension should minimally counter the decoupled buoyancy force along the SUS lattice, the additional perpendicular force onto the lattice frame will now exert an addition upending moment around the hinge. Therefore, the tension in the cable must be satisfied as in equation 3.7.

$$\sum F_{\perp} = T_{cable}\cos(\varphi) - \sin\varphi \cdot b_{box} \tag{3.7}$$

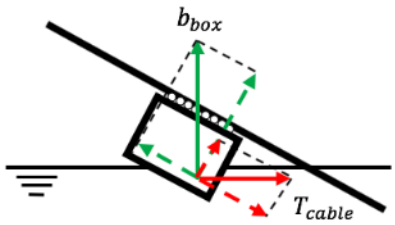

Figure 3.18: SUS 3 Buoyancy module loads

The loads within SUS 3 are presented in figure 3.19. Here the red line is the maximal buoyancy experienced by the module, which is about 97 MN. The maximal tension force in the cable is about 90 MN. It is clear that the curves of the loads in SUS 2 are quite different from the curves seen there. At first the buoyancy module is quite dominant as in the load curves of SUS 2. Except after about 45 degrees the tension force is getting more dominant than the buoyancy force. When decoupling the loads as in figure 3.18, the transferred perpendicular load to the latticed frame, $T_{cable}\sin(\varphi)$, has a larger value. This load is the additional upending moment due to pulling the buoyancy module horizontally against the lattice.

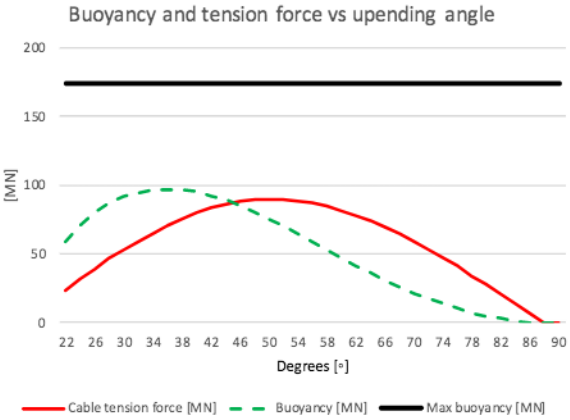

Figure 3.19: SUS 3 Buoyancy and tension force

3.5. Concept choice

All concepts have their advantages and weaknesses. To choose the best concept, multiple criteria should be considered before doing a detailed examination of the most optimal concept. At first the whole installation cycle is evaluated. There are four stages within the installation of wind turbines using the concept. Each concept is examined on transportation, submersing, upending and wind turbine lowering.

SUS 1: 'Hydraulic upend'

The SUS 1 concept will need quite a large vessel to transport the whole system, it cannot manoeuvre on its own. This is a negative point, although the upside would be that its stability can be guaranteed due its large water plane area. The lowering of the concept is done by deballasting the frame by pumping out water. This should be guided by the transportation vessel. As drift forces would be quite significant for such a large vessel lots of thrusters or tugs are needed. Upending the wind turbine using a hydraulic cylinder would be rather controlled, though the practical implementation is questionable as bending loads do not work well with hydraulic cylinders. The water depth it can operate strongly depends on the water depth limit of hydraulic cylinders and is therefore likely unfit for larger depths as controls

need significantly better pressure protection. The handling of the operating system is done from a separate vessel as the structure is fully submerged. Although dry control systems can be realised, this could lead to additional complications as control systems should be coupled to the SUS. Lowering the wind turbine will require an additional lifting mechanism which is still undetermined. This would most likely be a crane type winch system.

SUS 2: 'Buoyant upend 1'
The SUS 2 concept is a vessel itself and needs no additional transportation construction. It could either have its own propulsion or could use towing vessels to manoeuvre it to its destination. The stability of the whole structure is depending very much on the motions between the two floating body and could give some complication structurally as these bodies are quite far from each other. Also, the width of SUS 2 is smaller than SUS 1 and could be subjected to roll heavily, for that the SUS 2 will need design improvements. During lowering of the vessel, tanks are deballasted and is guided by either spuds or a jack up/down system. Using these guides the SUS system is lower and finally anchored to the seabed. The controls are preferably done from a separate vessel although a control station could be place on the jacking system which stay above the water line. The upending is done by a hoisting winch pulling the buoyancy module down. This buoyancy module will be influenced by wave loads which is unfavourable. The upending is dynamically more complicated than SUS 1, only requires less energy as buoyancy is used to create an upending force. Pulling the buoyancy along the SUS lattice works quite efficient in the first stage of the upend, however further on the effect of the buoyancy force upending the SUS lattice decreases. To able the upend the buoyancy module needs to be pull down excessively to generate little upending moment. When the wind turbine is upended the same hoisting system can be used to lower the turbine. By using the buoyancy module as a counter weight the winches are relieved from most loads.

SUS 3: 'Buoyant upend 1'
Finally, the SUS 3 concept is an altered version to the SUS 2 concept and has similar strengths and weaknesses. The main difference lies at the upending. Namely, the buoyancy module is pulled along the water line instead of toward the hinge. Therefore, it needs less buoyancy and thus energy than SUS 2 at which quite some energy is lost on pulling the buoyancy module down. As the cables operate in a free space, they might need an addition guiding system. As for the SUS 2, the cables could be well controlled as its path goes along the SUS lattice. The downside of this is that the cable does need to be handled submerged, which is unfavourable for SUS 2 compared to SUS 3.

Load evaluation
Another comparison between the different concepts is the experienced static load trough out the upending cycle. In table 3.3 all load of the considered concepts are presented.

Table 3.3: Preliminary SUS concept load evaluation

Parameter	SUS 1	SUS 2	SUS 3	Units
Weight system	6622	6064	6064	tonne
Maximal buoyancy	151	162	97	MN
Maximal load	188	145	90	MN

Concept evaluation
Considering the operational facets of the SUS concepts the hydraulic system would be the costliest and therefore a high CAPEX. And considering the additional transportation vessels dynamic positioning the OPEX would also be quite high. Also, the hydraulic cylinder handling would requires optimisation structurally as both axial and bending loads are very high. When concepts need many compensating systems to make it work, it is normally not a good concept. Taken all this into account, the SUS 1 concept is not favourable.

The last two concepts are quite similar, though one is chosen for further work. Both concepts would have similar CAPEX and OPEX as they do not differ as much. As the loads and buoyancy of the SUS 3 compared to the SUS 3 are significantly lower the obvious choice would be SUS 3. Though handling cables this way would require some additional attention. Apart for the efficiency, cost of energy consumption and equipment would also dramatically decrease when less loads are needed. Taken into account all strengths and weaknesses a multi criteria analysis can give insight. In table 3.4 the concepts are all graded for each criteria.

Table 3.4: Multi Criteria Analysis SUS concepts

Criteria	SUS 1	SUS 2	SUS 3
Transportation	9	7	7
Submersing	7	8	8
Upending	5	7	9
Lowering turbine	5	7	7
Loads	4	7	9
CAPEX	5	8	8
OPEX	4	7	8
Total average	5.57	7.29	8

The first concept scores the lowest and for the SUS 2 and SUS 3 are not really far apart. As the horizontal pulling of SUS 3 will have lower loads and therefore will be more efficient in energy usage the SUS 3 is the most optimal concept within these three concepts. Therefore, the SUS 3: 'Buoyant upend 2' will be further analysed from here.

4

Dynamic model of SUS 3

In this chapter the design of all subsystems is explained and elaborated on how these systems are modelled. The model is divided into four substructures; the upending latticed framework, the buoyancy module, the wind turbine and the base which will be sunk to the seabed. The first two will be modelled to experience hydrodynamic loads and the base will pass on the load though the hinge to the seabed. The first three substructures are divided into smaller sections depending on their geometry to calculated gravitational, buoyant and environmental load.

4.1. Model philosophy

As the concept is different than any other installation method known within offshore installation there is need for a sophisticated model which incorporates the motion and the relevant environmental loads. The configuration of the model can be change rather easy, as all geometric values can be set as well as the environmental parameters. The model should be able to capture the motion of the SUS from the moment it is anchored to the seabed till it has reached a vertical position. During this motion the tension force of the cable and the environmental loads are the only loads resulting in upending the frame.

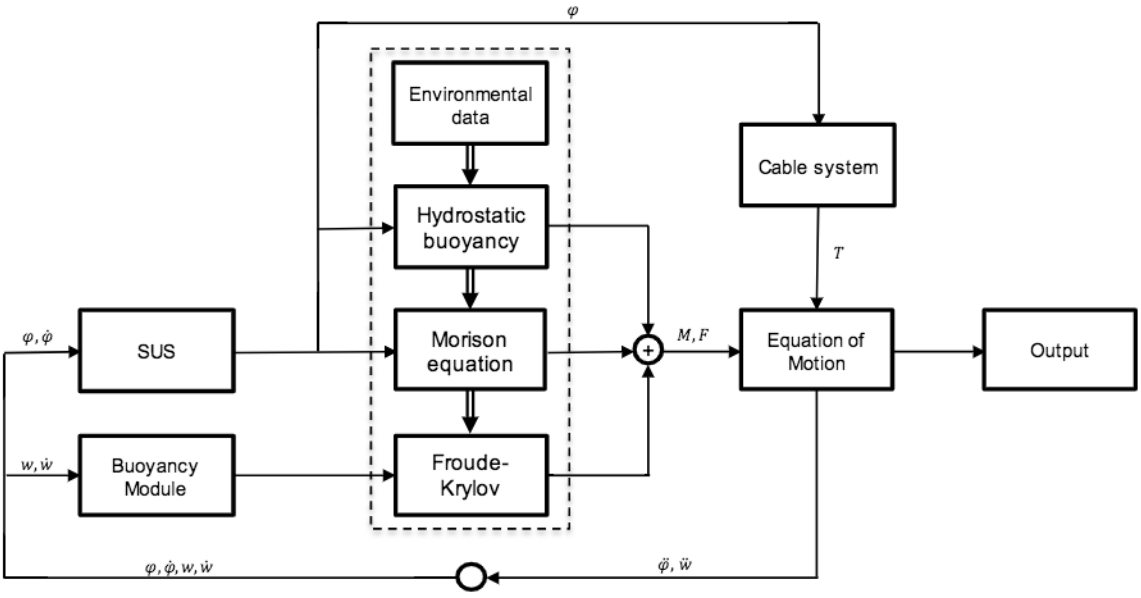

Figure 4.1: SUS model scheme

As a start the model has to create geometric data of the subsystems, which is explained in the next section. For each time step the location, the corresponding buoyancy and environmental load of the subsystems is calculated. These loads are then put into an equation of motion which then calculates the movement numerically. The model operates in time domain and is translated to frequency domain for further analysis. Figure 4.1 illustrates the model in blocks. At first the model will incorporate 1 Degree Of Freedom (DOF). The angle of the SUS lattice φ and a fixed buoyancy module. Doing so the dynamic behaviour of the SUS at varying positions of the buoyancy module can be analysed. The next step is to upend the SUS by moving the buoyancy module along the SUS latticed framework. To verify and optimise the model and SUS the behaviour is tested on various tension force input characteristics. Using the characteristics of the fixed buoyancy module and the dynamic movement a optimal tension force can be found.

4.2. Geometry

The sizing of the SUS depends on the wind turbines it will install. As these increases to over 150 meters hub height in the near future, the size of these turbines is taken to be 200 meter including foundation. The foundation is model as a longer turbine tower. Thus, accounting for 150 meters hub height and 50 meters water depth. For these kinds of turbines the latticed framework of the SUS will then reach about 215 meters. During this research this length is kept constant, however as the SUS is still in concept-phase this and other parameters are modelled such that they can easily be adjusted or tuned.

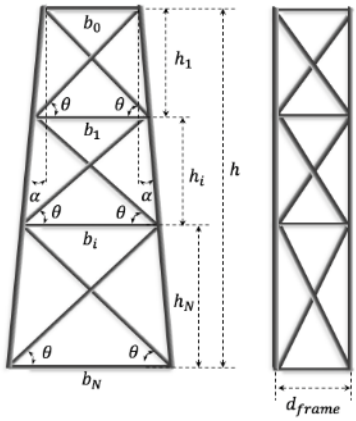

Figure 4.2: SUS latticed framework parameters

4.2.1. SUS lattice

The framework of the SUS is taken similar as latticed jacket like structures, the design is not fully optimized as structural loads are not yet known. The geometric calculation for these structures are well known within offshore technology. The structure is divided into bays, which are geometrically equal, as in figure 4.2. Because the structure is geometrically equal, the parameter m can be calculated, which defines the equality. Therefore, each bay i has the same dimension, as in equation 4.1.

$$dim_{i+1} = m \cdot dim_i \tag{4.1}$$

Hereafter, the geometric parameter m can be found from the outer dimensions of the frame with equation 4.2. With m known, the bay heights van be calculated with the equation 4.3.

$$m = \left(\frac{b_n}{b_0}\right)^{\frac{1}{N}} \tag{4.2}$$

where; m = geometric parameter [-]
b_n = bottom horizontal $[m]$
b_0 = top horizontal $[m]$
N = number of sections within the frame [-]
i = $1 \cdots N$

With m known, the bay heights van be calculated with the equation 4.3.

$$\left.\begin{aligned} h &= \sum_{i=1}^{N} h_i = h_1 + m \cdot h_1 + \ldots + m^{N-1} \cdot h_1 \\ &= h_1 \sum_{i-1}^{N} m^{i-1} = \frac{m^N - 1}{m - 1} \end{aligned}\right\} \rightarrow h_1 = h\frac{m-1}{m^N - 1} \tag{4.3}$$

where; h = height of the structure $[m]$
h_i = section height $[m]$

The brace angles, θ, are calculated with equation 4.4. As the α is the same for both sides the brace angles are similar for each side.

$$\tan\theta = \frac{h_i}{b_i - h_i \cdot \tan\alpha_1} \tag{4.4}$$

where; θ = brace angle $[^o]$
α = bay angle $[^o]$

For the depth of the frame, d_{frame}, there will be no addition batter angle. So from the side the structure will look as in figure 4.2. Now the basic parameters of the structure modelled, the positions of the joints of each beam is determined. The joints represent the nodes of the structure and between these nodes, the relevant beams are modelled into multiple beam sections. The lattice can be modelled either fully x-braced or k-braced. To be conservative in the weight, strength and environmental loads the lattice is x-braced during this research. The internal strength of the structure is calculated when the mechanics of SUS concept is optimized.

Knowing the basic parameters, the geometric model can be built by first finding all nodes. Where after, these nodes are coupled to representing beams. For the SUS frame, the beams are then divided into cylindrical segments, similar as strip theory. For each strip the mass and buoyancy are calculated with equations 4.5 and 4.6.

$$m_i = \rho_s \pi \frac{D^2 - (D-2t)^2}{4} \delta l_i \tag{4.5}$$

$$b_i = \rho_w \pi \frac{D^2}{4} \delta l_i \tag{4.6}$$

First the model calculates the area and length of each segment, hereafter the mass based on the material density of steel. To assess the buoyancy, the centre of the segment is tested for its submerged state. The locations of these segments are used to calculate the effective force and moment at the centre of rotation at the seabed with equations 4.7 and 4.8.

$$F_{SUS} = \begin{bmatrix} F_x \\ F_y \\ F_z \end{bmatrix} = \sum_{i=1}^{N} \begin{bmatrix} 0 \\ 0 \\ (m_i - b_i)g \end{bmatrix} \tag{4.7}$$

$$M_{SUS} = \begin{bmatrix} M_x \\ M_y \\ M_z \end{bmatrix} = \sum_{i=1}^{N} \begin{bmatrix} x \\ -r_i cos\varphi_i \\ r_i sin\varphi_i \end{bmatrix} \times \begin{bmatrix} 0 \\ 0 \\ (m_i - b_i)g \end{bmatrix} \tag{4.8}$$

where; m_i = Mass of segment $[kg]$
b_i = Buoyancy of segment $[kg]$
φ_i = Local inclined angle $[rad]$
r_i = Local radius to hinge $[m]$
δl_i = Length segment $[m]$
ρ_s = Density of steel $[^{kg}/_{m^3}]$
ρ_w = Density of water $[^{kg}/_{m^3}]$
D = Diameter of segment $[m]$
t = Thickness segment $[m]$
g = Gravitational constant $[^{m}/_{s^2}]$

Note that a design flaw is that during the calculation of the buoyancy of the SUS frame only the centre of the segment is considered to access its submerged state. Therefore, the model either overestimates or underestimates the buoyancy. Taking small enough segments would result in the model to have minor influence although it should be large enough to compromise on simulation time.

4.2.2. Buoyancy module

The buoyancy module will be modelled as a rectangular barge for simplicity. When there are no waves involved the buoyancy module can be modelled as rectangle. However, when waves are included the surface elevation will vary over the water plane area of the buoyancy module. Therefore, the module is divided in segments, similar as the arm frame. In this case the segments are divided into cubic section, as shown in figure 4.3.

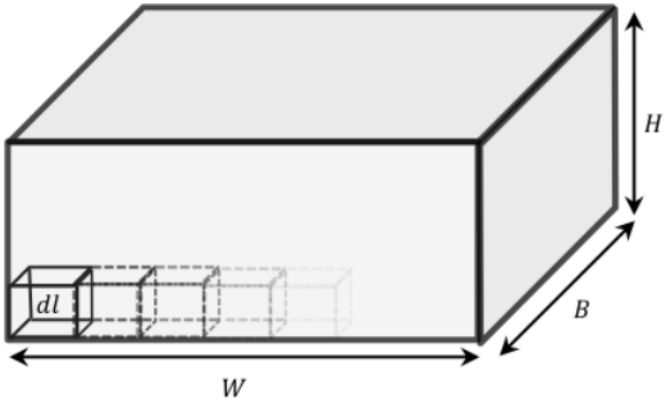

Figure 4.3: Buoyancy module segments

For each segment it is determined whether it has an edge or multiple edges in contact with water or air. These edges represent the mass of each segment and are calculated with equation 4.9. As the wall thickness is universal for each segment, the CoG of the buoyancy module is located in the middle of the rectangle. To find the buoyancy of the module, each segment is tested on its submerged state. hereafter, the buoyancy is calculated using equation 4.10.

$$m_i = n_i \rho_s \delta l^2 t \tag{4.9}$$

$$b_i = \rho_w A_{wl} \delta l \tag{4.10}$$

where; A_{wl} = Surface area
n_i = Number of panels

For most segments the buoyancy is maximal when submerged, however at the waterline these segments can be partly submerged. To evaluate this, it requires the inclined angle of

the latticed framework, φ, and more importantly the draft, T. The equivalent draft of the segment is found by calculating the difference between the most submerged point of the segment and the water surface. To already account for the surface elevation of the waves, for later simulations, the surface elevation is added as additional draft, resulting equations 4.11.

$$\begin{aligned} z_{bottom} &= z_{centre} - \frac{L}{2}\sin\varphi - \frac{H}{2}\cos\varphi \\ T &= z_{bottom} + \eta \end{aligned} \tag{4.11}$$

Figure 4.4 shows the six possible submerged states. The first two states are either totally submerged or above the water surface. The states are distinguished as in equation 4.12. In the third state the submerged area consists of only a triangle, whereas in the next two states should be accounted for an additional parallelogram. In the last state the area above the surface is subtracted from the maximum buoyancy. For each state the equivalent area and CoB are determined to eventually calculate the upending moment. The formulas for the CoB and volume of each state are found in appendix A.

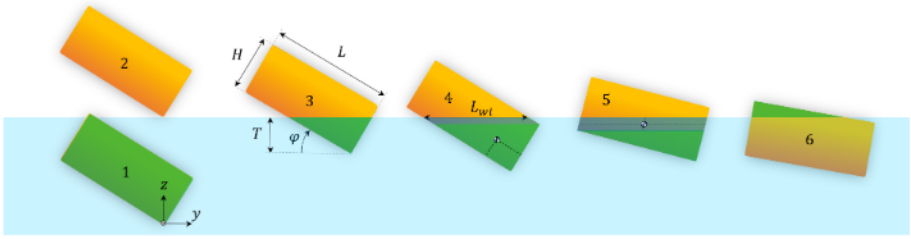

Figure 4.4: Submerged states of the buoyancy box

1. $T \geq T_{max}$
2. $T < 0$
3. $T \leq L\sin\varphi \;\;\&\;\; T \leq H\cos\varphi$
4. $T \leq L\sin\varphi \;\;\&\;\; T > H\cos\varphi$
5. $T > L\sin\varphi \;\;\&\;\; T \leq H\cos\varphi$
6. $T > L\sin\varphi \;\;\&\;\; T > H\cos\varphi$

(4.12)

Another reason for using smaller segments for the model is the hydrodynamic loads. As these loads also vary over the whole box. For each edge it will experience different loads due current and waves and are calculated accordingly. The segments positioned at the surface have the same dilemma as the buoyancy as these are only partly submerged. Therefore, the equivalent area will also be used to evaluate these loads at the free surface.
While the buoyancy and weight are known the force and moment at the connection between the SUS lattice, which is defined with equation 4.15, and the buoyancy module can be calculated with equations 4.13 and 4.14.

$$F_{box} = \begin{bmatrix} F_x \\ F_y \\ F_z \end{bmatrix} = \sum_{i=1}^{N} \begin{bmatrix} 0 \\ 0 \\ (m_i - b_i)g \end{bmatrix} \tag{4.13}$$

$$M_{box} = \begin{bmatrix} M_x \\ M_y \\ M_z \end{bmatrix} = \sum_{i=1}^{N} \begin{bmatrix} x_{box} \\ y_{box} \\ z_{box} \end{bmatrix} \times \begin{bmatrix} 0 \\ 0 \\ (m_i - b_i)g \end{bmatrix} \tag{4.14}$$

$$\begin{bmatrix} x_{box} \\ y_{box} \\ z_{box} \end{bmatrix} = \begin{bmatrix} x_i \\ y_i + r\cos\varphi + d_o\sin\varphi \\ z_i + r\sin\varphi - d_o\cos\varphi \end{bmatrix} \tag{4.15}$$

4.2.3. Wind turbine

For the wind turbine, only its mass is of interest. As the hydrodynamic loads are neglected. The mass of the nacelle and its wing blades is taken as a point load to simplify the calculation. The tower on the other hand is varying over the SUS frame, therefore it is calculated using segments. These segments are divided over length and radius. Turbine towers are tapered, therefore the radius changes over distance. The model simplifies this by decreasing the radius as the length increases. For future research, the hydrodynamic loads of these turbine slices are also divided into a pie, as illustrated in figure 4.5.

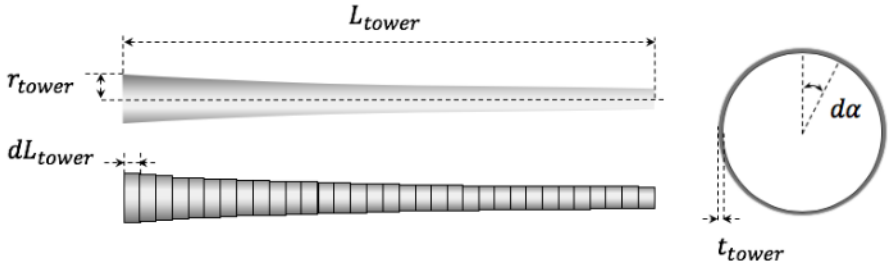

Figure 4.5: Tower sliced model

With these slices the mass can be calculated with equations in 4.16.

$$r_{tower}(i) = \frac{D_{bottom}}{2} - \frac{D_{bottom} - D_{top}}{2L_{tower}} dL_{tower} \cdot i$$
$$m_{tower}(i) = \left(2r_{tower}(i) \cdot t_{tower} - t_{tower}^2\right) \cdot \pi \cdot \rho_{steel} \cdot dL_{tower} \tag{4.16}$$

where; r_{tower} = Radius of the tower at segment i
D_{bottom} = Diameter of tower at the bottom
D_{top} = Diameter of tower at the top
t_{tower} = Wall thickness tower
L_{tower} = Length tower
dL_{tower} = Segment height of the tower

4.3. Environmental loading

The wave loads consist of varies load components. The theory that should be used for the model depends on the wave length and the geometry of the structure. The SUS concept has multiple bodies with different geometric size. The model distinguishes the SUS lattice and the buoyancy module. For wave loads this would also be the most logical procedure. The lattice structure of the SUS has slender beams and the buoyancy module is significantly bigger in size. The domains for each sub structure should be distinguished following figure 4.6.

The figure shows there are 6 different domains and corresponding wave theory should be used for the calculations of loads on the structure. During offshore installation operations waves should be relatively mild, therefore the H/D factor will be fairly low. The diameters of the beam from the SUS will be around 1 or 2 meters. For a H_s of 1 to 3 m the corresponding H/D factor will then be somewhere around 1 or 2. As for the buoyancy module the factor will be lower as the dimensions will be ranging from 10 to 30 meters and thus a quite higher H/D factor. To find the correct domain the wave length and therefore first the wave period should be known. As the SUS will operate in the North Sea, Jonswap is used to find the wave characteristics. Within this wave model it is found reasonable that the wave period and wave height lay in a interval shown in equation 4.17.

$$3.6 < \frac{T_p}{\sqrt{H_s}} < 5 \tag{4.17}$$

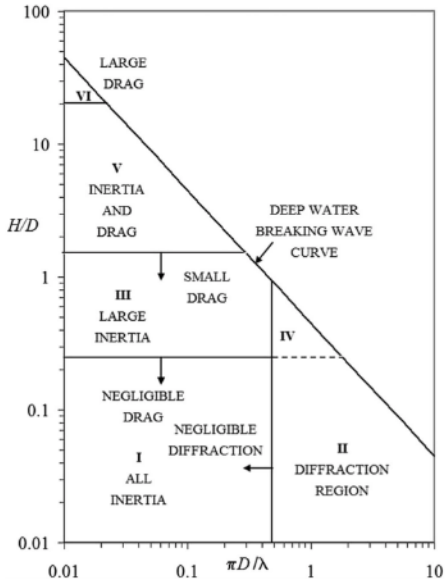

Figure 4.6: Wave load domains

Knowing the wave period for taken a significant wave height, the wave length can be calculated with equation 4.18.

$$\lambda = \frac{g}{2\pi} T_p^2 \tanh(2\pi \frac{d}{\lambda}) \tag{4.18}$$

With a corresponding wave period, T_p, of 3.6 to 5 and at a water depth, d, of 40 meters this will result in a wavelength between 20.2m to 77.8m. For diffraction to be negligible the parameters should agree equation 4.19, meaning the diameter of the structure should be lower than 3.2m. Which is the case for the lattice structure, however not for the buoyancy module.

$$\frac{\pi D}{\lambda} < \frac{1}{2} \tag{4.19}$$

Therefore, diffraction should be analysed using software ANSYS AQWA if the diffraction can significantly influence the load. If this is the case it should be added to the model.

4.3.1. SUS lattice

The hydrodynamic forces of the SUS latticed structure can be calculated using the Morison equation B.14. Doing so the drag and added mass coefficients are of importance. These can be found by consulting figure 4.7.

The KC value can be found using equation 4.20 and the Sarpkaya beta, β, can be determined using equation 4.21.

$$KC = \frac{u_a \cdot T}{D} \tag{4.20}$$

where; KC = Keulegan Carpenter Number
u_a = Oscillating flow speed
T = Oscillating period
D = Diameter structure

$$\beta = \frac{Re}{KC} \tag{4.21}$$

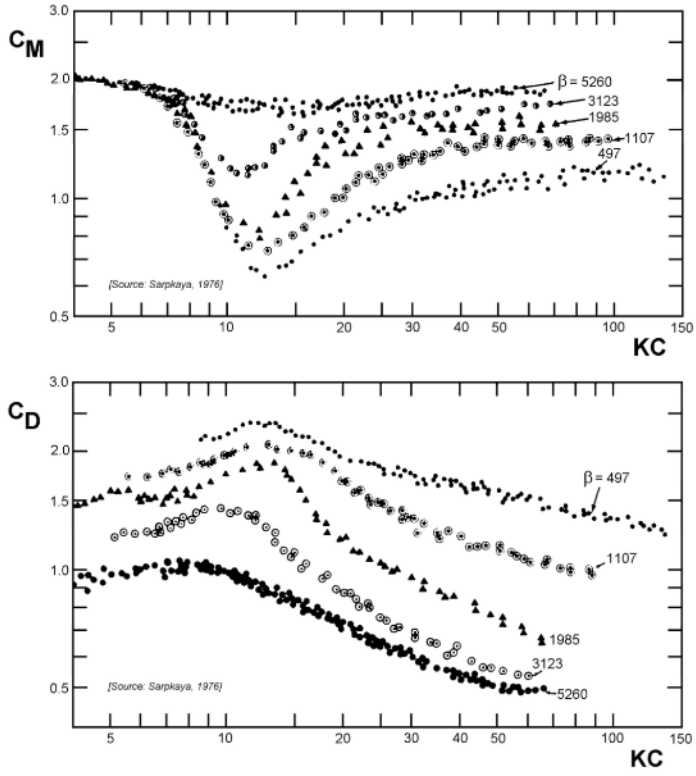

Figure 4.7: Drag and added mass coefficients for experimental results of Sarpkaya

where; β = Sarpkaya beta
$Re = \frac{u_a \cdot D}{\nu}$, Reynolds Number
ν = Kinematic viscosity

During operation the oscillating flow speed at the surface should not be very high as well as the time period, however as the diameter of the lattice is relatively small the KC number will maintain well below KC = 8. Therefore the C_m and C_d operate in a fairly constant range. As for the Reynolds Number and thus the Sarpkaya beta will be in order of 10^5, which is fairly high. Following these values it results in $C_m = 2$ and $C_d = 1.2$. At lower depths the oscillation speed would be much lower which would result in an even lower KC number and will not influence the Sarpkaya beta value as both Reynolds as KC depend on the oscillation speed. Therefore, the hydrodynamic coefficients C_m and C_d can be kept constant. Using Morison the wave drag loads can be calculated as in equations 4.22 and 4.23. The local speed of the segment and water particles at that segments are represented by equations 4.24 and 4.25. For each location the length to the hinge is expressed with r_i which is represented in equation 4.26.

$$\mathbf{F}_{SUS,drag} = \begin{bmatrix} F_x \\ F_y \\ F_z \end{bmatrix} = \sum_{i=1}^{N} C_d \frac{1}{2} \rho D \delta l \begin{bmatrix} \cos\beta_x^3 (u_{x,i} - v_{x,i}) |u_{x,i} - v_{x,i}| \\ \cos\beta_y^3 (u_{y,i} - v_{y,i}) |u_{y,i} - v_{y,i}| \\ \cos\beta_z^3 (u_{z,i} - v_{z,i}) |u_{z,i} - v_{z,i}| \end{bmatrix} \tag{4.22}$$

$$\mathbf{M}_{SUS,drag} = \begin{bmatrix} M_x \\ M_y \\ M_z \end{bmatrix} = \sum_{i=1}^{N} \begin{bmatrix} x \\ -r_i cos\varphi_i \\ r_i sin\varphi_i \end{bmatrix} \times C_d \frac{1}{2} \rho D \delta l \begin{bmatrix} \cos\beta_x^3 (u_{x,i} - v_{x,i}) |u_{x,i} - v_{x,i}| \\ \cos\beta_y^3 (u_{y,i} - v_{y,i}) |u_{y,i} - v_{y,i}| \\ \cos\beta_z^3 (u_{z,i} - v_{z,i}) |u_{z,i} - v_{z,i}| \end{bmatrix} \tag{4.23}$$

$$\mathbf{v_i} = \begin{bmatrix} 0 \\ r_i \dot{\varphi} sin\varphi_i \\ r_i \dot{\varphi} cos\varphi_i \end{bmatrix} \tag{4.24}$$

$$\mathbf{u_i} = \begin{bmatrix} u_{x,i} \\ u_{y,i} \\ u_{z,i} \end{bmatrix} \tag{4.25}$$

$$r_i = \sqrt{y_i^2 + z_i^2} \tag{4.26}$$

where; r_i = Orthogonal length to hinge axis of local of segment $[m]$
x_i = Local position in x of segment $[m]$
y_i = Local position in y of segment $[m]$
z_i = Local position in z of segment $[m]$
$\mathbf{v_i}$ = Local speed of segment $[m/s]$
$\mathbf{u_i}$ = Local speed of water particles at segment $[m/s]$

The Morison inertial loads consist of two parts, namely one for the oscillating part and another for the structure its acceleration. These are split as the oscillating waves contribution is known at each location, whereas the structure its contribution should be implemented into the added mass and inertial of the SUS lattice. Equations 4.27 and 4.28 represent the oscillating loads.

$$\mathbf{F}_{SUS,inertial} = \begin{bmatrix} F_x \\ F_y \\ F_z \end{bmatrix} = \sum_{i=1}^{N} C_m \frac{\pi}{4} \rho D^2 \delta l \begin{bmatrix} \cos\beta_x^2 \dot{u}_{x,i} \\ \cos\beta_y^2 \dot{u}_{y,i} \\ \cos\beta_z^2 \dot{u}_{z,i} \end{bmatrix} \tag{4.27}$$

$$\mathbf{M}_{SUS,inertial} = \begin{bmatrix} M_x \\ M_y \\ M_z \end{bmatrix} = \sum_{i=1}^{N} \begin{bmatrix} x \\ -r_i cos\varphi_i \\ r_i sin\varphi_i \end{bmatrix} \times C_m \frac{\pi}{4} \rho D^2 \delta l \begin{bmatrix} \cos\beta_x^2 \dot{u}_{x,i} \\ \cos\beta_y^2 \dot{u}_{y,i} \\ \cos\beta_z^2 \dot{u}_{z,i} \end{bmatrix} \tag{4.28}$$

Adding these up will result in the total load of the SUS lattice represented in equation 4.29 and 4.30.

$$\mathbf{F}_{SUS} = \mathbf{F}_{SUS,drag} + \mathbf{F}_{SUS,inertial} \tag{4.29}$$

$$\mathbf{M}_{SUS} = \mathbf{M}_{SUS,drag} + \mathbf{M}_{SUS,inertial} \tag{4.30}$$

The added mass and added inertial of the SUS lattice motion is calculated as in equations 4.31 and 4.32. In figure 4.8 the procedure is illustrated.

$$m_{SUS,add} = \sum_{i=1}^{N} C_a \frac{\pi}{4} \rho_w D^2 \delta l \tag{4.31}$$

$$J_{SUS,add} = \sum_{i=1}^{N} C_a \frac{\pi}{4} \rho D^2 r_i^2 \delta l \tag{4.32}$$

4.3.2. Buoyancy module

To calculate the induced force on the buoyancy module there are three methods, namely by simply calculating the buoyancy of the module exact, using box segments to verify the submerged parts, or Froude-Krylov induced pressure fields generated by undisturbed waves at each submerged edge plate. The first would only be applicable in still water as it does not distinguish waves. The second is applicable for waves and is limited to the mesh size of the box segments and needs additional hydrodynamic damping by induced drag on the structure its outer segments. And the last is calculates the static with Archimedes and dynamic pressure using undisturbed wave speed and structure speed. This last is the most accurate method to calculate the loads.

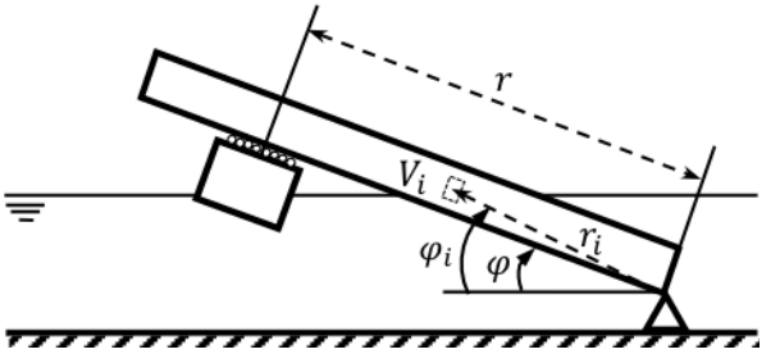

Figure 4.8: Numerically obtained added inertia

To estimate these loads the submerged area of buoyancy module is divided into plates. The plates experience different oscillating pressure due to the wave and the motion of the SUS. The load on these plates are calculated using the dynamic pressure due to drag from equation 4.34 combined with the hydro-static load from the hydro-static pressure on the plate as in equation B.16 in which the pressure is calculated with equations 4.33. The added mass due to the oscillations of the buoyancy module is calculated with equation 4.36.

$$\mathbf{F}_{box,static} = \begin{bmatrix} F_x \\ F_y \\ F_z \end{bmatrix} = \sum_{i=1}^{N} \rho_w g T_i A_i \overline{\mathbf{n}}_i \tag{4.33}$$

$$\mathbf{F}_{box,drag} = \begin{bmatrix} F_x \\ F_y \\ F_z \end{bmatrix} = \sum_{i=1}^{N} C_d \frac{1}{2} \rho_w A_{plate} \begin{bmatrix} (u_{x,i} - v_{x,i})|u_{x,i} - v_{x,i}| \\ (u_{y,i} - v_{y,i})|u_{y,i} - v_{y,i}| \\ (u_{z,i} - v_{z,i})|u_{z,i} - v_{z,i}| \end{bmatrix} \overline{\mathbf{n}}_i^2 \tag{4.34}$$

$$\mathbf{v_i} = \begin{bmatrix} 0 \\ r_i \dot{\varphi} sin\varphi_i \\ r_i \dot{\varphi} cos\varphi_i \end{bmatrix} \tag{4.35}$$

$$\mathbf{F}_{box,inertial} = \begin{bmatrix} F_x \\ F_y \\ F_z \end{bmatrix} = \sum_{i=1}^{N} C_m \rho_w V_{box,i} \begin{bmatrix} \dot{u}_{x,i} \\ \dot{u}_{y,i} \\ \dot{u}_{z,i} \end{bmatrix} \tag{4.36}$$

Combining all these loads results in the total hydrodynamic load, as in equation 4.37.

$$\mathbf{F}_{box} = \mathbf{F}_{box,static} + \mathbf{F}_{box,drag} + \mathbf{F}_{box,inertial} \tag{4.37}$$

The total moment around the buoyancy module is then calculated with these forces using equation 4.38.

$$\mathbf{M}_{box} = \mathbf{F}_{box} \times \begin{bmatrix} 0 \\ \sin\varphi_i r - \frac{d_o}{2}\cos\varphi \\ \cos\varphi_i r + \frac{d_o}{2}\sin\varphi \end{bmatrix} \tag{4.38}$$

The added mass is calculated for each submerged segment and is not dependent on any outer plates. This added mass, $m_{box,add}$ calculated with the displaced volume and is then integrated over the length of the arm to the hinge to find the added rotational inertia $J_{box,add}$. The equations are as in 4.39 and 4.40.

$$m_{box,add} = \sum_{i=1}^{N} (C_m - 1)\rho_w V_{box,i} \tag{4.39}$$

$$J_{box,add} = \sum_{i=1}^{N} (C_a)\rho V_{box,i} r_i^2 \tag{4.40}$$

The hydrodynamic coefficients C_m and C_d, the buoyancy module has similar values as the SUS lattice. It has a large diameter of around 24 to 36 meters and therefore a low KC value. A for the Reynolds number a higher diameter results in a higher value. These are the roughly recommended coefficients from the design codes of DNV [9].

4.3.3. Wind turbine

The turbine tower is divided into segments to be able to update the model on hydrodynamic and buoyancy. During this study the model will neglect these environmental loads, though the option remains to add in the future. As the buoyancy of the tower will only contribute positively in the upending moment it is considered that this method is conservative. Though the hydrodynamic loads can have a considerable part in the loads, especially for low angles, these are also neglected as within this model diffraction is not considered at this stage. In further research this should be calculated using software like ANSYS AQWA.

4.3.4. Cable system

The tension force of the cable is another important variable. The tension force is considered an external load on the connection of the buoyancy module and lattice frame. There are two input mechanisms considered, namely a controlled tension force input and a spring modelled cable at which the cable is reeled in at a chosen speed.
The controlled force is chosen as desired. It could be modelled as a constant, linear or controlled with a PID controller. The next chapter elaborates on this further.
The spring based cable is modelled with a predefined initial length at which the cable has a certain stiffness which is found with equation 4.41.

$$k_{cable} = \frac{E_{cable} A_{cable}}{L_{initial}} \tag{4.41}$$

The length between the buoyancy module its cable connection and the winch location above the waterline defines the length of the cable. While reeling the cable the cable is shortened and tension is built up into the cable. This tension results into the cable being stretched following k_{cable}, as in equation 4.42. For the upend the initial length of the cable is shortened with a certain reeling speed. As the stiffness depends on the initial length the stiffness is non-linear and will increase as it gets shorter.

$$\Delta L = L_{initial} - L_{cable} \tag{4.42}$$

$$L_{cable} = \sqrt{\left(h_{winch} + d - r\sin\varphi + \frac{d_o}{2}\cos\varphi\right)^2 + \left(r\sin\varphi + \frac{d_o}{2}\sin\varphi\right)^2} \tag{4.43}$$

4.4. Equation of motions

The motion of the SUS is captured with a single equation of motion and for a full analysis with two equations of motion. Doing two types of analysis the motion can be better understood. With the single equation motion the motion of the SUS with the buoyancy module at a fixed place is accessed to find its natural characteristics. Whereas for the double motion equation the full upend is analysed. The full derivation of these equations of motion are found in appendix A.

4.4.1. 1 Degree Of Freedom for SUS 3

To find the behaviour at the varies angles of the SUS operation, the model is tested for the rotation at the hinge with a fixed buoyancy module. At this point the model has 1 degree of freedom, namely φ. The behaviour of this system is captured as in figure 4.8 with the equation of motion, represented in equation 4.44.

$$A_1\ddot{\varphi} = B_1\dot{\varphi} + C_1\varphi + M_1 \tag{4.44}$$

where; A_1 = Inertial
B_1 = Damping
C_1 = Stiffness
F_1 = External load

Firstly, the rotational inertial of the system depends on the SUS and the lattice. Both have an added mass which is calculated numerically as explained earlier.

$$A_1 = J_{SUS} + J_{SUS,add} + J_{box} + J_{box,add} \tag{4.45}$$

The damping and stiffness of the system depend on the drag, inertial and buoyancy of the SUS lattice and the buoyancy module. They are calculated as effective loads and added to form the combined damping and stiffness load shown in 4.46.

$$B_1\dot{\varphi} + C_1\varphi = \left(\mathbf{M}_{SUS} + \mathbf{M}_{box}\right) \cdot \begin{bmatrix} 1 \\ 0 \\ 0 \end{bmatrix} \tag{4.46}$$

Finally, the external load exerted by the tension force of the cable. This is calculated with equation 4.47.

$$M_1 = M_{x,cable} = \left(\begin{bmatrix} 0 \\ r\cos\varphi - \frac{d_o}{2}\sin\varphi \\ r\sin\varphi + \frac{d_o}{2}\cos\varphi \end{bmatrix} \times \mathbf{T}_{cable} \right) \cdot \begin{bmatrix} 1 \\ 0 \\ 0 \end{bmatrix} \tag{4.47}$$

4.4.2. 2 Degree Of Freedom for SUS 3

The main purpose of the SUS concept is to upend a wind turbine. Therefore, a full simulation of upending the SUS is modelled. In addition to the previous model this model has another degree of freedom, namely L_{arm} or r. During the upend operation the buoyancy module is pulled down along the SUS lattice along axis r as in figure 4.9. As a result of that a second equation of motion is needed. The equation of motion is calculated using a Lagrangian approach and is fully elaborated in appendix A. The main addition is the coupling between the motion of the buoyancy module and the SUS lattice. When deriving the kinetic energy of the system this will result in equation 4.48.

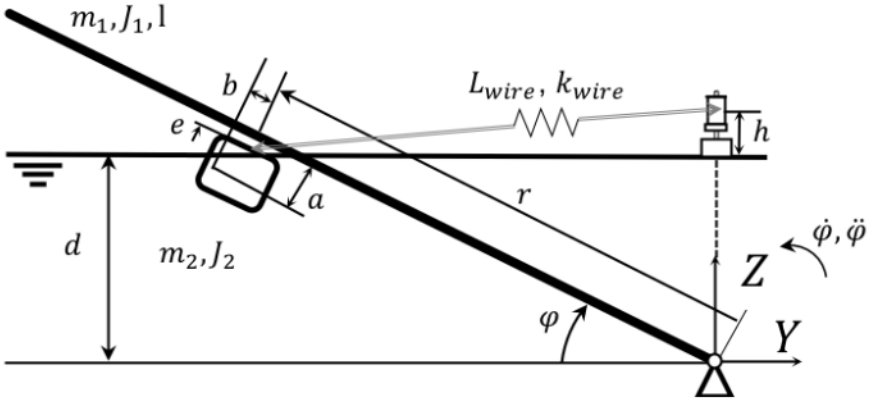

Figure 4.9: SUS 3: 2 Degree Of Freedom scheme

$$\mathbf{A_2}\begin{bmatrix} \ddot{\varphi} \\ \ddot{r} \end{bmatrix} = \mathbf{B_2}\begin{bmatrix} \dot{\varphi} \\ \dot{r} \end{bmatrix} + \mathbf{C_2}\begin{bmatrix} \varphi \\ r \end{bmatrix} + \mathbf{F_2} \tag{4.48}$$

The inertial part, A_2, will then become as in equation 4.49.

$$\mathbf{A_2} = \begin{bmatrix} J_{SUS} + J_{SUS,add} + J_{box} + J_{box,add} & m_{box}\left(\frac{H}{2} + e\right) \\ m_{box}\left(\frac{H}{2} + e\right) & m_{box} + m_{box,add} \end{bmatrix} \tag{4.49}$$

Second the hydrodynamic loads are found from the loads of the SUS lattice and the buoyancy module. An additional damping and friction are taking into account as these are present during the operation, though in this research these will be neglected as these are not known yet.

$$\mathbf{B_2}\begin{bmatrix} \dot{\varphi} \\ \dot{r} \end{bmatrix} + \mathbf{C_2}\begin{bmatrix} \varphi \\ r \end{bmatrix} = \begin{bmatrix} M_{SUS,x} + M_{box,x} + r(F_{box,z}\cos\varphi + F_{box,y}\sin\varphi) \\ F_{box,y}\cos\varphi - F_{box,z}\sin\varphi - \mu_f(F_{box,z}\cos\varphi + F_{box,y}\sin\varphi) - c_{box}\dot{r} \end{bmatrix} \quad (4.50)$$

$$\mathbf{F_2}\begin{bmatrix} r(F_{cable,z}\cos\varphi + F_{cable,y}\sin\varphi) \\ F_{cable,y}\cos\varphi - F_{cable,z}\sin\varphi - \mu_f F_{cable,z}\cos\varphi + F_{cable,y}\sin\varphi) \end{bmatrix} \quad (4.51)$$

where; r = Length along axis parallel of the SUS lattice $[m]$
$\dot{r}$ = Speed along axis parallel of the SUS lattice $[m/s]$
$\ddot{r}$ = Acceleration along axis parallel of the SUS lattice $[m/s^2]$
c_{box} = Damping of sliding mechanism $[Ns/m]$
M_{box} = Equivalent force due buoyancy and environmental load on the box $[Nm]$
F_{box} = Equivalent force due buoyancy and environmental load on the box $[N]$
F_{cable} = Tension of the cable $[N]$
μ_f = Friction coefficient of normal force in u direction $[-]$

With these equations the total motion of the SUS concept is captured. It is implemented into the model, where after the motion of the SUS can be analysed.

4.5. Model limitation

The model uses undisturbed waves, as it is a large structure it will generate radiation and experience diffraction which will disturb waves and influence results. Data from potential flow theory software can be used to find their significance and can be added if necessary. The radiation would dampen the motion quite significantly, therefore it can be stated that considering the radiation this approach is conservative. Diffraction will result mostly in sway and surge motion, which are both not the most influencing parameters during this upend as the SUS is mostly heaving and pitching.
The added mass and drag coefficients are taken constant at every position and speed, though it is likely to change accordingly. Segment sized are taken small enough to capture most of the wave loads, so no high frequency wave loads can be detected as this is not of interest at this point.
Bodies in water also experience frictional resistance along the body plates, this could be modelled as additional damping or directly from the parallel speed along each plate. This could dampen the buoyancy module its movement. It is not incorporated into the model and could be added in a later stage. Neglecting this can be considered as a conservative approach.

5

Results and evaluation

This chapter will evaluate and validate the model based on whether the results are realistic. Furthermore, characteristics of the SUS concept are evaluated and analysed. These are based on undisturbed water and 1 DOF and a full upend simulation with 2 DOFs.

5.1. Input parameters

The parameters used in the model are presented in table 5.1. Some parameters are denoted as var. These represent the parameters which are taken variable throughout this research. The water depth, d, is a crucial parameter as the SUS should be able to operate in various water depths. As well as the incoming wave angle φ_{wave} and the sea state based on the significant wave height, H_s, and peak period, T_p, are all variable to find the responses at several sea states. When these parameters are implemented the simulated model is displayed as in figures 5.1 and 5.2.

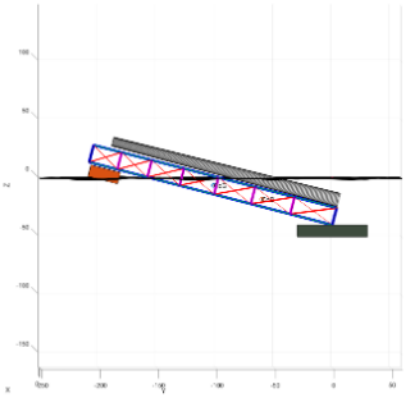

Figure 5.1: SUS 3 side view in simulation

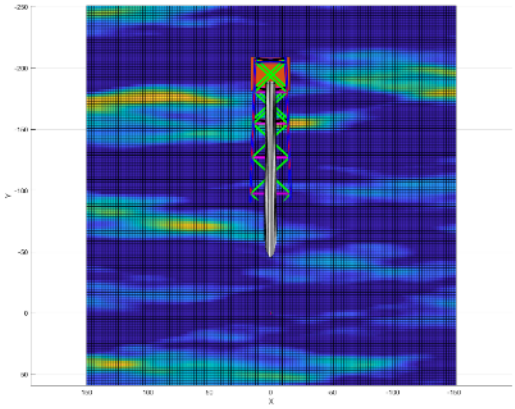

Figure 5.2: SUS 3 side view in simulation

5.2. Undisturbed water

Before simulating wave loads onto the SUS 3 the model is tested in still water. At this point the model does not incorporate disturbance of the water. At first the model finds the static equilibrium of the SUS with a fixed buoyancy module and the corresponding tension force. Hereafter a dynamic situation is tested as a 1 DOF system, where only the SUS can freely move in rotation around the hinge. Finally, the full 2 DOF system is tested by pulling the buoyancy module along the SUS lattice.

Table 5.1: Model parameters

Parameter	Value	Unit	Description
d	var	m	Water depth
φ_{wave}	var	deg	Incoming wave angle
ϑ_{spread}	30	deg	Wave spread
$u_{current}$	0	m/s	Current speed
$\vartheta_{current}$	0	deg	Current direction
ν	$1.35 \cdot 10^{-6}$	m^2/s	Kinematic viscosity
u_{wind}	0	m/s	Wind speed
θ_{wind}	0	deg	Wind direction
C_s	1	-	Wind drag coefficient
ρ_w	1027	kg/m^3	Density seawater
ρ_s	7850	kg/m^3	Density steel
H_s	var	m	Significant wave height
T_p	var	s	Peak period
b_N	40	m	Width bottom of the frame
b_0	25	m	Width top of the frame
d_o	2	m	Diameter outside frame
t_o	0.03	m	Thickness outside frame
d_i	1.5	m	Diameter inside frame
t_i	0.02	m	Thickness inside frame
h	215	m	Height frame
d_{frame}	15	m	Depth of the frame
N	7	-	Horizontal section in frame
n_{cross}	2	-	Number of diagonals in frame
dl	1	m	Beam interval size
C_d	1.2	-	Drag coefficient for SUS
C_m	2	-	Added mass coefficient for SUS
L	28	m	Length buoyancy module
H	12	m	Height buoyancy module
W	34	m	Width buoyancy module
dl_{box}	2	m	Mesh interval
L_{arm}	200	m	Initial length buoyancy for hinge
t_{box}	0.02	m	Thickness buoyancy module walls
C_d	1.2	-	Drag coefficient for buoyancy module
C_m	2	-	Added mass coefficient for buoyancy module
μ_f	0	-	Friction coefficient of buoyancy module roll system
c_{box}	0	Ns/m	Linear damping coefficient buoyancy module
D_{bottom}	12	m	Bottom diameter tower
D_{top}	8	m	Top diameter tower
L_{tower}	200	m	Length tower
dL_{tower}	1	m	Step length tower
$d\alpha$	1	m	Step circumferential tower
t_{tower}	0.04	m	Thickness steel
m_{nac}	1200	MT	Mass of nacelle and blades
q_{cable}	0	kg/m	Weight per meter cable
E_{cable}	$6000 \cdot 10^6$	kg/m^2	Elastic modulus cable
D_{cable}	0.072	m	Diameter
N_{cable}	5	-	Number of cables
δt	0.1	s	Time step
t	var	s	Time
φ_0	var	deg	Starting operation angle

5.2.1. Fixed static equilibrium

Firstly, a static situation is tested to find the characteristics of the system and find possible bottlenecks before dynamically accessing SUS 3. Based on the equilibrium at each angle φ the arms, loads and moments of the SUS can be plotted as in figure 5.3.

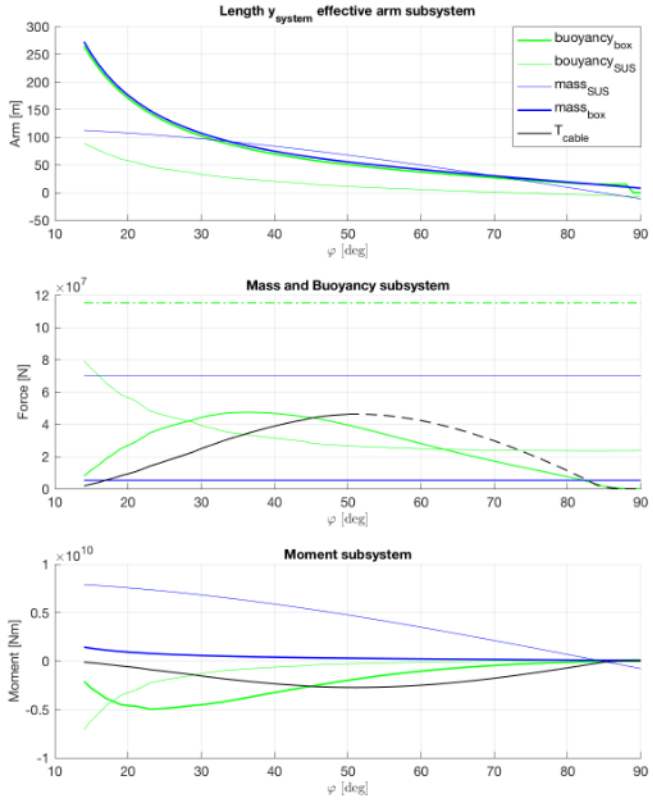

Figure 5.3: Arms, loads and moments of the SUS 3 under static equilibrium for 40 m water depth

The top graph illustrates the projected length, of the CoG or CoB of both the SUS lattice (thin line) and buoyancy module (thick line), to the hinge. The mass of the SUS is build up out of the weights of the SUS lattice, tower and nacelle. The arm of the buoyancy module can maximally be 200 meters as for the length of the frame. Therefore, it can be concluded that when starting the operation, the SUS 3 will have an inclination of about 17 degrees. Furthermore, the graph of the SUS mass suggests that after 85 degrees the arm will become negative and thus will exert a negative moment resulting in the SUS to turn further than 90 degrees.
The second graph shows a green dash-dot line which represents the buoyancy of the module when it is fully submerged. Another remark is the black dashed line of the tension force after 50 degrees. At this point the tension force should decrease accordingly while upending. Therefore, the tension force beyond 50 degrees should be design such that the speed of $\ddot{\varphi}$ is regulated to keep it relatively constant. Otherwise the SUS lattice should be designed such that if it passes 50 degrees it is retained by some sort of mechanism when using an input tension force. When the cable is reeled in with a constant speed there is no problem here.
In the last graph all effective moments are displayed. The upending buoyancy of the SUS lattice is gradually decreasing as it is emerging out of the water at higher angles, although it is most dominant for angles before 18 degrees. Overall the two most dominant upending moments are the buoyancy module and the tension force. Within the first 45 degrees the buoyancy module will be leading, where after the tension force dominates the upend movements. This latter fact implies that the dynamic behavior of the structure could be dominated

by this tension force.

5.2.2. Fixed buoyancy module

As the buoyancy module moves over the length of the frame the structures behavior changes. To find the change of this behaviour during upended a free decay test is simulated for various positions, so that the natural frequency, stiffness and damping characteristics can be found.

Free decay test

A free decay test is done to find the main characteristics of the free motion of the SUS concept. The motion should be captured using the equation of motion for rotation, as equation 5.1.

$$J\ddot{\varphi} + b_{damping}\ddot{\varphi} + k_{spring}\varphi = 0 \tag{5.1}$$

The model is tested for multiple water depths to evaluate the behavior as the buoyancy module position differs during upending. A set of three water depths are simulated, namely 30, 40 and 50 meters. For each position of the buoyancy module the tension force exerted by the cable is set to be such as the static equilibrium suggests. So, for most of the time the buoyancy module will be pulled down so that the forces along the r-axis are almost zero even though the buoyancy module is fixed at this point. The free decay test is done from 15 degrees in intervals of 5 degrees up to and including 45 degrees. At 50 degrees and further the system will get unstable using a constant tension force, as illustrated in the bottom graph of figure 5.3. At this point when φ is moving in any direction the tension would be either insufficient to return to its desired position or the tension force would be to high resulting in a continuous acceleration. Therefore, all decay tests beyond 50 degrees are neglected as at that point the tension force should be controlled by either modelling slack into the cable or with another control system such as a PID controller.

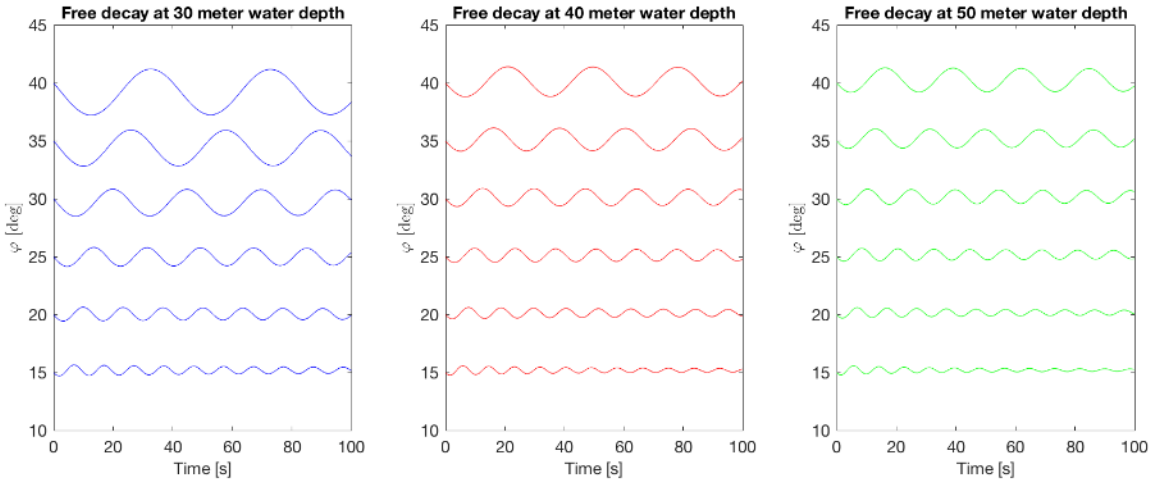

Figure 5.4: Free decay of SUS 3 model with 0.05 rad/s initial speed

In figure 5.4 the oscillations of the free decay tests are presented. The vertical axis shows the inclined angle of the SUS and the horizontal axis represents the time. At the initial state all tests are given a angular speed of 0.05 rad/s, where after they move freely. The set of free decay tests does not tests any further than 40 degrees, because for a water depth no 30 meters with an angle of 45 degrees a 100 seconds duration is not sufficient to capture enough oscillations to be analysed. As the current data gives sufficient insight into the characteristics of the data there is no reason to extend the test duration.

From the free decay test the corresponding period is determined as in figure 5.5. For this it is clear that the natural period T_n is fairly small for lower angles and comes close to the sea state frequency at which the SUS concept will operate. Ocean wave periods range from 1 to 30 seconds, however operating in mild weather at the North Sea periods above the 15 seconds can be avoided or chances of these waves can be minimized.
One of the most important parameters is the fixed position of the buoyancy module along the SUS lattice, which is displayed in figure 5.6. Here the length of the arm at the vertical axis is plotted against the inclined SUS angle. As the maximal r is 200 meters the first result data points of the free decay at 50 meters water depth are more or less fictional. The moment on the SUS is dominated by the buoyancy module, which exerts a spring force on the SUS lattice, and the length of the arm with the inclined angle, φ.

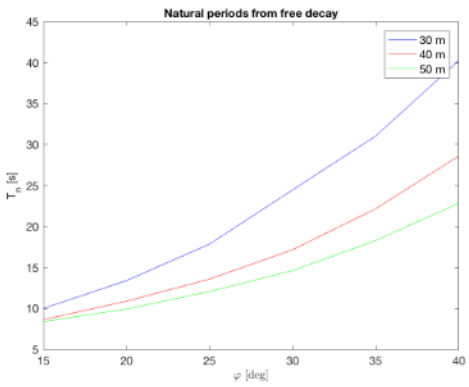

Figure 5.5: Natural periods from free decay test

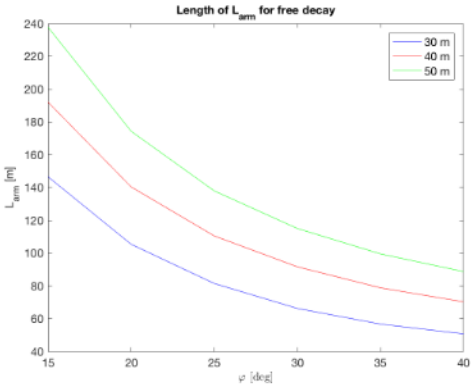

Figure 5.6: r of buoyancy module from free decay

$$T_n = 2\pi \sqrt{\frac{J_{total}}{k_{sys}}} \tag{5.2}$$

where; T_n = Natural period
J_{total} = Moment of inertia and the added mass
k_{sys} = Rotational spring stiffness of the whole SUS model

Using the period of oscillations from figure 5.4, one can calculate the total rotational spring stiffness of the system, k_{sys}, using equation 5.2. To verify this rotational spring stiffness it should match an analytical representation of the stiffness, which is equal to equation 5.3. As the φ changes during the oscillation the ratio between the heave motion of the buoyancy module and the pitch of the SUS lattice must be calculated. Although this is a non-linear problem it can be linearized for a small $\delta\varphi$, which is the case. Using the angle sum and difference identities equation 5.4 the nonlinear problem simplified.

$$k_{BOX} \approx \rho L_{wl} W g \cos^2(\varphi) L_{arm}^2 \tag{5.3}$$

$$\begin{gathered} sin(\varphi + \delta\varphi) = sin(\varphi) + \delta\varphi cos(\varphi) \\ \delta\varphi \approx 0 \end{gathered} \tag{5.4}$$

where; $L_w l$ = Waterline of the buoyancy module [m]
W = Width of the buoyancy module [m]
$\delta\varphi$ = Delta phi [rad]
J_{total} = Moment of inertia and the added mass [kg/mm]
k_{BOX} = Rotational spring stiffness of the buoyancy module [Nm/rad]

In figure 5.7 the stiffness of the free decay (k_{sys}), analytic buoyancy module stiffness (k_{BOX}) and that of the buoyancy of the SUS lattice (k_{SUS}) are found on the vertical axis plotted against the inclined SUS angle. The SUS spring stiffness is calculated from the added moment of the SUS, while φ is changing. The graph shows k_{sys} and k_{BOX} are quite covenant, although for low inclined angles there is a slight deviation. This can be explained by the influence of the buoyancy of the SUS lattice, which is displayed with the dashed-dot line. Adding the SUS and BOX would result in a near identical result which verifies the model as for angular stiffness.

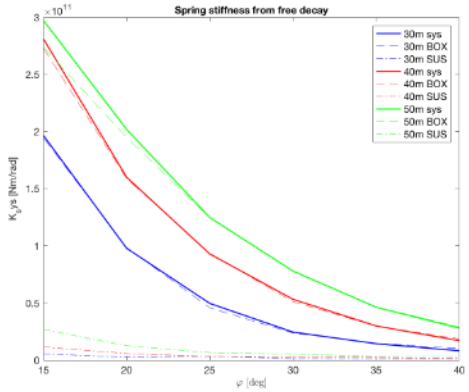

Figure 5.7: Stiffness from free decay

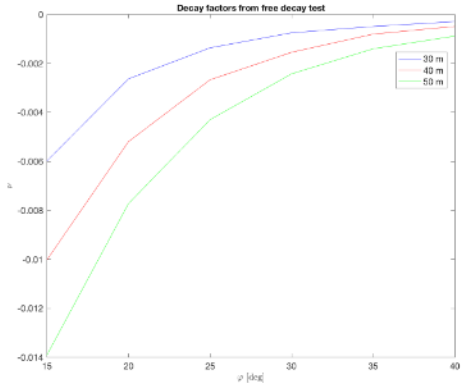

Figure 5.8: Decay factor

Another characteristic is damping, which can determine by calculating the decay of the system. By first detrending the curves, finding the periods and amplitudes using zero crossings, an exponential decay can be found. Fitting these in equation 5.5 results in the decay coefficients, which are displayed in figure 5.8.
As the motion has no coupled movement due the buoyancy module movement, thus L_{arm} is constant, this method is valid. For coupled motion between the movement of φ and w simultaneous is neglected during this part.

$$\varphi e^{-\nu t} cos(\omega_n t) \tag{5.5}$$

where; ν = Damping ratio [-]
ω_n = Natural frequency [$\frac{rad}{s}$]
t = Time [s]

Using this decay factor, the damping and non-dimensional damping coefficient can be calculated with equations 5.6 and 5.7.

$$2\nu = \frac{b_{damping}}{J_{total}} \tag{5.6}$$

$$\kappa = \frac{\nu}{\omega_n} \tag{5.7}$$

where; $b_{damping}$ = Damping ratio [$\frac{Nm}{s/rad}$]
κ = Non-dimensional damping coefficient [-]

Figure 5.9 and 5.10 display the development of the damping and non-dimensional damping during the upend. The graph shows a clear decrease of the damping and non-dimensional damping. The non-dimensional damping shows a near linear decrease which is likely correlated with L_{arm}, as the effectiveness of the damping is depending on the arm length around the hinge.

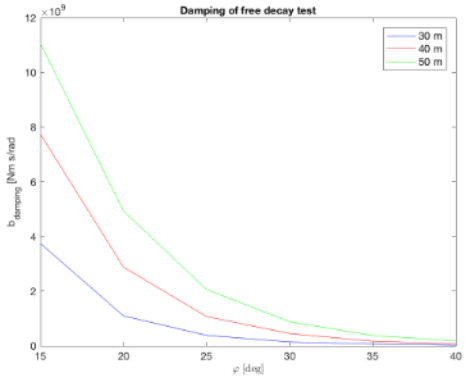

Figure 5.9: Damping from free decay test

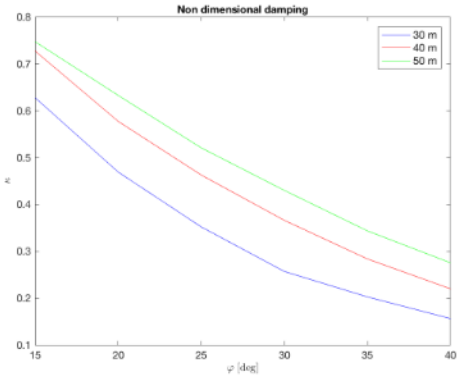

Figure 5.10: Non dimensional damping from free decay

For an simple simulation this data can be back filling into the equation of motion. This will could make future simulations easier. As the damping is only valid for the natural frequency, these simulations would only be valid at excitation loads coinciding with the natural frequency.

5.2.3. Dynamic upend simulation

The main purpose of the SUS concept is to upend a wind turbine. The objective is to find the optimal upending process of the SUS system. Within the model the only parameter that is controlled during the simulation is the tension force of the cable system. Therefore, it is the only testable parameter. To test what kind of control type should be applied to the SUS concept a series of tension force test is done. These tests are done as illustrated in figure 5.11. Each of these types is discussed and evaluated on their upending. The criterion of success is fairly simple and is described as following.

$$\varphi > 85° \begin{cases} \text{Successful} & T > T_{critical} \\ \text{Unsuccessful} & T < T_{critical} \end{cases}$$

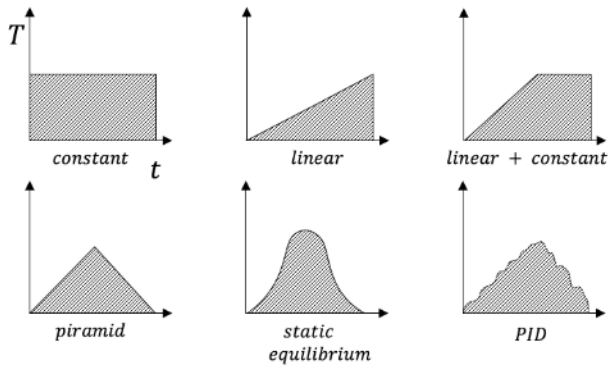

Figure 5.11: Controlled tension force types for upend simulation

Constant tension force

It is desirable that the control type is as simple as possible. Therefore, the first test done with a constant tension force in the cable. The goal here is to find a critical tension force at which the upend is successful. In figures 5.12 and 5.13 two simulation results are displayed. The first graph shows the inclined angle φ on the vertical axis, whereas the second graph shows the length of the buoyancy module along the SUS lattice. These tests have a constant tension

force of 30 MN and 32.5 MN. The lower tension force will reach its maximum till about 60°, were after it falls back to a about 30°. The higher tension clearly passes the 90° and thus a success. Meaning the $T_{critical}$ is somewhere in between these two tension forces, although for simplicity it is safe to $T_{critical}$ = 32.5 MN.

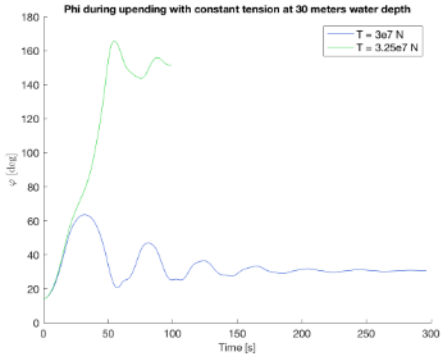

Figure 5.12: φ during upending with constant tension

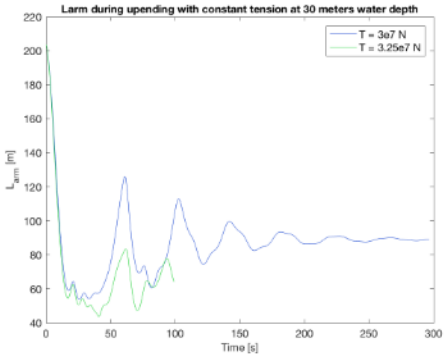

Figure 5.13: r during upending with constant tension

From a practical point of view, a direct constant tension is quite unrealistic as the tension force would have some kind of built up. Nevertheless, when a direct constant tension is initiated the buoyancy module will have an enormous acceleration along the SUS lattice. Figure 5.13 suggest that the buoyancy module travels 140 meters within 20 seconds. This is suggesting a maximal speed of about 10 m/s. Which seems reasonable considering that the drag will find an equilibrium with the drag, as in $T_{cable} \approx F_d = C_d \frac{1}{2} \rho u^2 A$. Although this acceleration would be undesirable.
The full upend with the critical tension force is done in 50 seconds. Due to the enormous upending moment of the buoyancy module the SUS lattice is accelerated rather quick, these speeds and accelerations are not desired.

Linear tension force

A linear increasing tension force would result in a more graduate upend motion as the graph in figure 5.14 illustrates. There are three types of tension force control, one is constantly linearly increasing, and two in which the tension force stays constant or linearly decreases at a certain point.

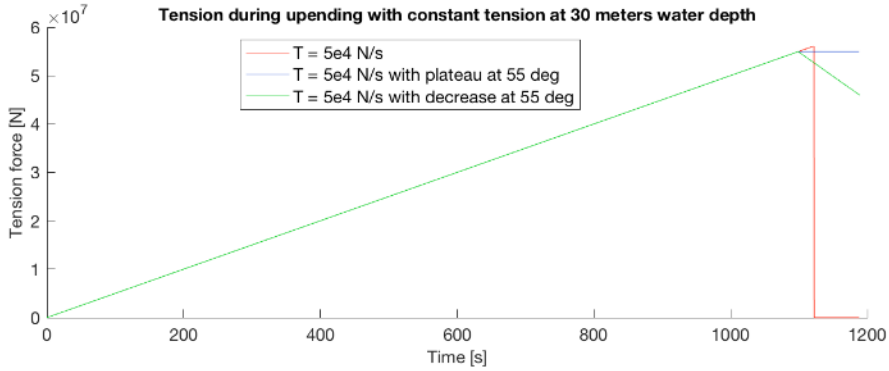

Figure 5.14: Tension force during upending with linear type tension

Again after 50°, the tension force is clearly too high as less tension force is needed at his stage. The SUS lattice is accelerated too quickly, therefore after 50° a linear increasing tension force is not desired for higher angles. Though the linear tension force increase would be really well for constant upending angle before 50°. This can be considered for further re-

PID control	Value	Units
Proportional	300	$[MNs/rad]$
Integral 300	$[MN/rad]$	
Derivative	1	$[MNs^2/rad]$

Table 5.2: Upending PID tension control

search.

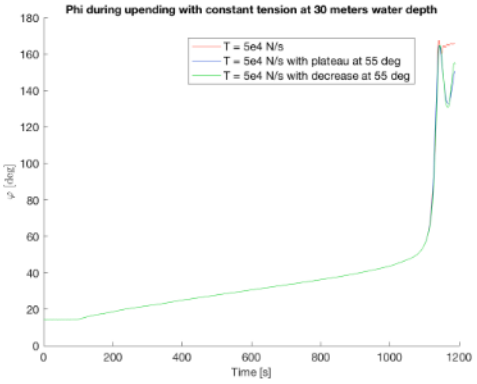

Figure 5.15: φ during upending with constant tension

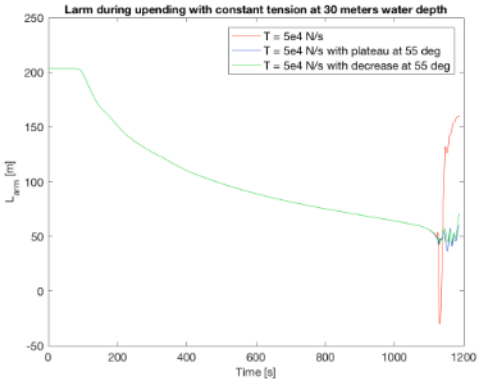

Figure 5.16: r during upending with constant tension

Static equilibrium and PID controlled tension force

Another method is to use the tension force needed for a static equilibrium. This way the position should eventually match the corresponding tension force as in figure 5.3. As the upending angle is delayed compared the corresponding tension force at the desired angle, the tension force would be insufficient using the exact tension force from the static equilibrium. Therefore, an additional 5 percent is added to overcome this problem. In figure 5.17 the path of the tension force is illustrated.

As an addition to this static equilibrium tension force, a PID controlled mechanism can be added. This will compensate for the offset in angle, angular velocity and accelerations. The PID then controls the output speed of the operation, which is 0,001 $^{rad}/_{s}$. In figure 5.17 the tension force during upending is illustrated. This tension is controlled with parameters presented in table 5.2. These could be further tested for better performance.

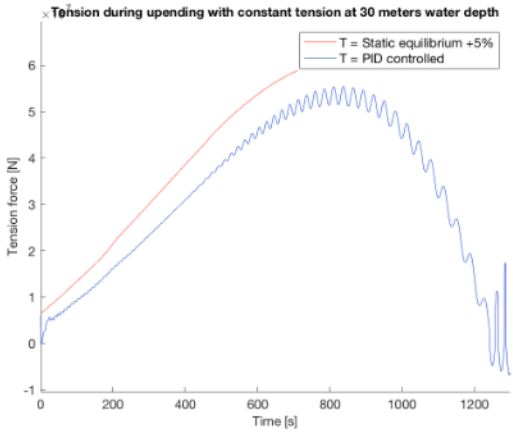

Figure 5.17: T during upending with statically stable and PID controlled tension

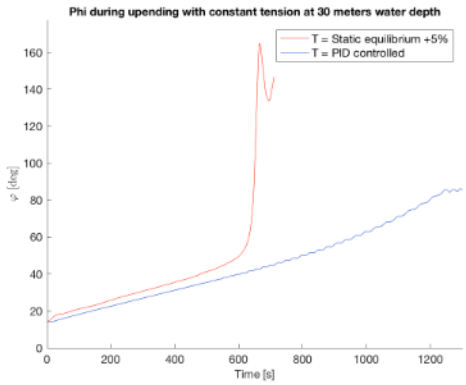

Figure 5.18: φ during upending with statically stable and PID controlled tension

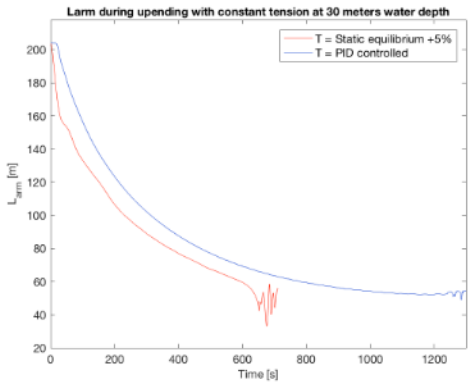

Figure 5.19: r during upending with statically stable and PID controlled tension

In figure 5.18 and 5.19 the motion path of φ and r or L_{arm} are displayed. The static equilibrium tension force is capable of upending the SUS, although similar as the linear tension force the system is unstable beyond 50°. Therefore, this type of tension force to upend the system is discarded. The PID controlled tension force show a significantly improved result considering the phase after 50°. Though at the last stage φ is slightly oscillating, which could be optimised by tweaking the PID parameters during upending. The PID controlled tension is the only tension type capable of upending the SUS in a controlled matter. Therefore, this method would be desired for the SUS.

Reeling cable

Though the PID controlled tension force is the desired tension force method at this point, a more practical approach of upending is to use a more realistic method. As the tension is controlled by a winch, another method is to gradually reel in the cable and thereby exert a tension force where the cable acts as a spring. This is a realistic operational approach. Figure 5.20 show the tension force during such an upend.

The tension force oscillates quite heavily which is the result of the coupled motion of the

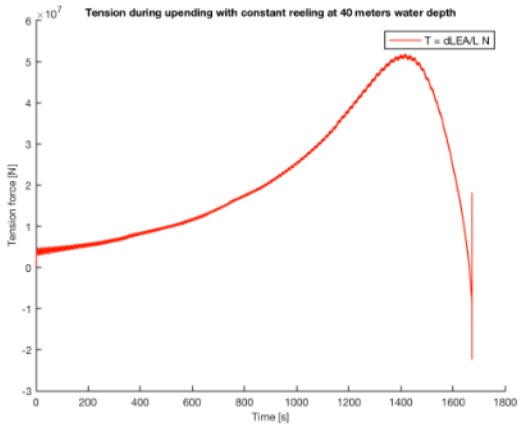

Figure 5.20: T during upending with reeling cable

SUS lattice and movement of the buoyancy module along the SUS lattice. These oscillations depend strongly on the stiffness of the cable. In this case there are 20 cables reeling in the buoyancy module. As the length of the cable decreases during the upend the stiffness increases drastically following $k = \frac{EA}{L}$. This will result in that the model cannot follow this motion sufficiently using time steps of 0.5 seconds. This can be handled by decreasing the time step and increasing the initial length of the cable. As the modelling time would with

smaller time steps an increase of initial cable length is combined with a smaller time step.

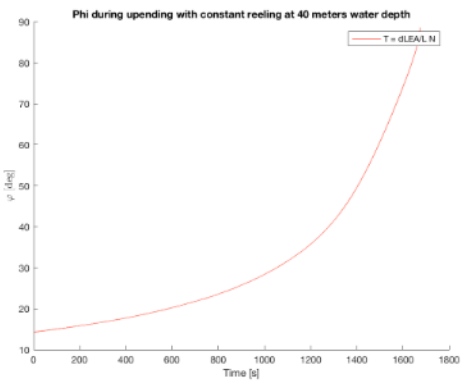

Figure 5.21: φ during upending with reeling cable

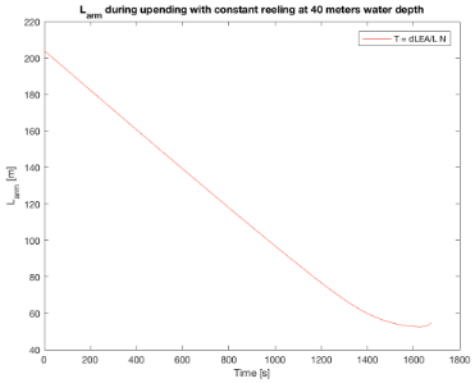

Figure 5.22: r during upending with reeling cable

The upending speed with respect to φ and position of r is illustrated in figures 5.21 and 5.22. At first the upending rotation is fairly slow where after beyond 30° it speeds up. This is the result of reeling the cable with a constant speed as the distance to the buoyancy module is strongly correlated to $cos\varphi$. To improve this the reeling speed should be depending on the position of the buoyancy module such as the length of the cable at the static equilibrium tension suggests. This is done in the following simulation. As the reeling of the cable gives the most constant results it is the most optimal chose from all evaluated upend methods.

5.3. Environmental loading

In this section the environmental loads are added to the upending simulation. The model is design to test multiple sea states and their direction. The goal is to find the limit of operating the SUS 3. For all results the upending is done such that the cable is reeled in ensuring a near constant radial speed upending the wind turbine within 30 minutes. This cable is modeled as a spring resulting in the cable to stretch to the equivalent length so that it has sufficient tension force. This will result to some deviation from a constant $\dot{\varphi}$.

5.3.1. Upend simulation time response

The goal of the simulation is to estimate the critical wave height in which the SUS 3 can upend. The most critical parameter to find this limit is motion of the wind turbines top tower; the nacelle, rotor and blades. A maximal acceleration of 0.1 g will be used as a maximum installation acceleration. However, this value depends on the turbine manufacturers which is unknown. This value can very well be lower or higher.

While SUS 3 installs a turbine in waves, with a significant wave height of 1 meter, a peak period of 4.5 seconds and incoming wave angle of 270^o, the response of the motions φ and r will be as in the graphs from figures 5.23 and 5.24. Figure 5.23 displays the motion in φ during upending. In the bottom graph the inclined angle, φ, of the SUS 3 is presented. It rises from about 0.253 to $\pi/2$ radians in less than half an hour. The motion seems quite linear, tough it has a slight variation from being linear. This is the result of the needed tension force during the upend, thus a larger stretch of the cable which gives a smaller angle φ.
When the upending is at its end, the SUS goes past its vertical equilibrium position and accelerates further on from about 85^o. At this point the SUS is stopped by a to be design mechanism. The upward movement at the end of the time response can therefore be neglected. The simulation is stopped at 90^o as the upend is successful. The rotational acceleration, $\ddot{\varphi}$, shows higher amplitudes at the beginning and end of the upending. The first part is the result of the natural frequency of the SUS 3 system is near that of the wave frequency. The

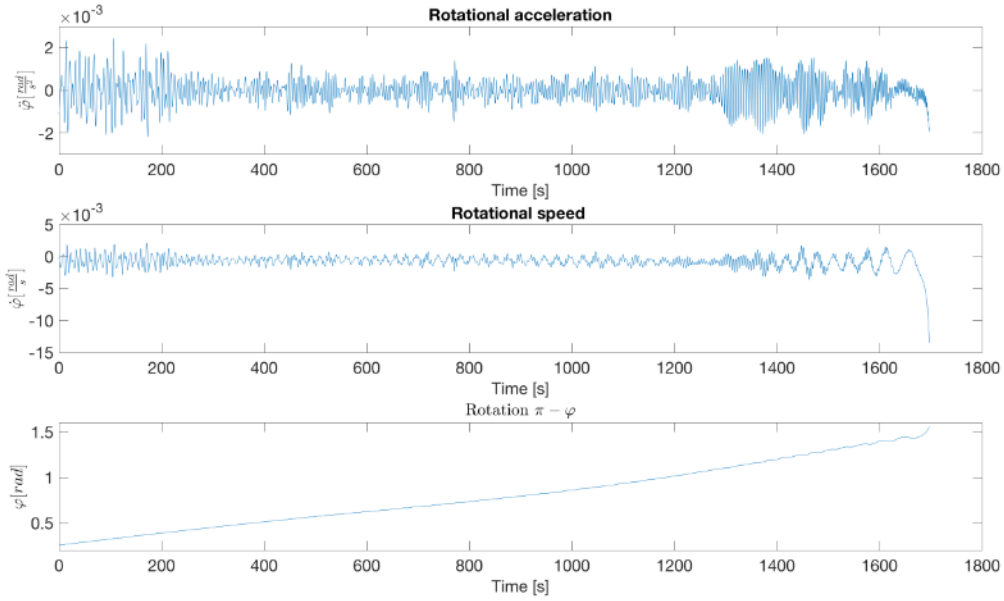

Figure 5.23: Motion of SUS in φ at Hs = 1, T_p = 4.5 and φ_{wave} = 270^o during upending

high amplitudes in the last phase are likely a result of the buoyancy modules response, from which the movement in r is more relevant. The motion in r is displayed through the graphs in figure 5.24.

Here in the last phase the acceleration ($\ddot{r}$) and speed ($\dot{r}$) are quite high. At this point the ten-

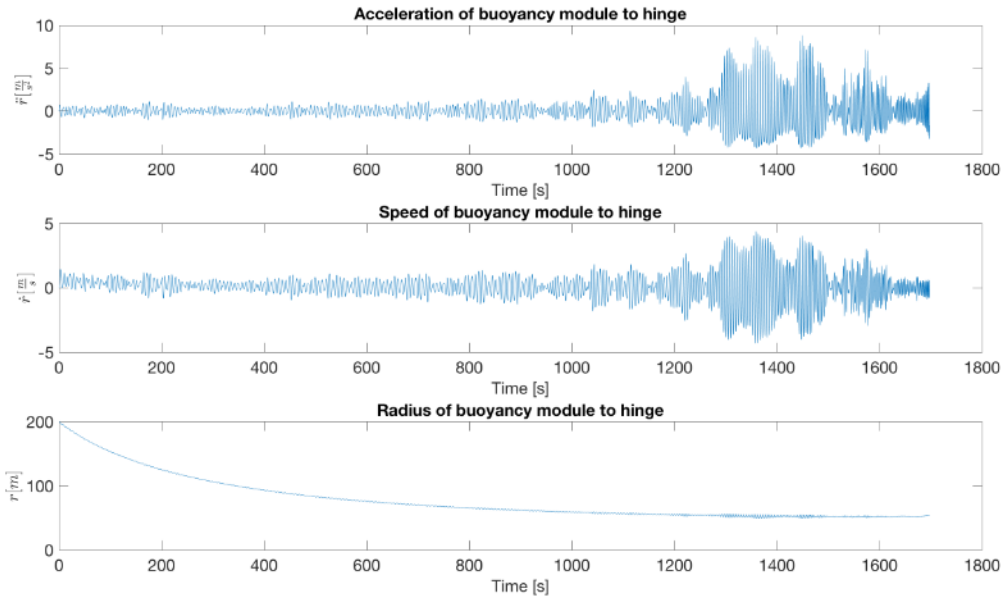

Figure 5.24: Motion of SUS in r at Hs = 1, T_p = 4.5 and φ_{wave} = 270^o during upending

sion force of the cable mainly does the work upending the SUS. Therefore, little resistance at the buoyancy module can result in quite significant oscillation amplitudes due environmental loads. The damping of the motion in r relies only on the drag on perpendicular panels of the buoyancy module, in reality the damping will be larger. There will be skin friction, eddies

and radiation damping, all of these damping mechanisms are not accounted for. This will significantly decrease the motion of the buoyancy module. The buoyancy module will need additional damping to smoothen the motion of the module and have more control over the point of application of the winch.

When higher waves with a larger significant wave height and peak period are present the

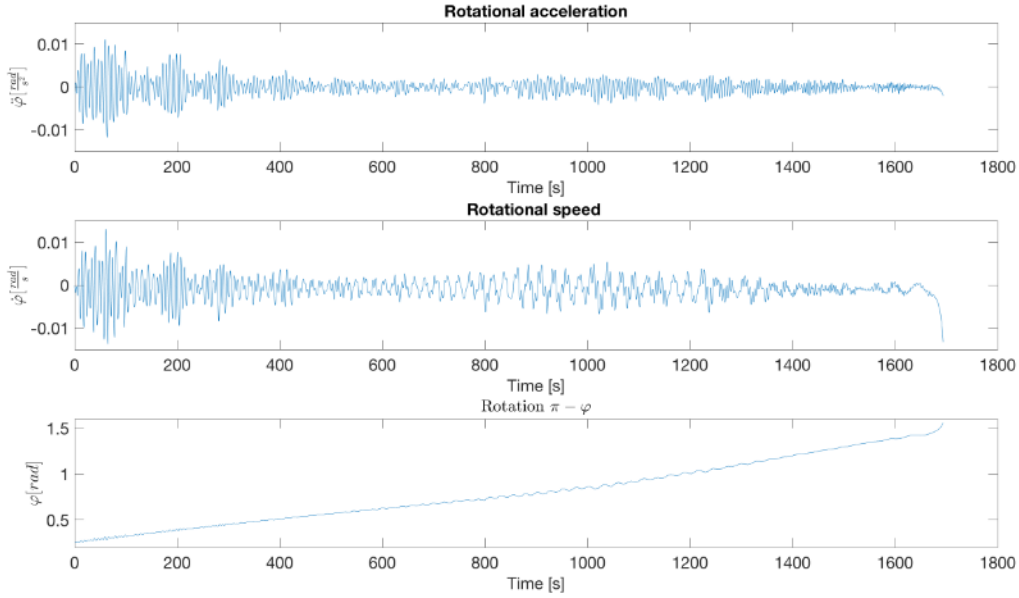

Figure 5.25: Motion of SUS in φ at Hs = 2, T_p = 6.5 and φ_{wave} = 270^o during upending

time response will tend to be most critical during the begin of upend. Figure 5.25 shows the response of the rotation for a significant wave height of 2 meter, a peak period of 6.5 seconds and incoming wave angle of 270^o. Clearly the first phase of the upending is critical for the operation as the rotational accelerations are high. At the end of the simulation are relatively small, though the amplitudes of φ are higher.

The maximal rotational acceleration of the SUS concept is needed for determination of the maximal wave characteristics. In table 5.3 the maximal rotational acceleration, $\ddot{\varphi}$, are given for multiple wave characteristics. The natural period of the SUS 3 ranges from 7 to 10 in the beginning of the upend, therefore the highest amplitudes occur around these peak periods. As the results are from a time response, the amplitudes represent a possible maximal amplitude. Because the time span in which the beginning of the upend takes place is 300 seconds, waves may be low during this period. Although it is not an exact response it does give quite a good estimation on how high these amplitudes would be.

H_s,T_p	4.5	5.5	6.5	7.5	8.5	9.5
0.5	1.9	3.9				
1.0	2.4	6.3	7.0			
1.5	5.9	7.5	8.0	9.9		
2.0	5.2	8.4	11.7	10.6	8.5	
2.5	7.7	10.0	11.3	12.0	113	10.9
3.0				11.0	12.7	15.7
3.5					14.8	

Table 5.3: Maximal rotational acceleration of SUS 3 at first 300 seconds of upend [$10^{-3}\frac{rad}{s^2}$]

The wave characteristics where it is safe to upend the wind turbine are described as in the statement 5.8. The limits of offshore lifting for weight between 2,500 and 10,000 tonne

are about 0.10 g. By multiplying the maximal rotational acceleration, $\ddot{\varphi}$, with the radius to the nacelle as in equation 5.9 the actual acceleration of the tower assembly is obtained. This acceleration should be lower than the limiting acceleration of 0.1 g for it to be safe for upending.

$$a_{nacelle} \leq 0.1g \tag{5.8}$$

$$a_{nacelle} = r_{nacelle}\ddot{\varphi}_{max} \tag{5.9}$$

In table 5.4 the maximal rotation acceleration of φ is given. The radius of the top tower assembly is taken to be 200 m. Comparing these accelerations with the limit of 0.1 g, which is 0.981 $^{m}/_{s^2}$, the upend would only be possible with a H_s of 0.5 m or with a H_s of 1.0 m and a T_p of less than 4.5. This would result in a workability of about 16 percent considering 2.1, which is fairly low. An upside is that the radiation and diffraction are not yet incorporated into the simulation, which means the acceleration response would be dampened a fair amount. Therefore, these loads should be added to the simulation in the future to get a better result.

H_s,T_p	4.5	5.5	6.5	7.5	8.5	9.5
0.5	0.38	0.78				
1.0	0.48	1.26	1.40			
1.5	1.18	1.50	1.60	1.98		
2.0	1.04	1.68	2.34	2.12	1.7	
2.5	1.54	2.00	2.26	2.4	2.26	2.18
3.0				2.20	2.54	3.14
3.5					2.96	

Table 5.4: Maximal acceleration of top tower assembly at first 300 seconds of upend [$\frac{m}{s^2}$]

When these additional loads are not sufficient to dampen these accelerations there is still no problem yet. As the SUS 3 is in design phase there are a lot of solutions possible to decrease the amplitude of these accelerations. By increasing either the mass or added mass the structures natural period increases which makes it less reactive to these wave conditions. Adding mass would be unfavourable tough, as this would affect structural design. Hydrodynamic added mass is more fit in this case. This can be realised by adding fins or plates on the structure. Another option would decrease the hydrodynamic spring coefficient by optimizing the buoyancy modules geometry.

Taken that the performance of the SUS 3 can be optimized for the beginning of the upend

H_s,T_p	4.5	5.5	6.5	7.5	8.5	9.5
0.5	0.80	1.12				
1.0	2.05	2.44	3.76			
1.5	2.63	3.12	4.08	3.80		
2.0	3.04	3.89	4.18	4.25	3.65	
2.5	3.10	4.18	4.62	4.77	4.67	4.76
3.0				5.87	4.94	4.86
3.5					6.28	

Table 5.5: Maximal acceleration of SUS 3 at second part of upend [$10^{-3}\,\frac{rad}{s^2}$]

it is interesting to analyse the performance of the SUS for the second phase of upending. In table 5.5 the maximal rotational acceleration of the second phase are given. Using equation 5.9 to find the accelerations at the nacelle will result in table 5.6. Here the performance is lots better, it could operate in waves with a H_s of 2.5 m. This is about the conditions that is desired for installing wind turbines as the workability would then be 75 percent.

H_s,T_p	4.5	5.5	6.5	7.5	8.5	9.5
0.5	0.172	0.224				
1.0	0.441	0.488	0.752			
1.5	0.565	0.624	0.816	0.760		
2.0	0.654	0.778	0.836	0.850	0.730	
2.5	0.667	0.836	0.924	0.954	0.934	0.952
3.0				1.174	0.988	0.972
3.5					1.256	

Table 5.6: Maximal acceleration of top tower assembly at second part of upend [$\frac{m}{s^2}$]

5.3.2. Frequency response of upend simulation

From the time domain upend simulation a frequency response can be obtained. Doing so the critical frequencies during upending can be found. The response of φ is used to create an amplitude spectrum of the simulation. When a waves with a significant wave height of 1.5 meter, a peak period of 5.5 seconds and incoming wave angle of 270^o are experienced during the upending the frequency response of φ will be as in figure 5.26. Figure 5.27 shows the Jonswap wave spectrum used during the simulation.

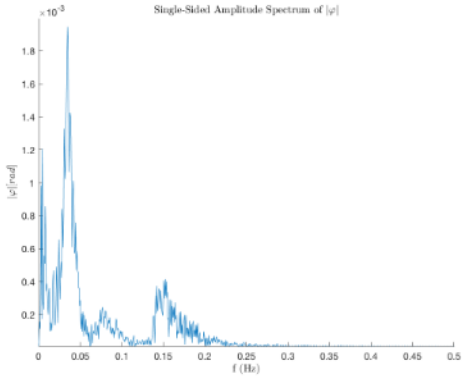

Figure 5.26: Frequency response of φ during a upend simulation with Hs = 1.5, T_p = 5.5 and φ_{wave} = 270^o

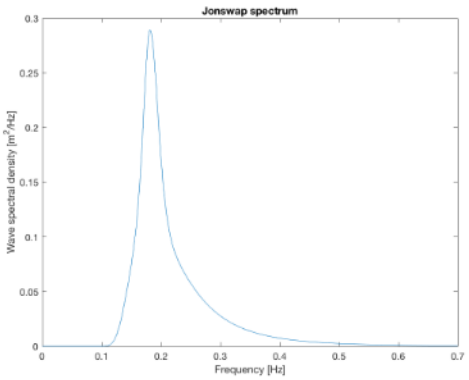

Figure 5.27: Jonswap spectrum of Hs = 1.5, T_p = 5.5 waves

On the vertical axis the maximal amplitude of φ during the whole upend and on the horizontal axis the frequency these amplitudes occur. The highest amplitudes occur at a frequency of 0.03477, which is a 28.76 seconds period. The second peak sits at 0.007931 corresponding with a 126 seconds period. The third peak corresponds to the frequencies of the wave excitation, which can be found in figure 5.27.
As the SUS can positioning itself it can manoeuvre such that the incoming waves are exerting the SUS as desired. Therefore, more insight is needed on the behavior of waves coming from all sorts of angles. And as the natural frequency of the system changes as φ changes during the upend, the time response is divided into time blocks. This will also be useful for analysing the different upend angles, finding where the critical stages of the upend simulation. The time response is divided into six time blocks as in figure 5.28.

This procedure will be repeated for incoming angles from 90 to 270 degrees, taking steps of 15 degrees. The incoming waves that are moving towards the SUS 3 are illustrated in figure 5.29. Only half of the circle is computed, as the SUS is symmetric the other half can be mirrored. Each time response with different incoming wave angles is then split into these six time blocks. Hereafter, the frequency response is generated from these time responses. In figures 5.30 to 5.32 the frequency responses of an upend during the first half are illustrated.

Each directional frequency plot has the direction of the incoming waves at polar axis and the frequency at the radius axis. The colors represent the amplitude of φ, corresponding with the color bar at the right of these figures. Figure 5.30 shows the very start of the upending, the excitation of the SUS mainly stays in a bandwidth of 0.07 to 0.2 Hz. The high frequency outer

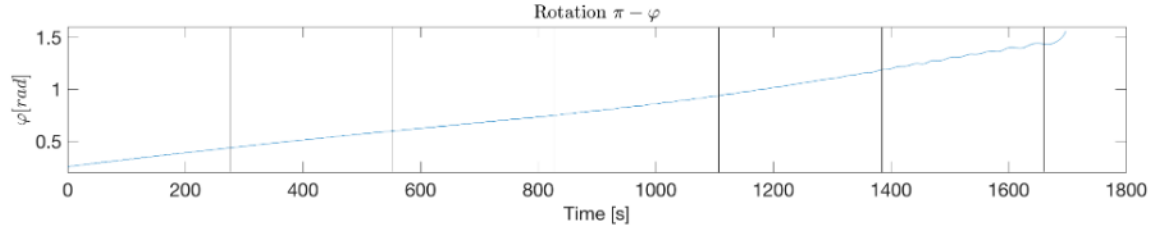

Figure 5.28: Division of time response into 6 blocks

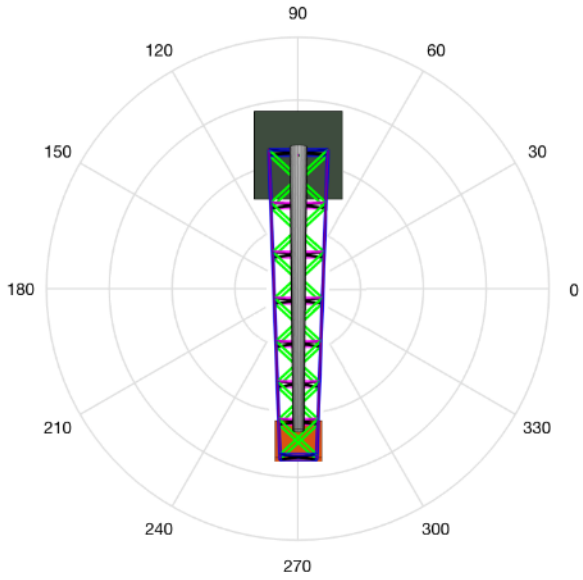

Figure 5.29: SUS 3 under different incoming wave angles

ring is the result of the wave impact, whereas the low frequency inner ring corresponds with the natural frequency of the SUS 3 at these angles. The plot shows a clear higher excitation for head waves coming from between 255 and 285 degrees. When the upend is progressing to higher angles the outer ring higher frequency amplitudes tend to fade away. Instead the amplitudes at lower frequencies increase as the SUS 3 is upended to higher angles.

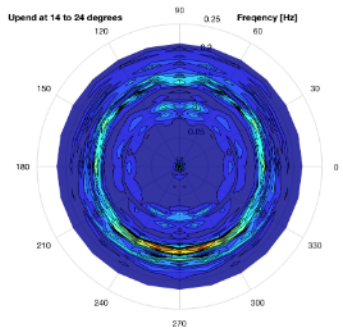

Figure 5.30: Directional frequency response of φ at 14 to 24 degrees upend

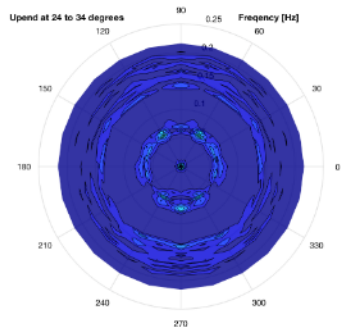

Figure 5.31: Directional frequency response of φ at 24 to 34 degrees upend

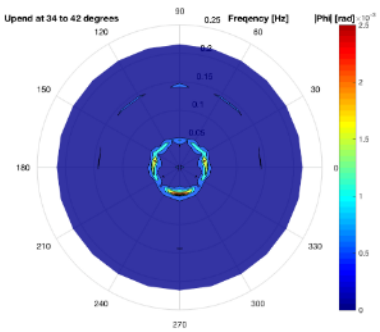

Figure 5.32: Directional frequency response of φ at 34 to 42 degrees upend

The figures 5.33 to 5.35 illustrate the directional frequency response during second half of the upend. These figures have a different scale in frequency and amplitude compared to the first three directional frequency responses. Now the inner ring with lower frequencies has more significance as the natural frequency increases during the upend. As the SUS is upend further the head and following waves are the only significant concerning amplitude in

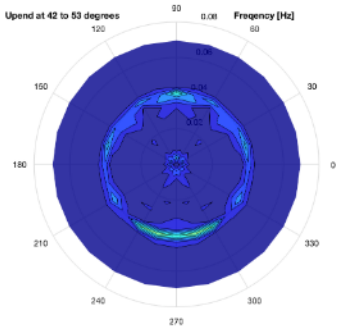

Figure 5.33: Directional frequency response of φ at 42 to 53 degrees upend

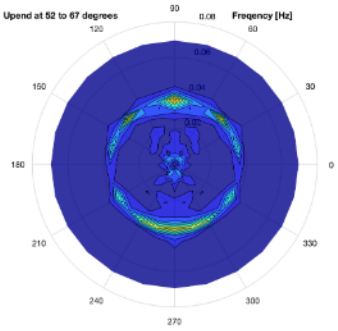

Figure 5.34: Directional frequency response of φ at 52 to 67 degrees upend

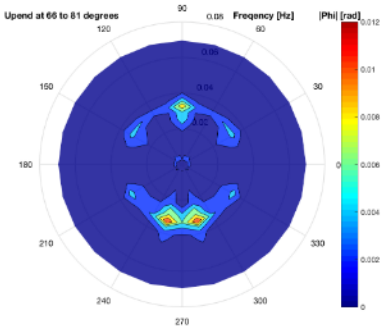

Figure 5.35: Directional frequency response of φ at 66 to 81 degrees upend

φ.
In table 5.7 all relevant data from the directional frequency responses are summarized. For most amplitudes the maximal value occurs with head waves and some at following waves. Overall it can be concluded that beam waves are most critical during upending. Therefore, all simulations are done using head waves.

	Outer ring			Inner ring		
Block	f [Hz]	$\lvert\varphi\rvert \cdot 10^{-3}[rad]$	φ_{wave} [^{o}]	f [Hz]	$\lvert\varphi\rvert \cdot 10^{-3}[rad]$	φ_{wave} [^{o}]
14-24	0.150	2.36	255~285	0.106	1.08 (0.90)	75~105 (270)
24-34	0.143	1.32 (0.77)	75~105 (270)	0.066	0.78	270
34-42	0.143	0.76	90	0.048	2.90	270
42-53	-	≤0.2	-	0.040	6.84	255~285
52-67	-	≤0.2	-	0.037	9.92 (8.54)	90 (270)
66-81	-	≤0.2	-	0.032	12.14	255~285

Table 5.7: Peak amplitudes of $|\varphi|$ with corresponding frequency and incoming wave angle

A similar procedure can be done for the acceleration for each wave direction. This is of interest as the limitation of upending is based on the maximal rotational acceleration. In figure 5.36 the frequency response of an upend simulation is shown. Clearly the higher acceleration peak occurs at higher frequencies which concurs with wave excitation frequencies.

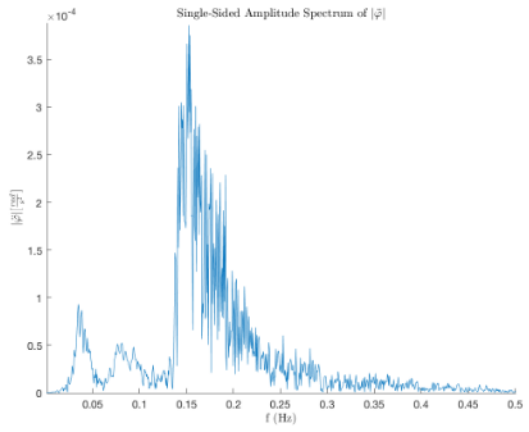

Figure 5.36: Frequency response of $\ddot{\varphi}$ during a upend simulation with Hs = 1.5, T_p = 5.5 and φ_{wave} = 270^o

The frequency response of the rotational acceleration for different time blocks are displayed in figures 5.37 5.42. The amplitude of the outside higher frequency ring decreases quite fast in the first half of the simulation. In the second half the amplitudes increase

slightly again around 60 degrees. The inner high frequency ring tends to keep quite the same amplitudes, although the frequency decreases.

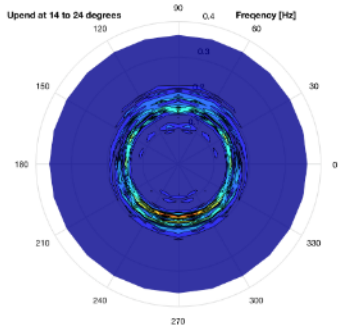

Figure 5.37: Directional frequency response of $\ddot{\varphi}$ at 14 to 24 degrees upend

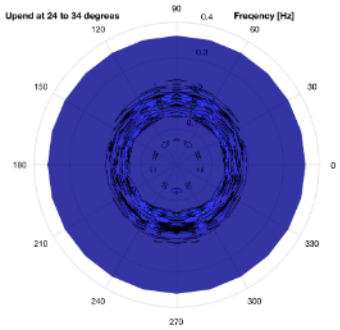

Figure 5.38: Directional frequency response of $\ddot{\varphi}$ at 24 to 34 degrees upend

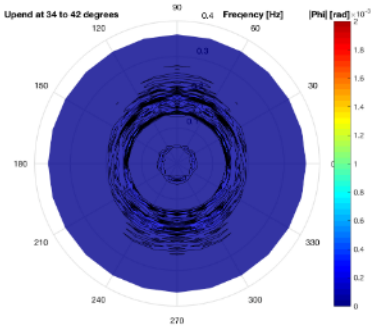

Figure 5.39: Directional frequency response of $\ddot{\varphi}$ at 34 to 42 degrees upend

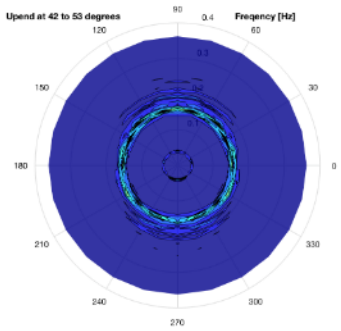

Figure 5.40: Directional frequency response of $\ddot{\varphi}$ at 42 to 53 degrees upend

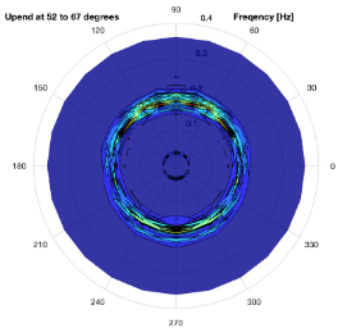

Figure 5.41: Directional frequency response of $\ddot{\varphi}$ at 52 to 67 degrees upend

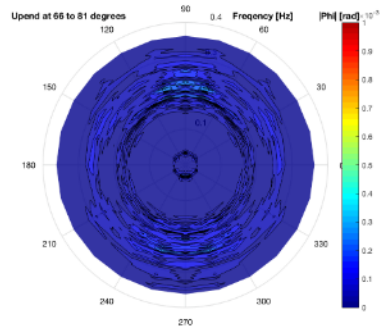

Figure 5.42: Directional frequency response of $\ddot{\varphi}$ at 66 to 81 degrees upend

In table 5.8 the maximal amplitudes of the rotational accelerations are summarised. Similar as table 5.7, the maximal amplitudes correspond predominantly with head waves. A main difference is the maximum occurs at the higher frequency which correspond with the wave excitation. This again suggest that the beginning phase of upending is critical for the workability of the SUS 3.

	Outer ring			Inner ring		
Block	f [Hz]	$\lvert\ddot{\varphi}\rvert \cdot 10^{-4}[rad]$	φ_{wave} [^{o}]	f [Hz]	$\lvert\ddot{\varphi}\rvert \cdot 10^{-4}[rad]$	φ_{wave} [^{o}]
14-24	0.150	21.03	270	0.106	5.00 (2.63)	75 ~ 105 (270)
24-34	0.139	6.05	270	0.073	2.38	270
34-42	0.143	5.86 (4.21)	90 (270)	0.048	2.57	270
42-53	0.154	9.28 (3.66)	30, 150 (270)	0.040	3.75	270
52-67	0.179	10.37 (7.06)	75 ~ 105 (270)	0.037	5.37 (4.51)	90 (270)
66-81	0.223	3.4 (2.83)	75 ~ 105 (270)	0.032	5.14	255~285

Table 5.8: Peak amplitudes of $|\ddot{\varphi}|$ with corresponding frequency and incoming wave angle

5.3.3. Forces and moments on the SUS 3

In this subsection the loads on the structure are presented. As the loads substantial, it is needed to elaborate these loads to optimise the design. In figure 5.43 the forces on the SUS lattice and moments around the hinge due to the SUS lattice are illustrated. The figure shows that the force in Z direction is quite significant as the buoyancy of the SUS lattice is largest at the start. The hydrodynamic loads associated with the Morison equation extent to a maximal amplitude load of $4.4{\cdot}10^5$ N in Z direction with significant wave of 1 meter.

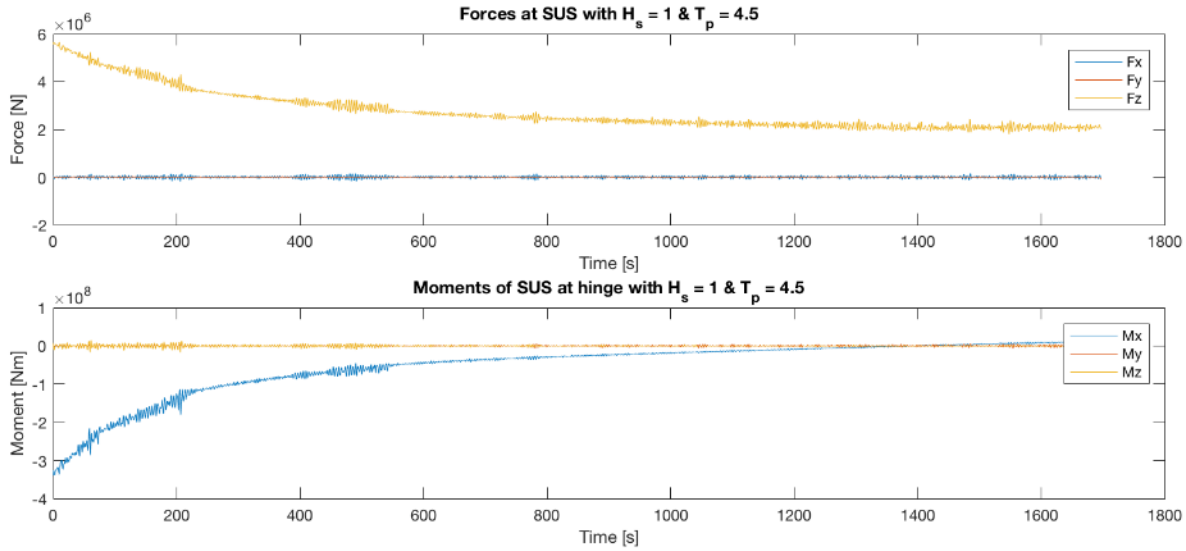

Figure 5.43: Loads of SUS at Hs = 1, T_p = 4.5 and φ_{wave} = 270^o during upending

The forces and moments on the buoyancy module are illustrated in figure 5.44. Interesting here is the high oscillatory loads in the later phase of upending. As the buoyancy module has a fairly small self-weight pushing it downward and the winch is pulling it in Y direction it is almost free to move in Z direction. This would actually be damped due radiation damping at this point, which is not incorporated into the model.

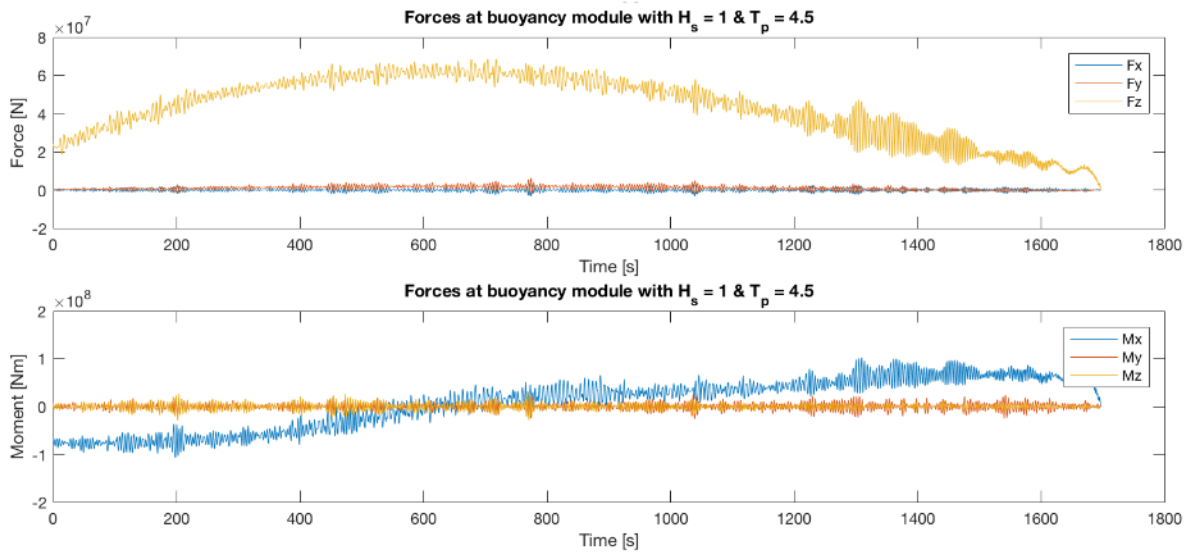

Figure 5.44: Loads of buoyancy module at Hs = 1, T_p = 4.5 and φ_{wave} = 270^o during upending

Parameter	Value	Unit	Description
D_{spud}	8	m	Diameter of spudcan
d_{spud}	1	m	Depth of spudcan
e_{spud}	2	m	Eccentricity of spudcan
$H_{floater}$	10	m	Height of the submerged floater
$L_{floater}$	10	m	Length of the submerged floater
$W_{floater}$	10	m	Width of the submerged floater
$m_{floater}$	500	tonne	Mass of the submerged floater
y_{water}	10.03	$[kN/m^3]$	Unit weight seawater
y_{sat}	19	$[kN/m^3]$	Unit weigth saturated sand
$\varphi_{friction}$	32	$[^o]$	Friction angle of sand deposit
a	-0.112	[-]	Rotation along cross-sections M_2H_3 and H_3H_2
h_0	0.122	[-]	Size parameter
m_0	0.075	[-]	Size parameter
q_0	0.033	[-]	Size parameter
β_1	0.76	[-]	Shape factor
β_2	0.76	[-]	Shape factor

Table 5.9: Input values of the spudcans and soil conditions

5.3.4. Loads at the seabed through spudcans

The environmental loads are transferred to the seabed via the submerged barge together with the weight of the SUS and the wind turbine. The moment around the hinge on the other hand can be neglect as this load is terminated due free rotation around the hinge. Another load is the force exerted by the winch. This will result in loads as in figure 5.45.

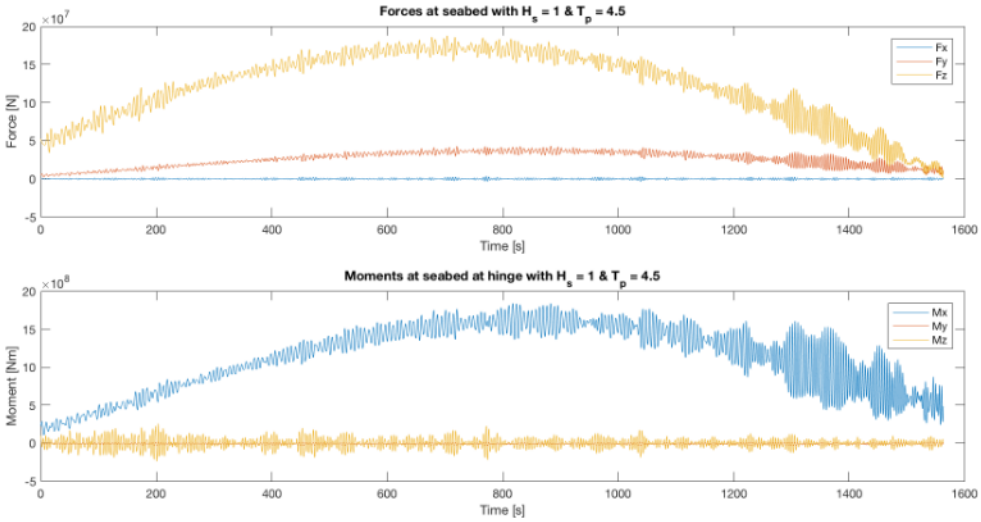

Figure 5.45: Loads at the seabed with Hs = 1, T_p = 4.5 and φ_{wave} = 270^o during upending

The design for anchoring the SUS is not yet designed. For now, the loads are distributed over four spudcans to estimate how the SUS would perform in sandy soils using these spudcans. In figure 5.46 the lay out is given for the simplistic situation. And table 5.9 gives the values used for the calculation.

The loads are equally divided over the spudcans. The loads of the SUS 3 are passed along with forces only. So, all moments are neglected, which will result in a 2D yield locus. For the system to be sufficiently fixed the loads should stay within this locus.

Figure 5.47 shows the corresponding yield locus during the upend. The vertical axis represents the shear loads and the horizontal axis represents the axial load. The data shown is a time response of the loads on the spudcans during upending. They move along the shear

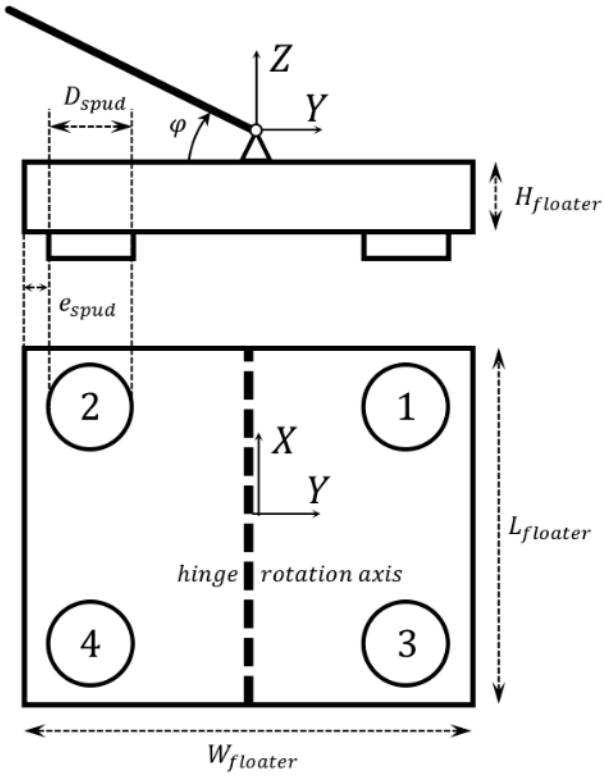

Figure 5.46: Spudcan layout at submersed floater

and axial axis as the wave loads and upending angle change. The minimum axial preload for such a spud is 41.5 MN. The axial preload needed for a fit yield curve is 456.7 MN, which is not desirable as this means a weight of 47.000 tonne is needed to preload the SUS. From the graph an ideal axial loading, V, can be obtained. For this case this would be about 200 MN. This would result into the data shifting to the right and all loads being under the locus curve.

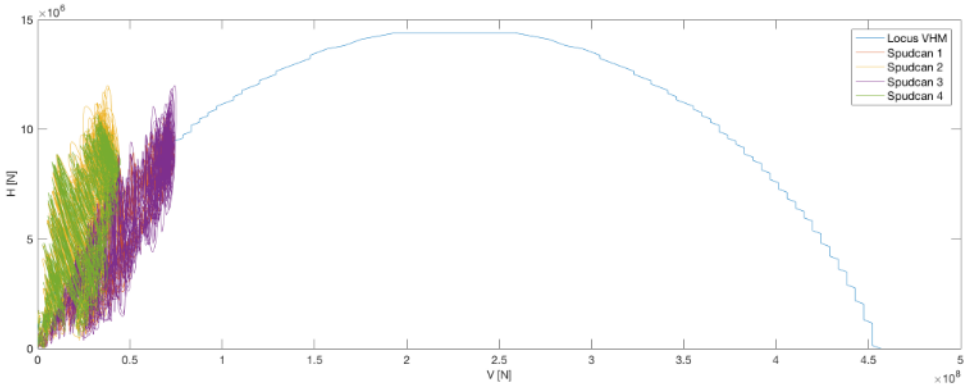

Figure 5.47: Yield locus with waves at Hs = 1, T_p = 4.5 and φ_{wave} = 270^o during upending

Although these spudcans could work the design should be made such that large axial preload as above is not needed. As the shear loads are mainly why the loads do not fit in the locus a better method would be to extend its shear capacity by using vertical plates for instance. Thus can be concluded spudcans are not the most really optimal and other anchoring methods should be accessed in future research. In table 5.10 the maximal shear loads are presented. From this table can be concluded that the shear loads do not increase

much when large wave occur. Although this data gives an indication on how much load the anchoring system should comprehend, wind loads should be added to have an even better estimate. Especially when the SUS is at a vertical position.

H_s,T_p	4.5	5.5	6.5	7.5	8.5	9.5
0.5	12.7	13.6				
1.0	12.0	15.7	18.6			
1.5	15.1	18.0	20.4	19.6		
2.0	16.6	20.6	18.5	21.2	18.5	
2.5	17.6	20.8	23.8	22.2	16.3	20.4
3.0				22.9	19.0	23.0
3.5					20.5	

Table 5.10: Maximal shear load, H, at spudcans during installation [MN]

5.4. Model validation

In this section the model is validated based on energy balance during the simulation. Also, other output variables are presented to validate the significance of the simulation. As the SUS is a new lifting method there are no similar models to reference this model to. Therefore, the model is validated by looking at how realistic the simulation performs.
For this validation a simulation of a 100 second upend is used, which is fairly quick considering the size of the structure. In figure 5.48 the rotational motion of φ is presented for position, speed and acceleration over time. Looking at the bottom graph the rotation is operating smoothly towards the desired vertical position, $\pi/2$. The speed and acceleration of the SUS oscillate a fair amount as the buoyancy module is reeled in rather fast. This movement is presented similar in figure 5.49. In the begin phase of upending the buoyancy has little resistance from the buoyancy module as its reeled in. Therefore, the buoyancy module can be accelerated to 6.7 m/s^2. This is not realistic as the power of such a winch should be 400 MW. Though it gives insight in the movement of system. Again, as the end of the simulation the buoyancy module starts to oscillate quite heavily as there is little restrain of the cable tension force.

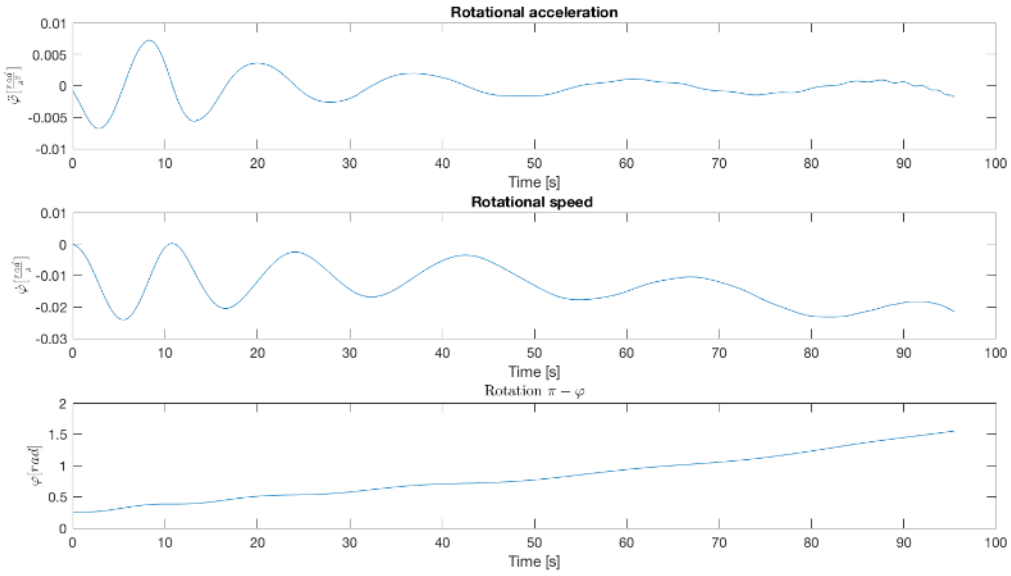

Figure 5.48: φ during 100 seconds upend with no environmental loading

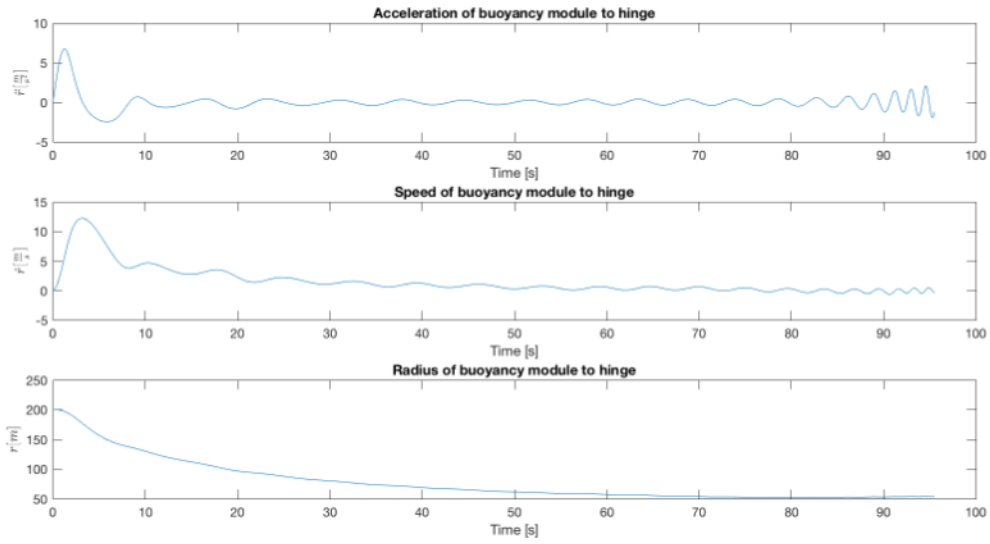

Figure 5.49: r during 100 seconds upend with no environmental loading

In figure 5.50 the mass, buoyancy and there effective distance of each subsystem towards the hinge. This effective distance represents the vector projection in Y axis from the radius towards the hinge.
As the graph illustrates the masses of these subsystems do not vary as these are fixed, though the buoyancy changes during the simulation. The buoyancy of the buoyancy module, which is denoted as 'Buoy BOX' does not move smoothly as the module is reeled in quicker than the SUS lattice can be upended due to its high inertial. Later in the simulation, the buoyancy module moves more smoothly as the angle between the applied force of the cable move more orthogonal from the r movement of the buoyancy module.
The buoyancy of the SUS lattices, denoted as 'Buoy Arm', decreases gradually. As the SUS is a latticed structure it does not decrease perfectly smooth as beams, parallel to the water surface, can suddenly occur. Within the model the buoyancy of each beam is either on or off. This results in jumps of buoyancy within the simulation as shown most clearly between 70 to 80 seconds. This result into spikes in movement of the buoyancy module as well as the SUS lattice. It can be considered a modeling flaw and could be corrected by testing the submerged state of each beam.
In the second graph the effective distance of these masses and buoyancy of the subsystems are presented. Here, all subsystem moves rather smoothly towards zero or beyond as this is the vertical upended position. The subsystems that move over the zenith of the hinge are all except buoyancy module. The jumps of the SUS lattice are again clearly visible and are undesired spikes, they could result in high acceleration spikes corrupting the data. Although these spikes would be of a short duration and as the buoyancy impact of the SUS lattice is significantly less than the buoyancy module, these spikes are negligible for now.
In figure 5.51 the energy of the SUS 3 is illustrated. The horizontal and vertical axis represented time and energy respectively. The blue line represents the kinetic and potential energy of the SUS. This includes all moving bodies, potential energy of these bodies and the kinetic spring force within the cable. The red line represents the work done by the winch and the yellow line is the effective energy loss during the upending.
From the applied work is 13 percent energy is lost during the upend as a result of drag loads. As the speed of the buoyancy module is moving rather fast at the starting phase of the upend simulation the energy loss is most significant. Hereafter the buoyancy module is moving slightly back towards an equilibrium. The drag loads from this movement have a positive effect on the energy balance of the system. From this graph the simulation can be considered roughly correct as the work is applied and the energy gained move as expected.

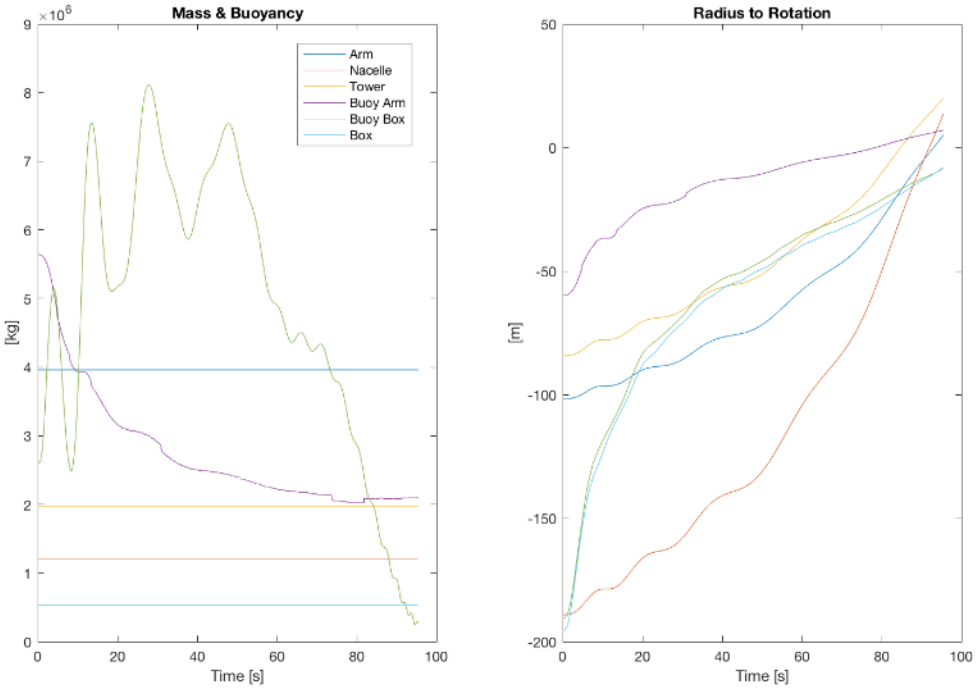

Figure 5.50: Mass, buoyancy and effective arm in Y-axis during 100 seconds upend with no environmental loading

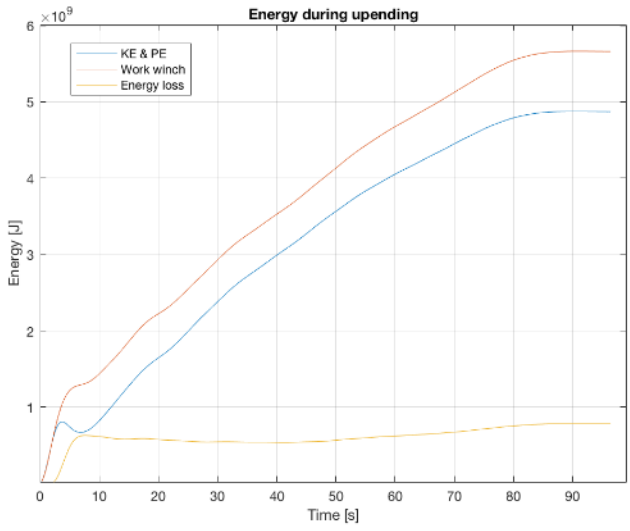

Figure 5.51: Energy of SUS 3 during 100 seconds upend with no environmental loading

When including wave loads the energy of the system would become as in figure 5.52. Here the buoyancy module moves more slowly and will not have large drag energy loss in the starting phase. Instead due the waves the SUS is elevated as the buoyancy increases. This results into less resistance to move while the buoyancy module is lifted above the water surface as when waves go up and down. This results into that the system needs less energy than it gains at the end. Beforehand the simulation this result was expected as the buoyancy module naturally moves more freely when resistance is lower. This energy gain can even be optimized by controlling the winch, reeling the cable when resistance is low.

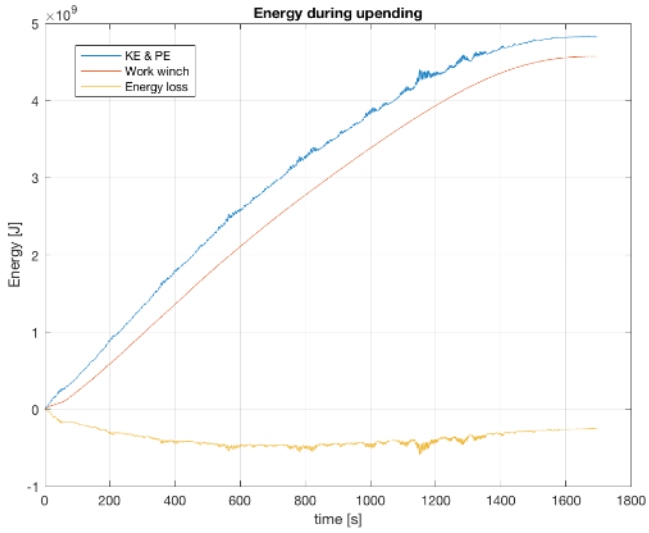

Figure 5.52: Energy of SUS 3 during 1800 second simulation with Hs 1.5 m and Tp 5.5 s

6

Conclusions

This chapter elaborates on the conclusions that can be made based on the finding of this thesis. The goal of this thesis is to improve the Sitting Up System design and determine the dynamic behaviour of the structure during installation.
Before this thesis the concept for the SUS was based on a hydraulic system pushing the wind turbine to a vertical position, the SUS 1. Two new concepts were developed as the loads within these cylinders exceeded acceptable levels. The axial load need for an upend extended to 188 MN, which is the equivalent of 6 large cylinders. The two new concepts are based on a buoyant type upending combined with winches. The SUS 2 pulling the buoyancy module along the SUS lattice towards the submerged floater and the SUS 3 pulling from a structure just above the surface. These two systems proved to be needing less loads, at which especially the SUS 3 is needing little upending force. The SUS 2 needs 145 MN tension force, whereas the SUS 3 needs 90 MN tension force upending the wind turbine. Considering these loads the SUS 3 is the most optimal and therefore chosen as the concept to research.
The dynamic model of SUS 3 is design as a rigid model. Before the full simulation of the SUS, the buoyancy module is fixated and tested for its free decay response. This resulted in that the natural period increases during the upend as the buoyancy module moved. More importantly the natural period of the system at the beginning of upending the wind turbine operates near wave periods. The natural period of the fixed free decay started at 8-10 seconds and increase exponential to 30-40 seconds during the upend, depending on the depth the SUS operates.
From the free decay test a damping ratio is obtained. During the upending this decay factor decreases from 0.006-0.014 to about 0.001, which is fairly low. Considering there should be skin friction and radiation damping added to the model this factor could be a factor 10 higher. Therefore, the model is too conservative and via model testing or potential theory modelling the correct parameters can be updated.
The response of the SUS 3 during an upend depends increasingly on reeling mechanism. The system is tested for several types of reeling tension force application on the buoyancy module. The tension control tests are done with either a fixed input, PID controlled or with constant cable reeling. The first test with fixed input operates quite well in the first half of upending, when a linear increasing tension force is exerted. Although after about 50^o the SUS becomes unstable while the tension force is controlled. From the static equilibrium for each upending angle it is clear that the tension force changes parabolic. When the maximum needed tension force is passed, after 50^o, the SUS tends to move from its desired position as it has to little or too much tension. While upending before 50^o this give not any problem. Therefore, a tension force input does not sufficiently control the upend. The PID controlled tension force worked quite well, although its oscillations for the SUS are quite extensive. Lastly the constant reeling speed using a spring type cable operated best considering all tension force control mechanisms. There was no instability until 85^o at which the SUS needs to be stopped from falling further than the desired vertical position.
Wave loads are added to the model and using constant reeling the SUS is upended within 30

minutes. Even though the model is conservative the response of the structure in wave can be used to find critical phases during upending. From the directional frequency response, the highest loads and amplitudes occur predominantly from head waves (270^o) and secondly from following waves (90^o). Therefore, the motions and loads during head waves are considered to be the critical state. In general, the most critical phase is during the starting phase of upending. Before about 25^o the amplitudes of acceleration are highest while increasing the significant wave height. The maximum operational significant wave height of the SUS in the starting phase is 1 meter with a peak period of 4.5 seconds. This can be considered low, although this performance is quite good as radiation, skin friction and diffraction are not considered. The performance in after this 25^o looks a lot more prosperous as the maximal operational significant wave height would then be about 2.5 meters, which is acceptable performance.
The stability at the seabed is depending very much on shear forces. When the SUS uses spudcans for seabed anchoring the needed preload is quite high, therefore anchoring methods with more shear capacity should be design.
The energy needed to upend a wind turbine is about 13 percent more than the potential energy gain of the system while no waves are considered. When waves are applied to the simulation the energy gained from the waves results in a positive effect in upending. The energy gained by the waves corresponds to 5 percent of the total work applied. This makes the system very efficient in upending a wind turbine.

7

Discussion

In this chapter the methods used are discussion to validate the significance of this study. During this thesis the most optimal SUS concept from three concepts is chosen. For that concept, SUS 3, a dynamic model has been generated using Matlab. The purpose of this model is to use it to estimate wave loads on the structure capturing the motion of the structure. A key point is that the model is easily adaptable for new updates and able to update it with new insight or design features. The model is assuming the SUS to be rigid and therefore does not account for structural displacements of any kind. The wave theory used in this thesis is based on undisturbed waves. In other words, the motion of the structure will not influence the water particles, which in reality will be the case. By adding radiation and diffraction the dissipated energy of the vessel can be found during the simulation. These values can be found with software like ANSYS AQWA or by doing basin model testing and finding the characteristic of the radiation and diffraction during upending. The value of adding these characteristics is that the model would become more accurate approximation of the reality. Now the model does not use these values. Nevertheless, the results are showing that without these additional coefficients the conservative model works and shows the SUS 3 is capable of installing a wind turbine within acceptable wave conditions. Potential complications can occur during the first phase of upending. Here the SUS 3 operates close to its natural frequency. Without sufficient damping, the loads and excitation of the SUS are can become excessive high which is not desired.

Another assumption is the constant drag and added mass coefficient, which is not physically correct. The drag coefficient is very much depending on the speed on the water particles, though the influence of the drag is fairly low as the SUS 3 is mainly inertial dominated. The added mass coefficient is also taken constant which is also physically incorrect. The added mass coefficient of a vessel is depending on the excitation frequency. Lower frequencies have a higher added mass. The added mass also depends on distance between the water surface and the seabed. Normally when a structure is closer to the seabed the added mass would increase as the water has less free volume to displace water.

In the model buoyancy and wave loads of the tower from the wind turbine are not taken into account. This could influence the model its behaviour either positive or negative. The buoyancy and added mass of the structure can influence the motion significantly. In the first stages of upending this would help the system to be stiffer as the water plane area increase. Also, the inertial is increase as there is more added mass which is trapped inside the tower. When the tower has no trapped water, the buoyancy will have a positive effect on the upending moment. Whereas when the tower moves beyond the zenith of the hinge it will have a negative effect and will the SUS need more tension force to upend the structure.

The soil mechanics are done based on spud cans. As the shear loads on the seabed are the most concerning, spuds are most likely not the right fit for the SUS concept. Instead vertical plates could be used to create additional shear capacity.

8

Recommendations

In this chapter the recommendation for the SUS concept are stated. First the design optimisation can is discussed, were after the simulation model and further work.

8.1. SUS design optimisation

Although the SUS design preforms well in the simulation, there are lots of optimisations realisable. First of all, the main frame of the SUS lattice can be optimised for the structural and hydrodynamic loads it will encounter, however as light weight as possible to decrease lifting weight. The addition of SUS 4, which is an additional winch lifting the SUS lattice from the end on, will probably have a positive effect on the structural integrity of the system. Therefore, when accessing the structural performance of the SUS this should be considered. Another optimisation would be the shape of the buoyancy module. During upending the buoyancy module is flipped from a horizontal position to a vertical position. During this the water plane area changes rather constantly. As for the start of the upend it is desired to have a small water plan area though sufficient buoyancy. In the later stage of upending this would have less effect as the spring stiffness of the buoyancy module has little influence on the system. Another aspect with respect to the buoyancy module is the sailing conditions. At this point the buoyancy module has a large offset and can give quite some structural complications, here also a smaller water plane area would be beneficial. The buoyancy module could be designed such that these characteristics are met. For instance, a submerged wing type body given sufficient buoyancy while moving or in rest. Furthermore, in open water condition, with a fully assembled wind turbine, the vessel could have quite a bad roll behaviour, this can be improved by changing the buoyancy module into a double hulled like structure which improves the rotation inertial for this motion. Lastly, as evaluated earlier in the discussion, the spud cans could be adapted with more vertical area to have more shear capacity at the seabed. A possible solution could be vertical plates which possible can penetrate deeper into the soil.

8.2. Model optimisation

The model created to simulate the upending motion of the SUS is already capable of to capture the motions in undisturbed wave. The first thing that should be done is to make the simulation more efficient by rewriting the code into more elementary function. Meaning the geometry is now split into several loops calculating the load in the structure. This can be rewritten to single function capable of handling different geometries.
In further work, the coefficient of added mass and drag can be made parametric depending on the local speed and geometry size. Moreover, the model can be updated with radiation and diffraction, gained from software as ANSYS AQWA. This would to create an even more realistic simulation, especially for the buoyancy module. Apart from the hydrodynamic loads the model should be able to be updated to find structural loads throughout the whole frame work. This can then be used to structurally analyse the framing within the lattice and use

this data to simulate fatigue in another model.
Another environmental loading is wind which can be very crucial during upending and mostly crucial in upright position. The model is already equipped with some possible wind loads, although the possibilities are still very restrained and are not handled during this thesis. This can be easily updated and added to the model.

8.3. Further work

As the design of the SUS is not yet final, the model should be updated accordingly. It already gives quite some insight on how the structure behaves dynamically in waves as a rigid structure. For further research it is recommended that the design is checked for soil stability, structural behaviour and fatigue. Another research area would be its open water performance during sailing, as the structure consists of two floating bodies from which one is relatively small, the motion in pitch can be quite significant. This would result in that the SUS lattice will handle large bending oscillation. It is expected this will be quite a challenge and needs careful attention.

List of Figures

List of Tables

Bibliography

[1] Global offshore wind farms. URL www.4coffshore.com/offshorewind/.

[2] North sea bathymetry. URL https://www.noah-project.de/habitatatlas/.

[3] Haliade x 12 mw offshore turbine. URL https://www.ge.com/renewableenergy/wind-energy/offshore-wind/haliade-x-offshore-turbine.

[4] Hindcast north sea 0.033° 54.35n 5.3e. URL https://app.metoceanview.com/hindcast/sites/nsea/54.35/5.3#!

[5]

[6] *Nonlinear Froude-Krylov and viscous drag representations for wave energy converters in the computation/fidelity continuum", journal = "Ocean Engineering*, volume 141. 2017.

[7] Getting ready for the next generation of offshore wind projects. April 2019. URL https://www.jandenul.com/en/pressroom/press-releases/getting-ready-for-the-next-generation-of-offshore-wind-projects.

[8] International Energy Agency. *World Energy Outlook 2018*. 2018. doi: https://doi.org/https://doi.org/10.1787/weo-2018-en. URL https://www.oecd-ilibrary.org/content/publication/weo-2018-en.

[9] DNV. *Recommended practice Det Norske Veritas DNV-RP-H103 Modelling and analysis of marine operations*. April 2010.

[10] Leo H. Holthuijsen. *Waves in Oceanic and Coastal Waters*. Cambridge University Press, 2007. doi: 10.1017/CBO9780511618536.

[11] L. Miró I. Pineda. *Offshore Wind in Europe; Key trends and statistics 2017*. Wind Europe, February 2018. URL https://windeurope.org/wp-content/uploads/files/about-wind/statistics/WindEurope-Annual-Offshore-Statistics-2017.pdf.

[12] Peter Jamieson. *Innovation in Wind Turbine Design*. John Wiley Sons, Ltd, July 2011. ISBN 978-0-470-69981-2. doi: 10.1002/9781119975441.

[13] Peter Jamieson. *Innovation in Wind Turbine Design*. March 2018. ISBN 9781119137900. doi: 10.1002/9781119137924.

[14] J.M. Peeringa K.W. Hermans. *Future XLmonopile foundation design for a 10 MW wind turbine in deep water*. ECN, December 2016. URL https://www.ecn.nl/publicaties/PdfFetch.aspx?nr=ECN-E--16-069.

[15] J M J Journée and W W Massie. *Offshore Hydromechanics*. January 2001.

[16] Axelle Viré Michiel Zaaijer. *Introduction to wind turbines: physics and technology*. December 2017.

[17] M. Randolph and S. Gourvenec. *Offshore Geotechnical Engineering*. Taylor & Francis, 2011. ISBN 9781134022168. URL https://books.google.nl/books?id=yAlEff_zspUC.

[18] José Antonio Domínguez-Navarrob Roberto Lacal-Arántegu, José M. Yustab. *Offshore wind installation: Analysing the evidence behind improvements in T installation time*. 07 2017.

A

Lagrangian derivation of equation of motion

A.1. Langrange equation

The equation of motion can be found by using Lagrange Generalized Force method. To find it first the kinetic and potential energies of a system are derived, as in equation A.1.

$$\mathcal{L} = KE - PE \tag{A.1}$$

Kinetic energy is the energy a system has due to movement and can be transferred to potential energy which is the energy an object has at a given position relative to a reference point. In this case that can be gravitational or elastic energy. The kinetic energy and potential energy are described in equations A.2 and A.3.

$$KE = \frac{1}{2}m\dot{r}^2 + \frac{1}{2}J\dot{\varphi}^2 \tag{A.2}$$

$$PE = mgh + \frac{1}{2}k\Delta x^2 \tag{A.3}$$

Hereafter, the derivative of equation A.1 is taken with respect to its generalized coordinates, q_i. This derivation should then either be zero or equal to an external generalized forces Q_i, as shown in equation A.4.

$$\frac{\partial \mathcal{L}}{\partial q_i} - \frac{\partial}{\partial t}\left(\frac{\partial \mathcal{L}}{\partial \dot{q}_i}\right) = Q_i \tag{A.4}$$

A.2. Energies within SUS 3

The SUS 3 concept has two moving parts, namely a pendulum and a moving buoyancy module. In figure A.1 this is illustrated and explains the two degrees of freedom φ and r and the coordinate system they operate in. The pendulum, representing the SUS lattice, can only move in φ direction. Whereas the square, the buoyancy module, can move in φ and r direction. This buoyancy module has a small eccentricity, e, orthogonal to the pendulum. Furthermore, to be able to express eccentricity within the box due a non-uniform weight or added mass parameters a and b are used. The axis system is set up such that the pendulum is rotating around the x axis is anti-clockwise, however the position of φ is described clockwise as in figure A.1. The identity in equation A.5 shows that the angle can be described correctly in this order.

$$\begin{aligned} \sin(\pi - \varphi) &= \sin\varphi \\ \cos(\pi - \varphi) &= -\cos\varphi \end{aligned} \tag{A.5}$$

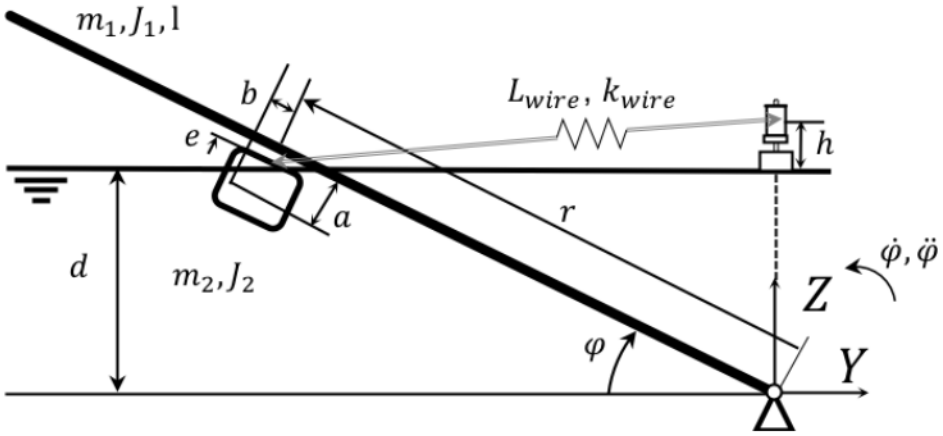

Figure A.1: Simplified model

The motion of the pendulum can be captured quick easily by its mass and inertial around the X-axis and the potential energy of its centre of gravity, CoG, and mass with respect the X-axis. For this simplified example this is taken as $l/2$.

A.2.1. General coordinates derivation for buoyancy module

The size of the buoyancy module is described with H, L and W which are the height, length and width respectively. Finding the kinetic energy of the buoyancy module requires some additional derivation as it depends on both r and φ. The centre of mass of the buoyancy module can be expressed with parameters a and b. Before finding the equation of motion using Lagrange the mass and buoyancy are rewritten in φ and r from the original axis system XYZ. Hereafter, the derivatives of these location are taken to find the speed at that location, as in equations A.6 to A.9.

$$Y = -(r+b)\cos\varphi - a\sin\varphi \tag{A.6}$$

$$Z = (r+b)\sin\varphi - a\cos\varphi \tag{A.7}$$

$$\dot{Y} = -\dot{r}\cos\varphi + (r+b)\sin\varphi\ \dot{\varphi} - a\cos\varphi\dot{\varphi} \tag{A.8}$$

$$\dot{Z} = \dot{r}\sin\varphi + (r+b)\cos\varphi\ \dot{\varphi} + a\sin\varphi\dot{\varphi} \tag{A.9}$$

The kinetic energy of the buoyancy module is calculated using the local speed in direction Y and Z squared, resulting in equations A.10 and A.11.

$$\begin{aligned}\dot{Y}^2 = {} & \dot{r}^2\cos^2\varphi + (r+b)^2\dot{\varphi}^2\sin^2\varphi + a^2\dot{\varphi}^2\cos^2\varphi \\ & - 2(r+b)\dot{r}\dot{\varphi}cos\varphi sin\varphi - 2(r+b)a\dot{\varphi}^2 + 2a\dot{r}\dot{\varphi}\cos^2\varphi\end{aligned} \tag{A.10}$$

$$\begin{aligned}\dot{Z}^2 = {} & \dot{r}^2\sin^2\varphi + (r+b)^2\dot{\varphi}^2\cos^2\varphi + a^2\dot{\varphi}^2\sin^2\varphi \\ & + 2(r+b)\dot{r}\dot{\varphi}cos\varphi sin\varphi + 2(r+b)a\dot{\varphi}^2 + 2a\dot{r}\dot{\varphi}\sin^2\varphi\end{aligned} \tag{A.11}$$

Adding these up will result in the total effective speed shown in equation A.12.

$$\dot{Y}^2 + \dot{Z}^2 = \dot{r}^2 + \left((r+b)^2 + a^2\right)\dot{\varphi}^2 + 2a\dot{r}\dot{\varphi} \tag{A.12}$$

A.2.2. Kinetic and potential energy of SUS 3

Substituting these functions into the kinetic energy of the system results into equation A.13. The mass of the pendulum is related to only φ. The equation for the buoyancy module results into 3 separate equations, namely an inertial in r and φ and another coupled component

depending on both. As the buoyancy module has a local moment of inertia J_2 and a moving parallel axis component and will become $J_{box} + m_2((r+b)^2 + a^2)$.

$$\begin{aligned} KE &= \frac{1}{2}J_1\dot{\varphi}^2 + \frac{1}{2}m_2\left(\dot{r}^2 + \left((r+b)^2 + a^2\right)\dot{\varphi}^2 + 2a\dot{r}\dot{\varphi}\right) \\ &= \frac{1}{2}(J_1 + J_2)\dot{\varphi}^2 + \frac{1}{2}m_2\dot{r}^2 + +m_2a\dot{r}\dot{\varphi} \end{aligned} \tag{A.13}$$

The potential energy of the weights is calculated using equation A.14. Here parameters a and b are $\frac{H}{2} + e$ and 0 respectively.

$$PE_{mass} = m_1 g\frac{l}{2}\sin\varphi + m_2 g\left(r\sin\varphi - (\frac{H}{2} + e)\cos\varphi\right) \tag{A.14}$$

where; H = Height buoyancy module $[m]$
e = eccentricity of buoyancy module $[m]$

A.2.3. Potential of cable system for SUS 3

Another additional potential is the spring stiffness of the cable which is modelled such that the spring has a specific stiffness depending on the length of the spring initial state or L_0. This initial length is found by initially find the equilibrium of the system without this spring. The actual length can be found with equation A.15.

$$L_{cable} = \sqrt{(d + h - r\sin\varphi)^2 + (r\cos\varphi)^2} \tag{A.15}$$

The potential energy of the cable can be formulated as in equation A.16.

$$PE_{cable} = \frac{1}{2}\frac{EA}{L_0}(L_{cable} - L_0)^2 \tag{A.16}$$

A.2.4. External loads for SUS 3

The system has two external loads, namely the buoyancy force and the reeling cable. These are both considered to put work into the system.

Buoyancy force

The buoyancy force is modelled as a generalized force on the structure such as in equation A.17. When deriving this function, a more extensive equation arises for V_2 and CoB_{Z2}. The buoyancy of the module can be expressed as a function of φ and r and as the volume and its CoB_{z2} has multiple derivations depending on its submerged state there is not one but six equations for the generalized force, as illustrated in A.2.

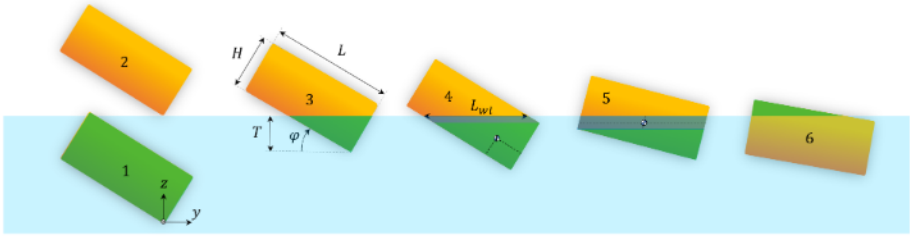

Figure A.2: Submerged situations of the buoyancy box

$$Q_{buoyancy} = \rho g(V_1\frac{d}{2} + V_2 CoB_{z2}) \tag{A.17}$$

These submerged states of the buoyancy and CoB_{z2} can be divided depending on the draft compared to its geometry, equation A.18. These equations are only valid for $0 < \varphi \leq \frac{\pi}{2}$ as the the lowest point is defined as the right lower corner of the buoyancy module at $\varphi = 0$.

1. $T \geq T_{max}$
2. $T < 0$
3. $T \leq L\sin\varphi \;\;\&\;\; T \leq H\cos\varphi$
4. $T \leq L\sin\varphi \;\;\&\;\; T > H\cos\varphi$
5. $T > L\sin\varphi \;\;\&\;\; T \leq H\cos\varphi$
6. $T > L\sin\varphi \;\;\&\;\; T > H\cos\varphi$

(A.18)

The draft, T, is calculated as in equation A.19 and is used as a parameter through out the derivation.

$$T = d - \left(r - \frac{L}{2}\right)sin\varphi + (e + H)cos\varphi \tag{A.19}$$

State 1:Fully submerged

$$V_2 = L\ H\ W \tag{A.20}$$

$$CoB_{z2} = d + (\frac{H}{2} + e)cos\varphi - r\ sin\varphi \tag{A.21}$$

State 2: Not submerged

$$V_2 = 0 \tag{A.22}$$

$$CoB_{z2} = 0 \tag{A.23}$$

State 3: Minimally submerged

$$V_2 = \frac{T^2}{2}(tan(\varphi) + \frac{1}{tan(\varphi)})W \tag{A.24}$$

$$CoB_{z2} = \frac{T}{3} \tag{A.25}$$

State 4: Submerged for one height but not the length

$$V_2 = \frac{T\ H}{sin\varphi} - \frac{H^2}{2tan\varphi}W \tag{A.26}$$

$$CoB_{z2} = \frac{(T^3 - (T - Hcos\varphi)^3)}{3(T^2 - (T - Hcos\varphi)^2)} \tag{A.27}$$

State 5: Submerged for one length but not the height

$$V_2 = \left(\frac{L^2}{2}tan\varphi + \frac{L}{cos\varphi}(T - Lsin\varphi)\right)W \tag{A.28}$$

$$CoB_{z2} = \frac{\frac{L^2T}{2}tan\varphi - \frac{L^2}{3}sin\varphi tan\varphi + (T - L*sin\varphi)^2\frac{L}{2cos\varphi}}{V_2/W} \tag{A.29}$$

State 6: Almost fully submerged

$$V_2 = W\ L\ H - \left(Lsin\varphi + Hcos\varphi - T\right)^2\left(tan\varphi + \frac{1}{tan\varphi}\right)\frac{W}{2} \tag{A.30}$$

$$CoB_{z2} = \frac{(\frac{H\ L}{2}(H\cos\varphi + L\sin\varphi) - \frac{1}{3}(H\cos\varphi + L\sin\varphi - T)^3(tan\varphi + \frac{1}{tan\varphi}))}{V_2/W} - (H\cos\varphi + L\sin\varphi - T) \tag{A.31}$$

Cable force

Another external load is the winch, which is decreasing the initial length of the cable, L_0. The work done by this winch can be calculated by simply multiplying the tension force in the cable with the decrease length as in equation A.32. The work is later added to finally upend the wind turbine.

$$\partial W_{cable} = \frac{EA}{L_0}(L_{cable} - L_0)\partial L_0 \tag{A.32}$$

A.3. Equation of motions using Lagrange derivation for SUS 3

Finally knowing all energies within the system, the derivation of the Lagrange can be calculated. First the partial derivative is taken of the time derivative of the general coordinates φ and r, where after the time derivative is taken as in equations A.33 and A.34. This derivation depends only on the kinetic energy. The derivations show the equation of motions will have a dependence with respect to each other. This is the result of the Coriolis force.

$$\frac{\partial}{\partial t}\left(\frac{\partial \mathcal{L}}{\partial \dot{\varphi}}\right) = (J_1 + J_2)\ddot{\varphi} + m_2 a\ddot{r} \tag{A.33}$$

$$\frac{\partial}{\partial t}\left(\frac{\partial \mathcal{L}}{\partial \dot{r}}\right) = m_2\ddot{r} + m_2 a\ddot{\varphi} \tag{A.34}$$

Then the Lagrange derivation with respect to the general coordinates is done for both the kinetic and the potential energy as in equations A.35 and A.36. The kinetic energy is involved in due to the centrifugal force of the moving buoyancy module and is therefore incorporated in equation A.35.

$$\begin{aligned}\frac{\partial \mathcal{L}}{\partial \varphi} = {} & m_1 g\frac{l}{2}\sin\varphi \\ & + m_2(r+b)\dot{\varphi}^2 \\ & + m_2 g\left(r\cos\varphi - \left(\frac{H}{2} + e\right)\sin\varphi\right) \\ & + EA(dr + hr)\cos\varphi\left(\frac{1}{L_{cable}} - \frac{1}{L_0}\right)\end{aligned} \tag{A.35}$$

$$\begin{aligned}\frac{\partial \mathcal{L}}{\partial r} = {} & m_2 g\sin\varphi \\ & + \frac{EA}{L_0}\left(r - (h+d)\sin\varphi\right)\left(\frac{1}{L_0} - \frac{1}{L_{cable}}\right)\end{aligned} \tag{A.36}$$

The buoyancy and centre of buoyancy depend on φ and r. These are located using the model and can be implemented as an external force. This way there is no need for a derivation with respect to the general coordinates. The cable is reeled in by a winch is also added as an external force on the system. This work is then transferred to the potential energy of the cable spring. These external moments are formulated as in equations A.37 and A.38. The effective distance in Y direction, CoB_{y2}, is calculated numerically.

$$Q_\varphi = \rho g(V_1\frac{d}{2\tan\varphi} + V_2 CoB_{y2} \tag{A.37}$$

$$Q_r = rhogV_2\cos\varphi \tag{A.38}$$

Finally, the Lagrange equation can be formulated as in equation A.39. This represents the equilibrium in still water and no cable is reeled in.

$$\begin{bmatrix} J_1 + J_2 & m_2 a \\ m_2 a & m_2 \end{bmatrix}\begin{bmatrix} \ddot{\varphi} \\ \ddot{r} \end{bmatrix} = \begin{bmatrix} {}^{\partial \mathcal{L}}/_{\partial \varphi} - Q_\varphi \\ {}^{\partial \mathcal{L}}/_{\partial r} - Q_r \end{bmatrix} \tag{A.39}$$

The system is upended by work delivered by reeling in the cable. This work is added, as in equation 4.42 by a piece of cable which is reeled in, ∂L_o. When no energy loss is considered, the work done by reeling the cable would be equal to the change of potential energy and kinetic energy of the SUS.

B

Hydrodynamic theory

In this section the methodology concerning hydrodynamic behaviour of structures in open water is presented, as well as the explanation of the relevant parameters which are chosen. The theory used for the hydrodynamic loads and wave properties are based on the literature of Journee [15], Leo H. Holthuijsen [10] and DNV [9].

B.1. Metocean characteristics

The whole wave spectrum as in figure B.1 shows the frequencies sea waves operate in. The SUS concept will operate in relatively short periods of 3 hours in relatively mild weather. The only frequencies that are accessed will be wind-generated waves. Swell is also neglected as these occur in coastal waters and during though weather.

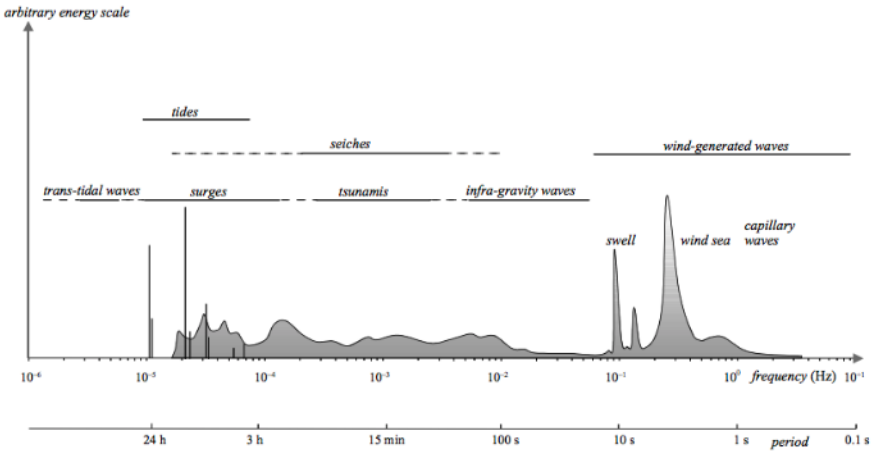

Figure B.1: Frequencies and periods of the vertical motions of the ocean surface (after Munk, 1950)

From the hindcast data the corresponding wave number, period and length are calculated with equations B.1, B.2 and B.3. From which the last is known as the dispersion relation.

$$k = \frac{2\pi}{\lambda} \tag{B.1}$$

$$T = \frac{2\pi}{\omega} \tag{B.2}$$

$$\lambda = \frac{2\pi}{\omega^2\ g} \tanh(\frac{2\pi\ d}{\lambda}) \tag{B.3}$$

where; k = Wave number $[\frac{1}{m}]$
λ = Wave length [m]
ω = Wave frequency $[\frac{rad}{s}]$
g = Gravitational constant $[\frac{m}{s^2}]$
d = Water depth

With these characteristics a wave spectrum can be generated in which the SUS concept will operate.

B.2. JONSWAP spectrum

As the North Sea is the ideal location for the SUS to install turbines JONSWAP is used as a reference wave spectrum for waves. The JONSWAP spectrum is an addition to the Pierson-Moskowitz spectrum in equation B.4. The PM spectrum is than enhanced with a peak factor creating the JONSWAP.

$$S_{PM} = \frac{A_{PM}}{\omega^5} e^{\frac{-\beta_{PM}}{\omega^4}} \tag{B.4}$$

$$S_{JONSWAP} = \frac{A_{PM}}{\omega^5} e^{\frac{-\beta_{PM}}{\omega^4}} \gamma^r \tag{B.5}$$

where; $A_{PM} = 320 \cdot \frac{H_s^2}{T_p^4}$
$\beta_{PM} = \frac{1950}{T_p^4}$
H_s = Significant wave-height [m]
T_p = Peak period [s]
γ = Peak-enhancement factor
$r = e^{-(\frac{\omega T_p - 1}{\sigma\sqrt{2}})^2}$
σ = Peak-width factor

The peak-enhancement factor is generally chosen to be $\gamma = 3.3$ and the peak-width factor is chosen $\sigma = 0.07$ before the peak frequency and $\sigma = 0.09$ after to make the spectrum wider for higher frequencies.

B.3. Stokes second-order waver theory

When calculating wave loads there can be chosen from a few wave theorems. Depending on the wave characteristics the correct wave theorem should be chosen. Most cases can be calculated with the most common used is linear airy wave theory. This theory is a linearized description of the propagation of gravity waves on the surface of a homogeneous fluid layer and is sufficient for most cases.

Figure B.2 illustrates all domains of theorem distinguishes them with the wave height (H), period (τ), depth (h) and gravitation (g). The area which the SUS will be tested in will ranges from 0 to 3 meters significant wave height and wave periods ranging from 2 to 10 second waves. Consulting figure B.2, this will result in that second order stokes theory should be used. The corresponding surface elevation, water particle velocities and accelerations are then calculated using equations B.6 to B.10.

$$\eta = \frac{H}{2}\cos(\theta) + \frac{\pi H^2 \cosh(kd)}{8\,\lambda \sinh^3(k\,d)} \cdot (2 + \cosh(2\,k\,d))\,\cos(2\theta) \tag{B.6}$$

where; $\theta = k\,x\cos(\mu) + k\,y\sin(\mu) - \omega t + \phi$ [rad]
ϕ = Phase angle [rad]

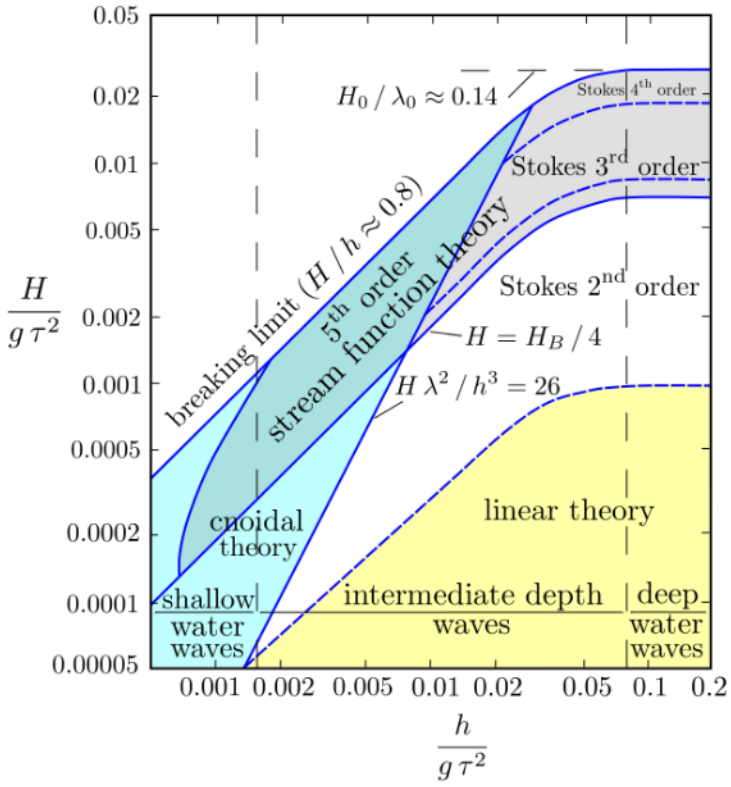

Figure B.2: Domains wave theorem

$$u = \frac{\omega H}{2}\frac{\cosh(k(d+z))}{\sinh(k\ d)}cos(\theta) + \frac{3\pi^2 H^2}{4T\lambda}\frac{\cosh(2k(z+d))}{\sinh^4(k\ d)}\cos(2\theta)$$
$$u_x = u\cos(\mu)$$
$$u_y = u\sin(\mu) \tag{B.7}$$

$$u_z = \frac{\omega\ H}{2}\frac{sinh(k(d+z)}{\sinh(kd)}\sin(\theta) + \frac{3\pi^2 H^2}{4T\lambda}\frac{\sin(2k(z+d))}{\sinh^4(k\ d)}\sin(2\theta) \tag{B.8}$$

$$a = \frac{\omega^2 H}{2}\frac{\cosh(k(d+z))}{\sinh(k\ d)}sin(\theta) + \frac{3\pi^3 H^2}{T^2\lambda}\frac{\cosh(2k(z+d))}{\sinh^4(k\ d)}\sin(2\theta)$$
$$a_x = a\cos(\mu)$$
$$a_y = a\sin(\mu) \tag{B.9}$$

$$a_z = -\frac{\omega^2 H(}{2}\frac{cosh(k(d+z)}{\sinh(k\ d)}\cos(\theta) - \frac{3\pi^3 H^2}{T^2\lambda}\frac{\sin(2k(z+d))}{\sinh^4(k\ d)}\cos(2\theta) \tag{B.10}$$

These water particle parameters are then calculated for a set of waves and then summed as in equation B.11, where after used to calculate the hydrodynamic loads on the structure.

$$\eta = \sum_{i=1}^{N} \eta(\omega_i)$$
$$u = \sum_{i=1}^{N} u(\omega_i) \tag{B.11}$$
$$a = \sum_{i=1}^{N} a(\omega_i)$$

B.4. Morison equation

For the calculation of wave loads there are also different theorems, one of these is the Morison equation. It is a semi-emperical formula which is used to calculate wave load on for slender structures. The formula was found by a heuristic approach ans has been proven to be fairly accurate for most cases. The general formulation, as in equation B.12, is build up out of an inertia part and a drag part. These are simply added together to find the oscillatory forces on the slender structure.

$$F = C_a\ \rho\ \dot{u}\ V + C_d\ \frac{1}{2}\ \rho\ u|u|\ A \tag{B.12}$$

When the body is moving the formula should be altered by subtracting the speed and acceleration of the body from the oscillatory flow, as in equation B.13. This is known as the relative velocity approach. The added mass of the acceleration is altered to C_m, which is $C_a + 1$. The plus 1 incorporates the Froude-Krylov force, this force is elaborated in the next section.

$$F = C_m\ \rho\ (\dot{u} - \dot{v})\ V + C_d\ \frac{1}{2}\ \rho(u - v)|u - v|\ A \tag{B.13}$$

As for this structure, an integration over the length is done. Each lattice member of the SUS is divided into nodes or segments, were after the forces are decoupled in x y and z direction. This is done by finding the projection of the water particles onto the cylinder, β.

$$F_m = C_a\ \frac{\pi}{4}\ \rho\ (\dot{u} - \dot{v})\ D^2\ \cos\beta^2\ l + C_d\ \frac{1}{2}\ \rho\ (u - v)|u - v|\ D \cos\beta^3\ l \tag{B.14}$$

where;
- ρ = Density sea water $[\frac{kg}{m^3}]$
- u = Water particle speed $[\frac{m}{s}]$
- $\dot{u}$ = Water particle acceleration also denoted as a $[\frac{m}{s^2}]$
- v = Body speed $[\frac{m}{s}]$
- $\dot{v}$ = Body acceleration $[\frac{m}{s^2}]$
- D = Diameter [m]
- l = Length segment [m]
- C_d = Drag coefficient
- C_a = Added mass coefficient
- C_m = $C_m = C_a + 1$
- β = Projected angle on x, y or z -axis

For each segment the projected angle β is calculated by finding the perpendicular component of directions in x y and z. Which can be calculated with equation B.15.

$$\cos\beta_x = \frac{\sqrt{(y_i - y_{i+1})^2 + (z_i - z_{i+1})^2}}{\sqrt{(x_i - x_{i+1})^2 + (y_i - y_{i+1})^2 + (z_i - z_{i+1})^2}} \tag{B.15}$$

B.5. Froude-Krylov

The Froude-Krylov is a formulation to calculate hydrodynamic load induces on floating structures by using the pressures generated in undisturbed waves and the pressure for the Archimedes Principle. It is used to calculate the non-viscous forces acting on a body. An addition to these non-viscous forces are loads from diffraction. The Froude-Krylov force is calculating using equation B.16.

$$F_{FK} = -\iint_{S_w} p\,\vec{n}\,ds \tag{B.16}$$

where; F_{FK} = Froude-Krylov force [N]
S_w = Wetted surface of body [m^2]
p = Pressure in undisturbed waves
$\vec{n}$ = Normal to the vertor from wetted surface into water

This theory can be used for structure that are to large to be slender. The buoyancy module is calculated using Froude-Krylov. In a journal of Giuseppe Giorgi [6] the errors of non linear Froude Krylov modelling showed that viscous drag is the dominant parameter. Therefore, using viscous drag in such a model errors stay within acceptable error margins.

C

Soil mechanics

The theory used for soil mechanics are found from 'Offshore Geotechnical Engineering' [17]. Similar as jack-up vessels, the SUS concept will most likely use spudcans to attach itself on to the seabed. While a spudcan is installed there are a four failure mechanisms that need to be calculated in order to validate its installation stability, these mechanisms are illustrated in figure C.1.

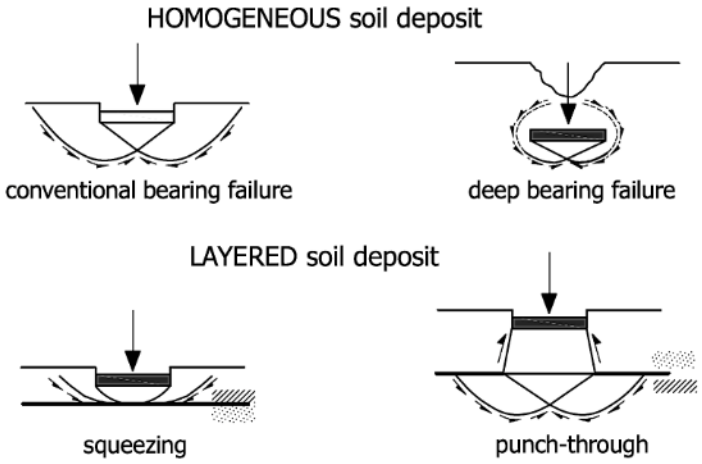

Figure C.1: Soil failure mechanisms for spudcans

When a soil deposit is homogeneous there are two mechanism which need to be tested, these are conventional bearing and deep bearing failure. Conventional bearing calculates the capacity of the soil considering the soil is maintaining in place. When deep bearing failure occurs the spudcan has a large penetration and is associated with clay. Due to the large penetration, cavity occurs with back-flow as a result. A flow-around mechanism will fill up the volume above the spud till finally it could stabilize to an equilibrium. For layer soil deposits there are also two failure mechanisms, namely squeezing and punch-through. With squeezing a spud is installed on a soft layer with a significantly harder underlying soil deposit. This could result in unstable foundation as the softer soil is squeezed against the harder soil, however the soil does not fully support the spud. The last mechanism is punch-through, in which the spud is pushed through a harder top layer. During this thesis only conventional bearing will be accessed.

The operational capacity is determined whit a yielding locus from combined loadings. As this research concerns the operational feasibility the upending it should be accessed. Figure C.2 illustrates the yielding locus in which the loads should maintain in order for to guarantee stability. The load are build up out of the vertical, horizontal, moment and torsional load, as

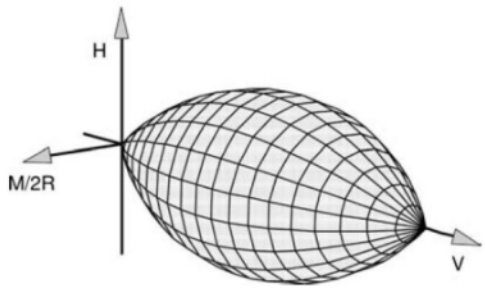

Figure C.2: Spudcan yield locus for operation performance

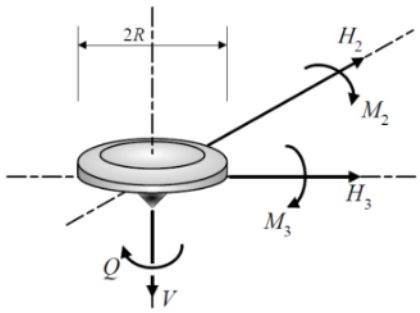

Figure C.3: VHM loading for operation performance

in figure C.3. The locus is calculated with equation C.1.

$$\left(\frac{H_3}{h_0V_0}\right)^2+\left(\frac{M_2/D}{m_0V_0}\right)^2-2a\frac{H_3M_2/D}{h_0m_0V_0}+\left(\frac{H_2}{h_0V_0}\right)^2+\left(\frac{M_3/D}{m_0V_0}\right)^2+2a\frac{H_2M_3/D}{h_0m_0V_0}+\left(\frac{Q/D}{q_0V_0}\right)^2-\left[\frac{\beta_1+\beta_2^{\beta_1+\beta_2}}{\beta_1^{\beta_1}\beta_2^{\beta_2}}\right]\left(\frac{V}{V_0}\right)^{2\beta_1}\left(1-\frac{V}{V_0}\right)^{2\beta_2}=0 \quad \text{(C.1)}$$

where;

V_0	= Preload load [N]
V	= Actual vertical load on spud [N]
H_2, H_3	= Shear force on spud [N]
M_2, M_3	= Moment on spud [Nm]
Q	= Torsion on spud [Nm]
D	= Diameter of spud [m]
h_0, m_0, v_0, q_0	= Governing size parameter for shear
a	= Defines the rotation of M_2H_3 and M_3H_2 cross-sections
β	= Shape parameter

D

Matlab code